Dissertation

submitted to the

Combined Faculty of Natural Sciences and Mathematics

of the Ruperto Carola University Heidelberg, Germany

for the degree of

Doctor of Natural Sciences

Presented by

M.Sc. Jørgen Benjaminsen

Born in: Tromsø, Norway

Oral examination: 26.02.2019

Investigating efficient apoptotic corpse removal by microglia in the developing brain

Referees: Prof. Dr. Detlev Arendt

Prof. Dr. Joachim Wittbrodt

Table of contents:

Abstract:

Every day millions of cells die in the human body, because of injury, infection, or to maintain homeostasis. The most common way for cells to die is through a process of controlled cell death, apoptosis, through which the body eliminates superfluous, or potentially damaged cells. However, ultimately this material needs to be removed, through phagocytosis, to avoid inflammation and secondary necrosis. Professional phagocytes deal with this by engulfing and digesting a large number of apoptotic cells. The throughput of this process is estimated to be several times the phagocytes own biomass in a 24 hour period. Here, I investigate the process by which engulfed apoptotic cell material is dealt with. To this end I have developed a correlative light and electron microscopy workflow that allows us to target a specific cell inside the brain of a zebrafish larvae. I have also made use of state of the art single plane illumination microscopy for tracking of the dynamic events involved in this process. By studying microglia in the optic tectum of zebrafish during a developmental stage characterized by high neuronal apoptosis I have discovered a role for the sugar-phosphate transporter Slc37a2 in shrinking phagosomes as well as a propensity for phagosomes to undergo fusion resulting in apoptotic corpses being trafficked towards a single compartment inside the cell. The broader relevance of these findings is expanded on through the development of a cell culture model to study this compartment which allowed us to characterize it in further detail. This compartment has a unique ultrastructure and a molecular signature indicating it is involved in lipid metabolism and possibly phagosome resolution.

Zusammenfassung:

Jeden Tag sterben im menschlichen Körper Millionen von Zellen, sei es durch Verletzungen, durch Infektionen oder zur Homöostase. In den meisten Fällen führt dazu ein kontrollierter Prozess, die Apoptose, zum Zelltod, mit dem Ziel überschüssige und potentiell beschädigte Zellen zu entfernen. Das dabei freiwerdende Material muss letztendlich durch Phagozytose beseitigt werden, damit es nicht zu Entzündungsreaktionen oder sekundärer Nekrose kommt. Phagozyten werden dieser Aufgabe gerecht, indem sie eine hohe Zahl von apoptotischen Zellen umfließen und verdauen. Der Umsatz dieses Vorgangs wird auf ein Vielfaches der eigenen Biomasse eines Phagozyten innerhalb von 24 Stunden geschätzt. In meiner Doktorarbeit habe ich untersucht, wie apoptotisches, umhülltes Zellmaterial verwertet wird. Dazu habe ich ein Verfahren entwickelt, das mithilfe von korrelierender Licht- und Elektronenmikroskopie ausgewählte Zellen im Gehirn von Larven des Zebrabärblings („Zebrafisch“) untersuchen kann. Daneben habe ich auch modernste Lichtscheibenmiskroskopie eingesetzt, um die dynamische Ereignisse zu verfolgen, die mit diesem Prozess einhergehen. Durch die Beobachtung von Mikroglia im Mittelhirndach (optic tectum) des Zebrabärblings während einer Entwicklungsstufe, die durch eine hohe neurale Apoptoserate gekennzeichnet ist, habe ich herausgefunden, dass der Zucker-Phosphattransporters Slc37a2 eine Rolle in schrumpfenden Phagosomen spielt und dass Phagosomen dazu neigen zu fusionieren und so apoptotische Überreste hin zu einem einzigen Kompartiment in der Zelle transportiert werden. Mit der Etablierung eines zellkulturbasierten Modells wird die allgemeine Relevanz dieser Ergebnisse näher untersucht; so konnten wir bereits das Kompartiment genauer charakterisieren. Das Kompartiment weist eine einzigartige Ultrastruktur auf und seine molekularen Merkmale deuten darauf hin, dass es am Lipidstoffwechsel und möglicherweise auch an der Auflösung von Phagosomen beteiligt ist.

List of abbreviations:

ATP: Adenosine TriPhosphate

BAI1: Brain Angiogenesis Inhibitor 1

BFP: Blue Fluorescent Protein

***blb*:** Bubblebrain

cAMP: cyclic Adenosine MonoPhosphate

CLEM: Correlative Light and Electron Microscopy

CPT: Camptothecin

CRISPR: Clustered Regularly Interspaced Short Palindromic Repeats

DMEM: Dulbecco's Modified Eagle's Medium

DMSO: DiMethyl SulfOxide

DNA: DioxyriboNucleic Acid

dpf: days post fertilization

EM: Electron Microscopy

ER: Endoplasmic Reticulum

ESCORT: Endosomal Sorting Complexes Required for Transport

FasL: Fas ligand

FBP17: F-BAR protein 17

FBS: Fetal Bovine Serum

G2A: G protein coupled receptor 132

G6P: Glucose-6-Phosphate

GA: GlutarAldehyde

GFP: Green Fluorescent Protein

GTP: Guanosine triphosphate

Ig: Immuno globulin

ILV's: IntraLuminal Vesicle's

KO: Knock Out

LAMP1/2: Lysosome-Associated Membrane Protein 1 and 2

LBPA: LysoBisPhosphatidic Acid

LPC: LysoPhosphatidylCholine

MFG-E8: Milk Fat Globulin Epidermal growth factor-factor 8

MPI: Max Planck Institute

MS: mass spectroscpy

mTORC1: mammalian Target for Rapamycin Complex 1

MVB's: MultiVesicular Bodies

µCT: x-ray micro tomography

NIRB: Near InfraRed Branding

PCR: Polymerase Chain Reaction

PFA: ParaFormAldehyde

PstSer: Phosphateidyl-Serin

PTU: N-PhenylthioUrea

RFP: Red Fluorescent Protein

RNA: RiboNucleic Acid

S1P: Sphingosine-1-Phosphate

SBFSEM: Serial Block Face Scanning Electron Microscope

sgRNAs: single guide RNAs

SLC: SoLute Carrier

SPIM: Single Plane Illumination Microscopy

TEM: Transmission Electron Microscopy

TIM4: T-cell Immunoglobulin Mucin receptor 4

TNF α: Tissue Necrosis Factor α

TRAIL: TNF-Related Apoptosis-Inducing Ligand

UA: Uranyl Acetate

UCP2: mitochondrial UnCoupling Protein 2

UTP: Uridine TriPhosphate

UV: Ultra Violet

WASP: Wiskott-Aldrich Syndrome Protein

WB: Western Blot

WIP: WASP-Interacting Protein

Z-VAD-fmk: carbobenzoxy-valyl-alanyl-aspartyl-[O-methyl]-fluoromethylketone

List of figures:

To my darling dearest, for your patience, your steadfastness and your companionship.

Det som du er, vær fullt og helt, ikke stykkevis og delt.

Henrik Ibsen, Brand

1 Introduction:

1.1 Cell death in homeostasis:

Death is a natural part of life, also for cells. The death of individual cells is often necessary for the continued well-being of the organism. This is the case from early embryonic development where cell death plays a crucial role in the sculpting of many tissues. A well-known example is tetrapod development where s tadpole's tail is lost as it metamorphize into an adult frog (Kerr, Harmon, and Searle 1974). Taking the evolutionary leap from amphibian to mammal, the loss of interdigital ectoderm that separates the digits relies on the same mechanism (Chen and Zhao 1998). From nematode to man developmental apoptosis is utilized to shape the body plan of the organism (Meier, Finch, and Evan 2000).

It also plays a role in adult homeostasis where senescent cells regularly die to make place for new healthy cells. Amongst the highest turnover rates can be found in red blood cells with an average lifespan of about 4 months (Connor, Pak, and Schroit 1994). As cells start to age they are replaced by newly differentiated cells, as senescent cells are less efficient at carrying out their biological function and their continued existence is to the detriment of the organism as a whole. In the case of injury or infection, the death of a few cells can safeguard many others. Cells are therefore programmed to elect suicide in an effort to contain a threat. It has been estimated that billions of cells die in the average adult human body every day (Renehan, Booth, and Potten 2001). There are however, many ways to die, and as it turns out some ways are to be preferred to others.

1.2 Mode of death, apoptosis:

Of the many ways a cell can die necrosis is by far be the most damaging for the organism. In short, necrosis is a non-voluntary, not controlled death where the plasma membrane ruptures and cytotoxic molecules are released into the surrounding tissue causing more cell death. It is highly inflammatory and can lead to the development of autoimmune disease (Nagata 2007, Nagata, Hanayama, and Kawane 2010).

Thus, in the evolution of multicellular organisms there has been a strong selection pressure for a mechanism by which cells can die in a controlled fashion such that the content of a dying cell could be contained. This mechanism, known as apoptosis, was initially described in 1972 (Kerr, Wyllie, and Currie 1972). Apoptotic cells have several hallmarks, unique morphological characteristics that make them easily discernable from living cells. These include condensation of the chromatin, condensation of the cell cytoplasm, and blebbing, or fragmentation, of the cell body (figure 1).

Both extracellular and intracellular signaling can eliciting an apoptotic response. The intrinsic pathway is responsible for developmental apoptosis, but can also be activated by DNA damage in a cell from ultra violet (UV) light exposure, or other genotoxic sources. This initiates a signaling

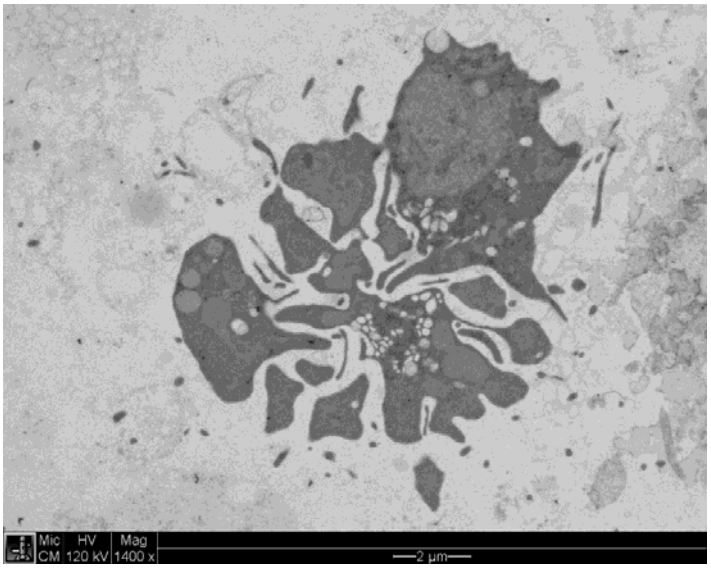

Figure 1: Apoptotic cell

Transmission electron micrograph of HeLa cell turned apoptotic by triggering the extracellular pathway through treatment with TRAIL.

cascade regulated by the Bcl-2 protein family and leads to the release of cytochrome C from mitochondria which activates caspase 9 followed by caspase 3 (Nagata 2018). The extrinsic pathway can be triggered by Fas ligand (FasL) or tissue necrosis factor α (TNF α) signaling, through their respective receptors, leading to activation of caspase 3 through caspase 8 (Nagata 2018). Downstream of caspase 3 the signaling cascade, and molecular machinery is the same regardless of the stimuli (Nagata 2018).

As a result, the cell shuts down all transcription and starts digesting itself from within. Importantly though, the plasma membrane remains intact, although it undergoes drastic changes to its lipid composition. In healthy viable cells certain lipids are highly concentrated on the outer leaflet of the membrane, while others are enriched on the inner leaflet. Maintaining this difference is achieved by three distinct processes; the translocation of a lipid from the outer to the inner leaflet referred to as “flip”, the reverse process mediated by a different set of enzymes called “flop”, and “scrambling”, the random movement from one bilayer to the other (Balasubramanian and Schroit 2003, Suzuki et al. 2010).

In apoptotic cells, translocation of phosphateidyl-serin (PstSer), an aminophospholipid normally confined to the inner leaflet of a cells plasma membrane (Seigneuret and Devaux 1984), to the outer leaflet, is considered a molecular fingerprint. It is mediated by the scramblase Xkr8, upon activation by caspase 3 (Suzuki et al. 2013), and is of great importance for removal of the apoptotic cell later.

Other mechanisms of controlled cell death have also been described, like pyroptosis which relies on different caspases, or necroptosis which is a failsafe mechanism for programmed cell death should caspases be inhibited, but unlike apoptosis which results in anti-inflammatory

signaling, these are responses to a potential threat and lead to a pro-inflammatory signaling (Tait, Ichim, and Green 2014).

1.3 Removing the corpses:

Apoptotic cells however, can only remain intact for a limited period of time. Eventually they will enter into secondary necrosis (Silva 2010), rupture and can potentially causing massive damage to the surrounding tissue (Sisirak et al. 2016). To avoid this, they are therefore removed by surrounding healthy cells through phagocytosis, also termed efferocytosis in the specific case of apoptotic cell removal (Erwig and Henson 2008). Efferocytosis can be carried out by a range of different cell types depending on the exact context. In vertebrates professional phagocytes patrol most tissues carrying out constant surveillance and are responsible for, among many other things, the removal of apoptotic cells. The professional phagocytes are of myeloid cell lineage and include neutrophils, dendritic cells, and most important for corpse removal, macrophages in their various tissue resident forms. Non-professional phagocytes, like epithelial cells can also carry out efferocytosis of dying neighbor cells and in the lower invertebrates, like nematodes corpse removal is entirely dependent on non-professional phagocytes (Horvitz, Ellis, and Sternberg 1982). A classification of a third type of phagocyte has also recently been proposed. The specialist phagocyte, refers to highly specialized support cells like the Sertoli cells in the testes or retinal epithelial cell in the eye, which include efferocytosis as one of their main tasks, but only for very specific target cells (Penberthy, Lysiak, and Ravichandran 2018). The exact description of corpse removal will therefore vary slightly on who is eating whom, however, the molecular mechanisms will be largely the same. The following description is given from the perspective of a professional

phagocyte, but with the exception of the first step, and some specific receptors, most of what I describe also applies to the other classes.

1.3.1 Attraction:

First the phagocyte must find its target. Several different molecules released by apoptotic cells have been identified which are capable of attracting phagocytes. These “find me” signals act through chemotactile gradients which are recognized by the phagocyte. Among the possible “find me” signals which have been proposed are lysophosphatidylcholine (LPC) (Lauber et al. 2003), sphingosine-1-phosphate (S1P) (Gude et al. 2008), fractalkine (Truman et al. 2008), ATP and UTP (Elliott et al. 2009), to mention a few. Many different receptors have also been identified for these various ‘find me’ ligands, for example G2A for LPC (Peter et al. 2008) and the purinergic $P2Y_2$ for nucleotides (Elliott et al. 2009). The reason for this plurality is poorly understood, however, it is widely hypothesized that they are required for different immune cells to act appropriately under differing in-vivo conditions, allowing them to modulate their response depending on the urgency required, the specific source of the signal and the needs of the surrounding tissue (Medina and Ravichandran 2016). How exactly this synergy is achieved is not known, and there is much controversy around the exact details. For LPC, for example, it has been argued that the concentrations required to stimulate phagocyte migration might not be physiologically relevant(Nagata, Hanayama, and Kawane 2010). In the case of S1P there are at least 5 different receptors (named $S1P_{1\text{-}5}$) expressed by macrophages, all capable of recognizing SP1. How the individual contribution of either one of these could be determined remains uncertain. The only traditional chemokine among the potential ligands for attraction is fractalkine which is recognized by CX3CR1, however, knockout mice

for this receptor did not show an increase in uncollected apoptotic or necrotic cells (Truman et al. 2008) indicating it might not play a crucial role in migration in-vivo.

The nucleotides ATP and UTP are the best studied in vivo, and although they are not suitable for long range signaling due to their short half-life in the extracellular space, it has been shown that a gradient can be maintained in a relay fashion, from cell to cell, by Ca+ and glutamate signaling (Sieger et al. 2012) There are, however, several ionotropic (P2X) and metabotropic (P2Y) purinergic receptors (Idzko, Ferrari, and Eltzschig 2014), and again, how these act synergistically is not at all understood.

In addition to their role in attraction "find me" signals have been shown to be involved in preparing the phagocyte for the meal to come. Fractalkine, for example, can stimulate the production of milk fat globulin epidermal growth factor-factor 8 (MFG-E8) by the phagocyte (Leonardi-Essmann et al. 2005, Miksa et al. 2007). This is a bridging molecule involved in the later recognition of apoptotic cells by the same phagocyte (Hanayama et al. 2002). In another example S1P was shown to have an anti-inflammatory effect on macrophages (Weigert et al. 2007) suggesting a role in keeping the clearance of the apoptotic cell immune-silent.

No doubt, elucidating the exact contribution of each of these players is going to be hard and for now we will have to settle for knowing that they are all involved in a complex set of interactions to facilitate the swift and harmless removal of apoptotic cells from the host body.

1.3.2 Recognition:

Once the target is reached, the phagocyte must distinguish it from neighboring cells. Just as with the receptors responsible for attraction there are many recognition receptors involved in the process of telling apoptotic and healthy cells apart. Ligands for these receptors are referred to as "eat me" signals. The best studied by far is the aforementioned PstSer which is

recognized either directly or indirectly by most of the known recognition receptors. Different sets of recognition receptors are expressed by different cell types, they are involved in the recognition of a wide variety of different substrates, and the sheer number of different receptors expressed by a single cell is bewildering (Arandjelovic and Ravichandran 2015).

Perhaps one of the best understood examples is the Brain Angiogenesis Inhibitor 1 (BAI1) which was identified as the receptor upstream of the ELMO/Dock180/Rac pathway (Park et al. 2007). However, it also moonlights in other functions like brain angiogenesis (Kaur et al. 2005) and myoblast fusion (Hochreiter-Hufford et al. 2013). It was named based on the initial discovery that it was involved in angiogenesis and showed particularly high expression in the mammalian brain. Low levels of expression have however, been reported in other tissues as well (Nishimori et al. 1997) with some indication that it is expressed by professional phagocytes in the peritoneum, colon, testes and thymus (Penberthy and Ravichandran 2016).

Another example, Stabilin, has also been shown to lead to actin polymerization, although through a different pathway, involving the intracellular adaptor protein GULP (Park, Kang, et al. 2008). It was initially described as a scavenger receptor with specificity for hyaluronan (McCourt et al. 1999, Zhou et al. 2000, Politz et al. 2002), but was later shown to also recognize bacterial low density lipoproteins (LDL) (Adachi and Tsujimoto 2002) as well as certain glycosylated proteins (Tamura et al. 2003) and more recently also PstSer (Park, Jung, et al. 2008).

Yet another example is the T-cell Immunoglobulin Mucin receptor 4 (TIM4). It is unclear whether this is a “tickling” or a “tethering” receptor, meaning if it leads to any intracellular signaling upon binding to a ligand, but its involvement in phagocytosis of apoptotic cells is well established (Park, Hochreiter-Hufford, and Ravichandran 2009, Flannagan et al. 2014,

Park et al. 2015). It does not rely on either the GULP or ELMO-DOCK180 pathway, and in fact the cytoplasmic tail of the protein is entirely dispensable (Park, Hochreiter-Hufford, and Ravichandran 2009). However, integrins, which can act as PstSer recognition receptors in their own right, have also been shown to function cooperatively with TIM-4 for signaling in vitro by forming complexes potentially capable of signaling (Flannagan et al. 2014). In this regard it is an interesting observation that comparative analysis of BAI1 and TIM4 knock downs in zebrafish yields different phenotypes in terms of how the phagocytic cup forms (Mazaheri et al. 2014).

A number of indirectly binding receptors have been identified as well. These receptors do not rely on binding any substrate on the apoptotic cells surface itself, rather they have soluble ligands that opsonize the apoptotic cell, and are then recognized by the receptor. Examples include the TAM family of receptor tyrosine kinases which can recognize Gas 6 and protein S (Lai and Lemke 1991, O'Bryan et al. 1991, Graham et al. 1994, Ohashi et al. 1995, Stitt et al. 1995, Nagata et al. 1996), or integrin αvβ5 which recognizes MFG-E8 (Hanayama et al. 2002). All these ligands, sometimes thought of as “eat me” signals in their own right, in turn bind to PstSer on the apoptotic cell.

There is also CD300a which binds PstSer and was described in its role in inhibiting inflammatory signaling. However, cells deficient in CD300a also showed decreased uptake of apoptotic cells, indicating a possible role in engulfment as well (Simhadri et al. 2012). In addition to ‘eat me’ signals there are also some ‘don’t eat me’ signals which are expressed on the surface of viable cells, to avoid being mistaken for an apoptotic target, such as CD31 (Brown et al. 2002) and CD47 (Gardai et al. 2005) detected by Signal Regulatory Protein α (SIRPα) (Barclay and Brown 2006).

Again, we can speculate that all these different receptors act synergistically for the efficient clearance of apoptotic cells, but the pluralistic nature of the receptors involved means elucidating the specific role of a single one is still beyond our grasp.

1.3.3 Engulfment:

Once recognized the target cell must now be engulfed by the phagocyte. This requires a series of cell shape changes which are triggered by the recognition receptors and mediated by actin polymerization (Kaplan 1977). Protrusions of the plasma membrane are extended along the surface of the target to form a phagocytic cup. The end result is that the target cell gets enclosed within the limiting membrane of a compartment called the phagosome.

The mechanism underlying the formation of the phagocytic cup has been a hot topic of debate. Two models were proposed, one mechanism was referred to as “zippering” and another “triggering” (Swanson and Baer 1995, Erwig and Henson 2008, Swanson 2008). According to the zippering model actin polymerization, induced by the initial binding of phagocytic receptors, would push more of the local membrane into proximity with the target. This would lead to a positive feedback loop with more receptor signaling, more actin polymerization and more membrane to come into proximity with the target, eventually engulfing the target entirely. The triggering model on the other hand postulated the requirement of a soluble “trigger-” or “tickle-signals” that would induce flailing pseudopods, often referred to as ruffles, to protrude from the phagocyte, which could capture nearby targets in loose pockets of plasma membrane that would later close in on themselves.

A morphological distinction was made to differentiate one from the other. Whereas zippering would produce tight fitting phagosomes containing nothing but the target particle, triggered phagosomes would result in a spacious phagosome, similar to macropinosomes, including a

"healthy gulp" of solute uptake (Erwig and Henson 2008). A good example of a zippering phagosome comes from the best studied phagocytosis receptor of all times, the Fcγ receptor responsible for recognizing immuno-globulin (Ig) opsonized targets (Griffin, Bianco, and Silverstein 1975). However, several species of pathogenic microorganisms have been demonstrated to elicit ruffling in phagocytes as a means to enter the host cell (Guerra et al. 2014) and can even induce the inadvertent uptake of non-pathogenic bacteria or inert beads this way. In the particular case of efferocytosis very strong evidence for a zippering phagosome has been provided and is now generally well accepted (Krysko et al. 2003, Krysko et al. 2006) with few exceptions (Erwig and Henson 2008).

Detailed molecular models have been presented for how a zippering phagosome forms (Levin, Grinstein, and Canton 2016). However, this relies heavily on observations of cytoskeleton to plasma membrane interactions in resting (not phagocytically active) cells (Ritchie et al. 2003, Kanchanawong et al. 2010), and engulfment of artificial target particles stimulating only a single recognition receptor not taking into account the natural diversity of both receptors and ligands.

There are two known pathways through which recognition receptors can activate actin polymerization. Both converging at the small GTPase Rac1 which in turn activates the Arp2/3 complex responsible for actin polymerization (Kinchen et al. 2005). The involvement of both pathways in efferocytosis, the GULP-ABCA1 pathway and the crkII-Dock180-ELMO pathway were discovered in a hallmark study in *Caenorhabditis. elegans* (Ellis, Jacobson, and Horvitz 1991) and are conserved from worm to human. While it has been proposed that they constitute somewhat of a redundancy, (Erwig and Henson 2008), for most cases of naturally

occurring phagocytic targets, and certainly in the case of efferocytosis, the set of recognition receptors expressed by the phagocyte would stimulate both pathways simultaneously.

As the distal margins of the phagosome comes into contact with each other the plasma membrane fuses with itself, sealing the phagosome. It is still unclear how the forces necessary for this joint fusion/fission event are generated, but there is some evidence that myosin is required (Swanson et al. 1999, Cox et al. 2002, Araki et al. 2003). At least parts of the machinery involved in clathrin coated pit closure is known to localize to forming phagosomes as well. F-BAR protein 17 (FBP17), known to facilitate actin polymerization through Arp 2/3, have also been shown to recruit Wiskott-Aldrich syndrome protein (WASP) as well as WASP-interacting protein (WIP) and dynamin-2 to forming phagosomes (Tsuboi et al. 2009, Levin, Grinstein, and Canton 2016).

1.3.4 Digestion:

Inside the phagosome the apoptotic cell can now be digested. To this end the phagosome undergoes a process of maturation. This happens through the sequential acquisition of Rabs, small GTPases that facilitates subsequent fusion events with compartments of the endocytic system (Roberts et al. 2000, Vieira et al. 2003).

While maturation is generally thought of as occurring after the phagosome is sealed, there are reports of endosomes fusing with the base of the phagocytic cup already during its formation (Bajno et al. 2000, Lee et al. 2007, Bohdanowicz et al. 2012). This has been suggested to be necessary to deliver sufficient membrane to the forming phagocytic cup, however, it is contested on the basis that the mesh of polymerized actin surrounding the phagosome would sterically hinder such fusion events from taking place (Mercanti et al. 2006).

First, the nascent phagosome acquires Rab5 followed by fusion with early endosomes (Roberts et al. 2000), then late endosomes, at which point they also acquire Rab7 (Vieira et al. 2003). At this point luminal pH starts to decrease and catalysis of the phagosomes luminal content can begin (Desjardins et al. 1994). Throughout this maturation the pH is progressively dropping (Maxfield and Yamashiro 1987), and the catabolic enzymes, like cathepsins, appear to be delivered in a sequential order (Claus et al. 1998). This is a very dynamic process and it is very difficult to know exactly how much can be inferred from studies in different cell types, and of different phagocytic targets. Macrophages and fibroblasts for example appear to digest apoptotic cells much faster than dendritic cells. Ig opsonized targets on the other hand are digested at the same slow rate in both macrophages and dendritic cells (Erwig et al. 2006). A lot of the details, especially concerning the temporal aspect of phagosome maturation therefore has to be established for individual systems.

Any biological material that has been ingested, whether it is an apoptotic cell or a potential pathogen, consists of a large variety of different materials. Proteins, lipids, sugars, DNA and RNA all need to be broken down into different components and this requires different enzymes. Cathepsins are responsible for the breakdown of protein first into peptides and then individual amino acids. Different cathepsins with different specific substrates are thought to arrive at the phagolysosome in a sequential manner (Claus et al. 1998, Flannagan, Jaumouille, and Grinstein 2012, Abraham 2015). Sphingomyelinase and several phospholipases have been found in phagosomes (Fischer et al. 2001, Trost et al. 2009, Wahe et al. 2010) that are capable of digesting lipids. While apoptotic cells are known to start digesting their own DNA prior to engulfment (Samejima and Earnshaw 2005), DNaseII is also reported to be delivered to phagosomes containing apoptotic cells and appears to be much more crucial to their degradation (Krieser et al. 2002). However, again we must be cautious of extrapolating too

much between different forms of phagocytosis as the activation state of cells greatly affect relative abundance of proteins in phagosomes as well as their phosphorylation states (Trost et al. 2009).

It has long been speculated that the phagocyte might be able to utilize much of the digested material for its own metabolism. Some evidence in support of this hypothesis comes from a study of mitochondrial uncoupling protein 2 (UCP2), involved in regulating mitochondrial membrane potential. This protein is upregulated in response to phagocytosis and mice with a deficiency in this gene are less effective in clearing apoptotic cells (Park et al. 2011). The underlying mechanism, however, remains largely unknown.

1.4 Phagosome resolution:

So far I have been discussing the mode by which apoptotic cells are effectively removed from a tissue. However, what happens to the engulfed material after it has been digested in the phagolysosome is still an open question. Furthermore, it is clear that the limiting membrane of the phagosome has to be disposed of, or recycled. This process is referred to as phagosome resolution. Several hypothesis have been put forward and below I will describe three possible models.

1.4.1 Hypothesis 1. Expelling the digested material from the cell:

Specialized lysosomes have long been known to fuse with the plasma membrane in many different cell types and this can serve a variety of different functions from plasma membrane repair to platelet activation and granule secretion (Reddy, Caler, and Andrews 2001, Silverstein and Febbraio 1992, Hirano et al. 1991). The idea that this could also be relevant for phagosome resolution comes from observations in the unicellular amoeba *Dictystelium. discoideum*, but it has also been proposed as a mechanism for phagocytes in multicellular

organisms to expel phagosomal content (Gotthardt et al. 2002). The most compelling argument for this comes from observations of macrophages exocytosing engulfed, opsonized beads upon stimulation by a secretion stimulant, GTP-γS , an analog of GTP (Di et al. 2002). There is, however, no evidence for this happening in-vivo. If this is indeed the way phagosomes resolve it would mean that the phagocyte takes a compartment full of what is essentially "useful" nutrients, and dumps it into the extracellular space, where it could even result in cytotoxicity.

1.4.2 Hypothesis 2. Nutrient uptake from lysosomes in an mTORC1 dependent manner:

A key player in cell metabolism is the mammalian target for rapamycin complex 1 (mTORC1) that regulates the extraction of nutrients, especially amino-acids, from storage lysosomes (Hara et al. 1998, Kim et al. 2002). While mainly studied in the context of autophagy, it was reported that this complex controls a late stage of the phagocytic pathway involving the fission of phagolysosomes into multiple lysosomes, from which nutrients can be extracted on demand under the control of mTROC1 (Krajcovic et al. 2013). Krajcovic et al. showed that macrophages grown in amino acid free medium could be rescued from starvation by engulfing and digesting apoptotic cells, providing further evidence that phagocytes are indeed capable of extracting nutrients from engulfed cells. Macrophages grown in regular growth medium however, did not show any evidence of increased mTORC1 activation after phagocytosis, questioning the relevance of this mechanism to general phagosome resolution.

1.4.3 Hypothesis 3. Extraction of metabolites over the phagosomes limiting membrane:

Proteomics studies of isolated endosomes and phagosomes have identified several solute carrier (SLC) transporter proteins which are capable of transporting various metabolites across the phagosomal membrane (Duclos et al. 2011, Jutras et al. 2008, Peltier, Hartlova, and

Trost 2017). By removing these metabolites from the lumen of the phagosome it has been hypothesized that water is extracted through aquaporins, known to localize to phagosomes, resulting in phagosome shrinkage (Levin, Grinstein, and Canton 2016). This decrease in phagosome volume, it has further been argued, is necessary in order for the limiting membrane to undergo the necessary fission events for its own resolution (Freeman and Grinstein 2018), an argument not considered for the fission of phagolysosomes into multiple lysosomes. This hypothesis relies largely on mechanisms already well known from studies of the endocytic system and the growing appreciation for the extensive overlap in the two pathways argues in favor of it.

1.4.3.1 Transporters known to localize to the endocytic/phagocytic pathway:

Among the SLC families known to localize to phagosomes specifically there are Slc2 which facilitates glucose transport, Slc12 for potassium/chloride transport, Slc37 for phosphate sugars transport and Slc38 for amino acid transport (Jutras et al. 2008). Early endosomes are known to possess Slc1a5 facilitating sodium-dependent neutral amino acid transport, Slc25a5 for adenine nucleotide transport among others, and late endosomes/lysosomes possess Slc15a2 for oligopeptide transport, Slc37a2 a putative glucose-6-phosphate (G6P) transporter and the putative sphingolipid transporter Spns1. (Duclos et al. 2011), as well as the nucleoside transporter Slc29a3 (Hsu et al. 2012). From these examples, and others, we know of transporters with substrates representing all the major metabolic pathways. Of special interest was the SLC37 family of transporters as previous unpublished work from our lab discovered a mutant for Slc37a2 with a striking phenotype linked to phagocytosis.

The SLC37 family consists of four members, the best characterized among these is Slc37a4 which is known to be important for myeloid cell function (Chou and Mansfield 2014, Cappello

et al. 2018)(Chou and Mansfield 2014, Cappello et.al 2018). It is ubiquitously expressed and involved in the regulation of blood glucose levels (Pan et al. 2009). It is a putative G6P transporter located to the ER where it is suggested to act in a functional complex either with G6Pase-α or G6Pase-β. Mutations in the latter is known to cause severe congenital neutropenia in humans (Chou, Jun, and Mansfield 2010b, a). While the other members, Slc37a1 and Slc37a3, also are associated with disease, breast and colorectal cancer, or hyperinsulimia, respectively (Iacopetta et al. 2010, Kikuchi et al. 2018, Proverbio et al. 2013) neither has been associated with phagocytosis or endocytosis.

Slc37a2 was initially discovered in a screen for genes upregulated by cAMP in RAW 264.7 cells. It is predicted to encode a 501 amino acid, 55 kD protein with a 43 % homology over 478 residues to the Arabidopsis thaliana glycerol-3-phosphate permease (Takahashi et al. 2000). The protein contains 12 transmembrane domains and gives a band of 50 – 70 kD by western blot due to N-linked glycosylation (Kim et al. 2007). Expression of Slc37a2 has been reported in liver, kidney and spleen (Pan et al. 2011), but unlike the more ubiquitously expressed Slc37a4 it is much more highly expressed in neutrophils and macrophages (Chou and Mansfield 2014). High expression levels were found to correlate with chronic inflammation in obese mice (Kim et al. 2007) and in dairy cattle mutations have been reported to lead to increased embryonic mortality (Fritz et al. 2013, Reinartz and Distl 2016). In mouse brains it is almost exclusively expressed in microglia according to the Barres Brain database. Based on its homology to Slc37a4 it was hypothesized that Slc37a2 also is a transporter for glucose-6-phosphate, and it has indeed been shown to be capable of both G6P/Pi and Pi/Pi exchanges in vitro. Unlike Slc37a4 it does not act in a functional complex with any phosphatase and does not appear to be involved in maintaining blood glucose levels (Pan et al. 2011).

Extraction across the membrane however, only solves one half of the problem of phagosome resolution. Proponents of this hypothesis therefore relies on the two mechanisms known from the endocytic pathway to explain membrane resolution.

1.4.3.2 Membrane resolution in the endocytic pathway:

In the endocytic pathways two different compartments are described as necessary to resolve the limiting membrane of endosomes. These are recycling endosomes and multivesicular bodies (MVB's). Recycling endosomes, as their name suggests, are involved in salvaging what can be reused of the limiting membrane and the proteins on it. This happens through outwards vesiculation, budding off by part of the endosomes limiting membrane, and recycling it back to the plasma membrane (Cox et al. 2000). These recycling events are primarily mediated by the small GTPases Rab4 and Rab11 and thought to occur during the early endosome/phagosome stage (Garin et al. 2001, Damiani et al. 2004).

MVB's on the other hand serve the opposite function. As the name suggests they contain intraluminal vesicles (ILV's) which are derived from the membrane of the MVB itself through a process of invagination facilitated by the endosomal sorting complexes required for transport (ESCORT) known to localize to phagosomes (Lee et al. 2005). The MVB classically a sub category of late endosomes is proposed to have some digestive properties of its own but has also been reported to undergo fusion with lysosomes to continue digestion (Matsuo et al. 2004).

It is important to note that neither of these mechanisms truly resolves the compartment though, in the sense that it never really ceases to exist. The full resolution of a phagosome is conceptually very difficult and has not really been thoroughly explored (Levin, Grinstein, and Canton 2016).

1.5 Microglia:

The professional phagocytes of the brain are the microglia, first described by Del Rio Hortega in 1919 (Sierra et al. 2016). They are tissue resident macrophages originating from hematopoietic monocytes early in development (Herbomel, Thisse, and Thisse 1999, Ginhoux et al. 2010). By colonizing the brain (Herbomel, Thisse, and Thisse 2001, Casano, Albert, and Peri 2016) they establish a self-renewing population that lasts for the lifespan of the organism (Ginhoux et al. 2010). In adult homeostasis they play many important roles including contributing to the maintenance of the blood brain barrier and removal of potential pathogens or other hazards. They are also implicated in a number of aging related disorders such as Alzheimer's disease, although whether their contribution is beneficial or detrimental is still largely debated (Aguzzi, Barres, and Bennett 2013, Rothhammer and Quintana 2015).

During development they play a particularly crucial role in refining neuronal connectivity through clearing apoptotic cells as well as pruning synapses (Bilimoria and Stevens 2015). The latter has been proposed to happen through the same mechanism as the former, as detailed above, but instead of engulfing a whole cell microglia are suggested to nibble off individual dendrites, a process referred to as trogocytosis. However, a recent electron microscopy study of microglia pruning dendrites is casting some serious doubt over whether these can be considered actual engulfment events (Weinhard et al. 2018).

Microglia are also known to be important for learning and memory formation, both through their ability to eliminate neurons and synapses, as well as through the secretion of neurotrophins that help stimulate and strengthen them (Parkhurst et al. 2013).

Classically microglia have been divided into two states based on the observation of two distinct morphological phenotypes. Highly branched microglia thought to be in a resting state,

and more rounded up cells thought to be active. However, as more advanced live imaging techniques became available it has become clear that this interpretation is somewhat of an oversimplification. A more rounded up cell shape is usually associated with amoeboid cell migration, but highly branched cells can still be very active, extending and retracting their branches to probe their environment and to identify their targets. While it was initially thought that the amoeboid cell shapes must be associated with a pathology we now know that there are several reasons for microglia to migrate, and not all of them are associated with inflammation (Nimmerjahn, Kirchhoff, and Helmchen 2005, Davalos et al. 2005).

1.6 Zebrafish as model system for studying efferocytosis:

Zebrafish embryos have been used as a tool to study developmental biology since the 1970's (Streisinger et al. 1981). Many facets of its development are therefore well characterized and understood. The ease of pharmacological manipulation, short generation time and large hatches from mating has made zebrafish a useful model for genetic screens which have been important for the identification of several novel genes and their functions (Mullins et al. 1994, Haffter and Nusslein-Volhard 1996, Driever et al. 1996). A well maintained and frequently updated database is available through the Sanger Institute's Zebrafish Genome Project further facilitating the use of genetic manipulation when working with zebrafish. Well established protocols for knock downs and knock outs are also available (Bedell, Westcot, and Ekker 2011, Hwang, Fu, Reyon, Maeder, Kaini, et al. 2013, Hwang, Fu, Reyon, Maeder, Tsai, et al. 2013, Sander and Joung 2014).

It offers an excellent model system in which to study the process of efferocytosis in vivo and under naturally occurring conditions. The ex-utero development and translucent properties of zebrafish embryos allows for direct observation of these events without any manipulation.

The innate immune system is well preserved within the vertebrate phylum and therefore highly similar between humans and zebrafish (Davidson and Zon 2004, Ellett et al. 2011, Renshaw and Trede 2012). Macrophages have been shown to differentiate from hematopoietic precursors and invade the brain at about 2.5 days post fertilization (dpf) to establish a microglial population (Herbomel, Thisse, and Thisse 1999, 2001). Around the same time a large number of neurons in the optic tectum undergo apoptosis and are removed by microglia (Peri and Nusslein-Volhard 2008). The optic tectum is conveniently positioned dorsally in the midbrain making it ideal for live imaging. Our lab has made use of these properties to study several aspects of microglial biology, from migration to brain colonization and neuronal phagocytosis (Sieger et al. 2012, Mazaheri et al. 2014, Moritz et al. 2015, Rossi et al. 2015, Casano, Albert, and Peri 2016).

2 Aim of project:

The aim of this project was to study the process by which professional phagocytes deal with the massive influx of material they are required to engulf as part of homeostasis. In particular I focused on microglia engulfing apoptotic neurons during zebrafish brain development as a model for this process. To this end it was necessary to establish imaging protocols and data analysis pipelines enabling me to track individual phagosomes over extended periods of time in this in vivo system. Previous work from the lab had identified a mutant line in which microglia developed a peculiar bloated phenotype which was shown to be strictly dependent on their phagocytic activity. As part of my effort to understand the process of effective cell clearance I uncovered the cell biological mechanisms by which this phenotype comes about. In order to study this process and investigate the cell morphology at an ultrastructural level I aimed to establish correlative light and electron microscopy pipeline capable of targeting a single specific cell inside the volume of a zebrafish brain.

3 Results:

3.1 Observing efferocytosis in vivo:

The three mechanisms described in the introduction for phagosome resolution, namely, lysosomal fusion with the plasma membrane, phagosome dispersion into lysosomes, and extraction of content across the membrane, are not necessarily mutually exclusive. They could represent different stages of phagosome maturation, or strategies utilized by different phagocytes under specific conditions. The vast majority of observations underlying all three are heavily focused on cell culture experiments and in-vivo data from *C. elegans.* While the latter is an excellent in-vivo system for investigating apoptotic cell removal, thanks to its very regular development and body plan, these phagocytes are not challenged with the same high throughput as professional phagocytes in vertebrates under in-vivo conditions. Our lab has therefore been using the zebrafish model for in-vivo observations using confocal microscopy. While this approach has been very successful in visualizing the formation of the phagocytic cup (Mazaheri et al. 2014) it is not sufficient to follow highly dynamic processes like the fate of individual phagosomes into the soma of the cell.

Thus, in collaboration with Nils Norlin, I applied Single Plane Illumination Microscopy (SPIM), a powerful new technology, characterized by low phototoxicity and capable of visualizing large in-vivo volumes at very high temporal resolution. We used this imaging technique in combination with two transgenic zebrafish lines. We visualized microglia using the either the *Tg(pU1::Gal4UAS::tagRFP)* or *Tg(mpeg::GFPcaax)* reporter line. Both promoters are macrophage specific and therefore also label microglia (Peri and Nusslein-Volhard 2008, Ellett et al. 2011). We simultaneously visualized apoptotic cells by crossing this line with another reporter line *Tg(ntb::LexPR-LexOP::secA5)*. There neurons express an Annexin5 BFP fusion

protein. Annexin5 is secreted by neurons as a natural opsonin for PstSer and the BFP therefore localizes to apoptotic cells (van Ham et al. 2010).

Imaging the entire optic tectum of zebrafish larvae with two channels, allowed us to follow phagosomes by acquiring stacks every 20 seconds for a few hours duration 3.1.1 A. This, however, resulted in datasets over 1 TB in size. In order to analyze these data sets they had to be reduced in size, which was achieved by cropping out individual microglia. However, due to their high motility each individual time point required the crop to be of a different area of the dataset. This challenge was overcome using the big data tracker tool developed for Fiji by Christian Tischer of the EMBL ALMF (https://github.com/tischi/fiji-plugin-bigDataTools). Utilizing this approach allowed us to make the following observations.

3.1.1 Formation of a phagosome:

As shown in figure 2 B the phagocytic cup forms around an apoptotic cell. A protrusion can be seen to extend from the microglia (green) towards the apoptotic cell (blue). As it reaches its target the phagocytic cup extends protrusions on either side of the apoptotic cell until they meet on the opposite side and the phagosome closes. The fully formed phagosome can be observed independently of the BFP marker, as an exclusion of the GFP marker. It is possible to follow the movement of this phagosome as it is retracted towards the soma of the cell. After it reaches the soma however, it intermingles with several other shadows (also phagosomes) and their dynamic movement makes it difficult to discern them from one another over time (figure 2 C).

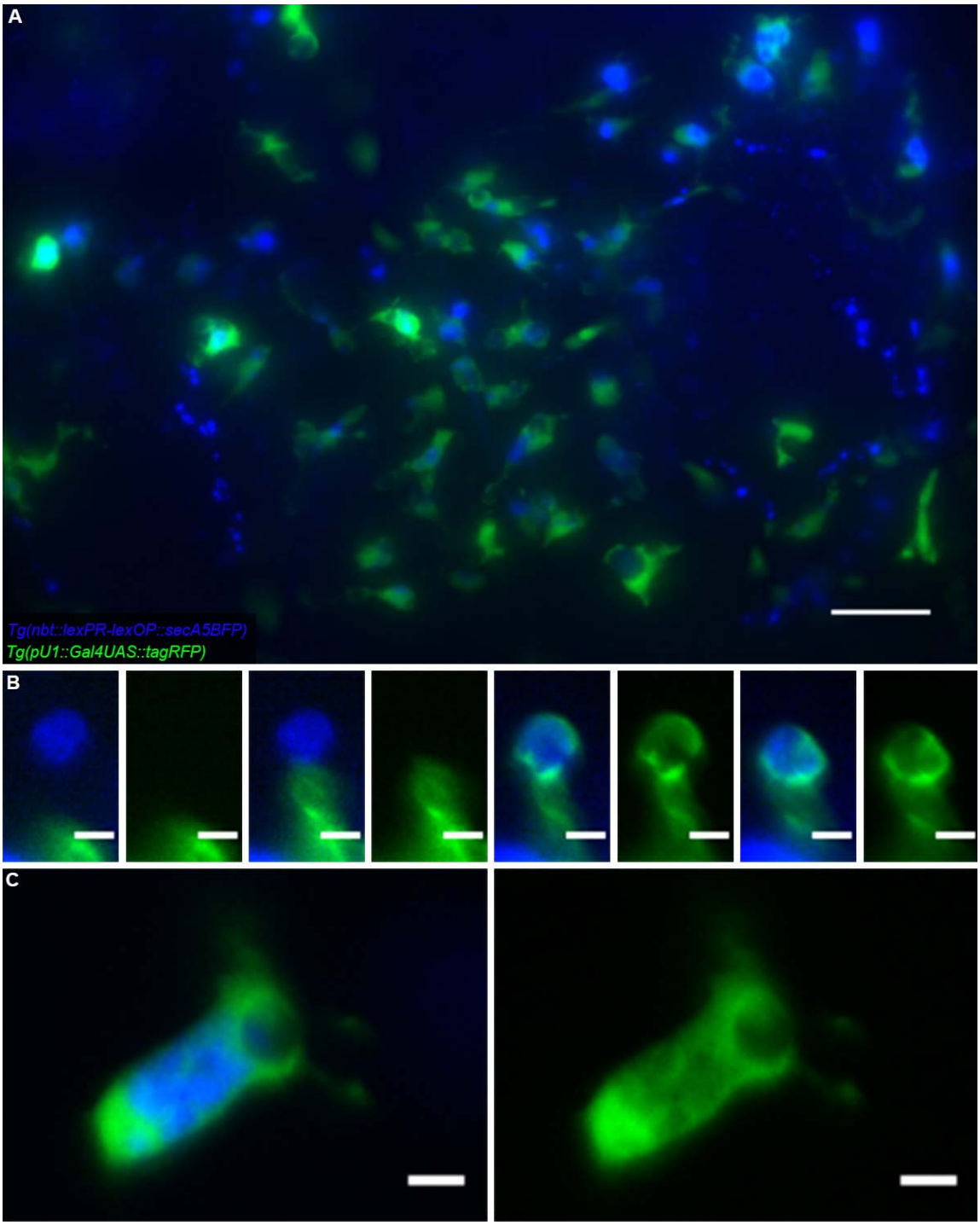

Figure 2: Observing efferocytosis in-vivo

(A) Overview of optic tectum of zebrafish larvae at 3 dpf. Microglia labeled with *Tg(pU1::Gal4UAS::tagRFP)* are coloured in green and apoptotic cells labeled with *Tg(nbt::lexPR-lexOP::secA5BFP)* are coloured in blue. Scale bar 30 µm. (B) Time series from A of forming phagosome. Scale bar 5 µm. (C) Soma of the microglia from B. Scale bar 5 µm. All images are projections of select z-planes.

3.1.2 Phagosomes both shrink and undergo homotypic fusion:

While most phagosomes had a fairly regular size (approximately 5 µm) upon formation, the phagosomes present in the soma of microglia had a much wider size distribution (figure 3 A and B). Extended tracking of individual phagosomes after they enter the soma of the cell enabled us to identify two ways in which this change in size distribution occurred. This analysis was achieved by isolating the center z-plane of each individual phagosome for each individual time point using the MtrackJ plugin for Fiji (https://imagescience.org/meijering/software/mtrackj/). Phagosome diameter was measured for every time point and a gradual reduction in size was observed over time for many of the phagosomes (figure 3 C and D). This size reduction did not coincide with any observation of smaller vesicle budding off from phagosomes, but rather appeared consistent with the hypothesis of extraction of metabolites across the phagosomal membrane.

Furthermore, extensive homotypic fusion was observed between phagosomes (figure 3 E-H). This explains why many phagosomes were found to be larger than they are upon formation. It has previously been proposed that phagosomes lack the ability to undergo homotypic fusion (Griffiths 1996), though some reports have already been made prior to ours (Harris and Cardelli 2002, Duclos et al. 2011). We do not know the mechanism by which this fusion is facilitated. Several proteins involved in membrane fusion, such as syntaxins, has been found in proteomics studies of phagosomes (Garin et al. 2001, Duclos et al. 2011), but just pairing the right fusion mediators together does not seem to be sufficient to regulate which compartments are allowed to interact with each other (Brandhorst et al. 2006). It is, however, well known that phagosomes fuse with endosomes and lysosomes and assuming there is transfer of membrane involved the resulting compartment would inherit the fusion capacity of both the phagosome and the endo/lysosome. The homotypic fusion we observe in our

study therefore would not necessarily require any special mechanism for fusion to occur, but could rely on the same mechanism already in place to facilitate the fusion events necessary for maturation.

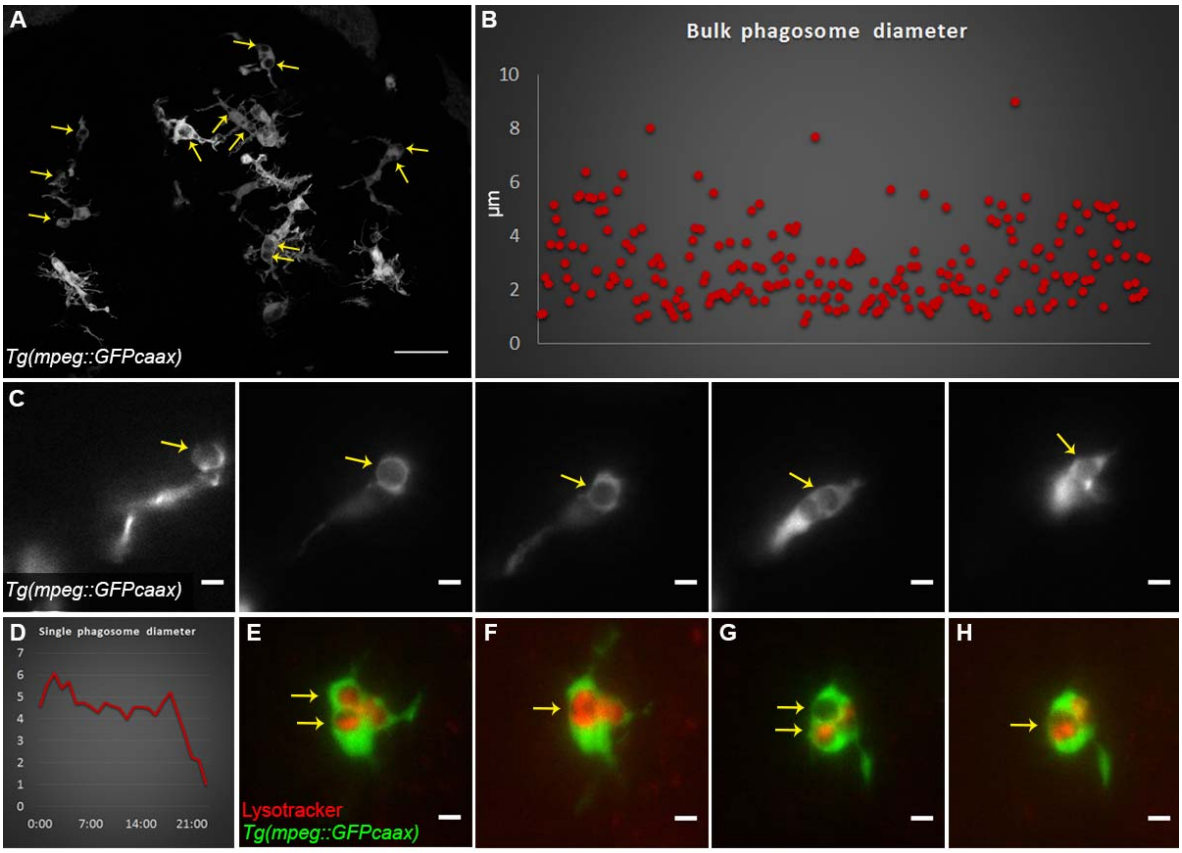

Figure 3: Phagosome shrinking and fusing

(A) Projection of data used for measuring bulk phagosome size. Arrows indicate some phagosomes. Scale bar 30 µm. (B) Diameter of phagosomes (µm). Each point represents one phagosome. N=3; n=228. (C) Select time point of a shrinking phagosome. Only the center z-plane shown. Arrow indicates the phagosome being tracked. Scale bar 5 µm. (D) Graph showing the size (µm) over time (min) of phagosome from C. (E-H) Examples of fusion events. Microglia coloured in green. Lysotracker coloured in red. (E) Arrows indicate two phagosomes about to fuse. (F) Arrow indicate the two phagosomes from E after fusion. (G) Arrows indicate two phagosomes about to fuse. (H) Arrow indicate the two phagosomes from G after fusion. Scale bar 5 µm. Microglia labeled with *Tg(mpeg::GFPcaax).*

I made no observation of microglia expelling residual material to the extracellular space through phagosome fusion with the plasma membrane. Whereas it is well documented that specialized lysosomes can fuse with the plasma membrane to perform very specific functions, the notion that this is the main method for professional phagocytes to deal with digested content is counterintuitive. While it is a perfectly sustainable way for unicellular organisms to excrete undesired waste, the apparent objective of phagocytosis in multicellular organism is very different. These cells phagocytize, not primarily to obtain nutrients, but to ensure the safety of the organism as a whole. Expelling indigestible materials would necessarily lead to an accumulation of waste products elsewhere. In fact, such accumulations are routinely observed in the context of pathology. In these circumstances the failure of cells to clear waste products are detrimental to the local tissue (Nagata 2007, Nagata, Hanayama, and Kawane 2010).

3.1.3 Phagosome shrinkage correlates with acidification:

If the observed shrinkage is the result of the extraction of metabolites it would have to occur after digestion. To investigate this, we applied a lysotracker dye to the sample prior to imaging. I observed phagosomes acidifying rapidly after engulfment often fusing with lysosomes as they were being retracted towards the soma of the cell. By plotting phagosome size against lysotracker intensity we found that there is indeed a correlation between acidification and size reduction (figure 4). This observation alone however, does not distinguish between size reduction through extraction of metabolites across the membrane or through fission events. It could conceivably be argued that the reduction in size we observed is indeed a result of fission events involving vesicles budding off from the phagosome that were too small to be resolved in our imagine data.

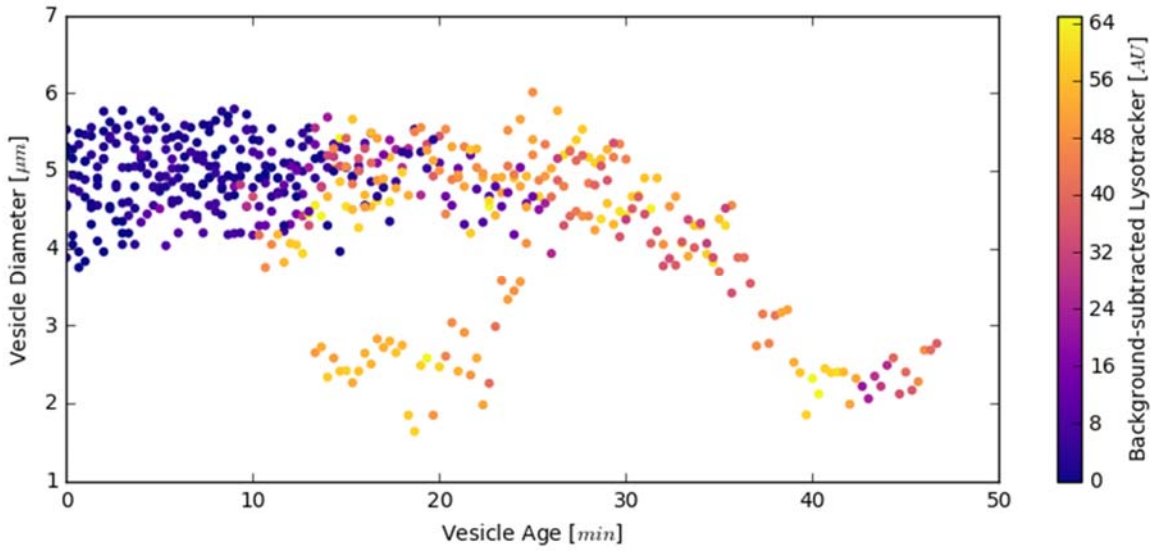

Figure 4: Phagosome shrinkage correlates with acidification

Plot showing phagosome size (µm) over time (min). The same phagosome is represented several times for different time points. Colour indicate lysotracker intensity.

3.1.4 Further exploring homotypic phagosome fusion:

To investigate the extent of homotypic fusion between phagosomes I tracked every newly formed phagosome in a cell and mapped out every fusion event. Strikingly, almost all the phagosomes I tracked underwent fusion, the only exceptions were tracks that were lost due to inconsistent image quality. This happened through a disorderly process by which some phagosomes fused with each other, while other phagosomes fused directly with compartments resulting from previous homotypic fusions. This eventually led to all tracks converging towards the same compartment.

For analysis of this data I collaborated with Jonas Hartmann who wrote a python script to make a graphical representation of phagosome fusion events. We called this a vesicle fusion tree and it enabled us to examine the data in relation to size and intensity measurements.

To ask if acidification was necessary for phagosome fusion we overlaid the lysotracker data with the vesicle fusion tree. This revealed no correlation between acidification and fusion events. As phagosomes acidify rather quickly, relative to the length of their track, most of the fusion events took place between compartments of which at least one was acidic. However, we did also observe rare examples of two lysotracker negative compartments undergoing fusion.

By also overlaying the size of phagosomes with the vesicle fusion tree we found that although not all phagosomes shrink prior to fusing with other compartments, the resulting compartment remains capable of reducing its size. This means that all phagosomes indeed undergo shrinkage, although this fact had previously been obstructed by the fusion events in my initial observations (figure 5).

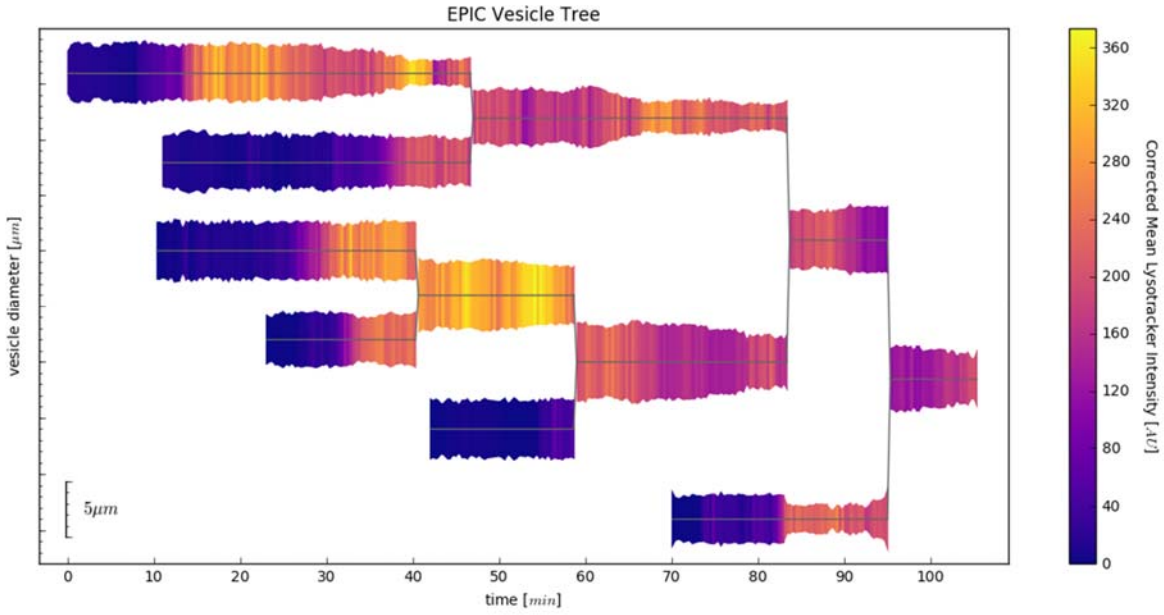

Figure 5: Vesicle fusion tree

Each line represents a phagosome tracked from its formation (left) through a series of fusion events. Thickness of the line represents vesicle diameter (µm). Colour indicates lysotracker intensity. Time in min.

3.2 Investigating homotypic fusion in cultured cells:

Phagosome maturation has largely been viewed from the perspective of individual compartments maturing along a linear path. Our observation, that fusion among phagosomes is common in professional phagocytes gives a new perspective. To test if this level of convergence among phagosomes is a general feature we designed a phagocytosis assay using cultured cells. RAW 264.7 macrophages were chosen as the phagocyte as they are easy to maintain, well characterized, and one of the most commonly used cell lines to study phagocytosis. To obtain apoptotic target cells we chose two transgenic HeLa Kyoto cell lines expressing different fluorophores. One expressing *Tg(H2B::GFP)*, the other *Tg(H2B::mCherry)*. These were co-cultured with the macrophages and turned apoptotic by adding the drug TRAIL, which selectively targets cancer cells (Wiley et al. 1995). Cultures where chemically fixed at 3, 6, and 9 hours post treatment and observed by confocal microscopy.

Among the macrophages that had engulfed both colour apoptotic HeLa cells we observed a time dependent coalescence towards one compartment. At three hours post treatment phagosomes were still spread out throughout the soma of the macrophage and each phagosome contained material fluorescent in only one colour. By six hours post treatment some phagosomes showed co-localization of both fluorophores in the same compartments, although phagosomes containing only a single fluorophore could still be observed. By nine hours post treatment phagocytically active macrophages had only a single compartment in which both fluorophores co-localized (figure 6).

The co-localization of both fluorophores was always associated with a dense structure visible in the bright field channel as well (figure 6 C). To exclude that what we observed as co-localization was auto fluorescence we therefore looked at macrophages fed with only a single

colored HeLa cells, or HeLa cells not expressing any fluorophore. In these cells the structure was only fluorescent in the expected channel, or not at all when no fluorophore was present. This was a very useful observation because it allowed us to identify the compartment at which phagosomes converged directly in cultured cells.

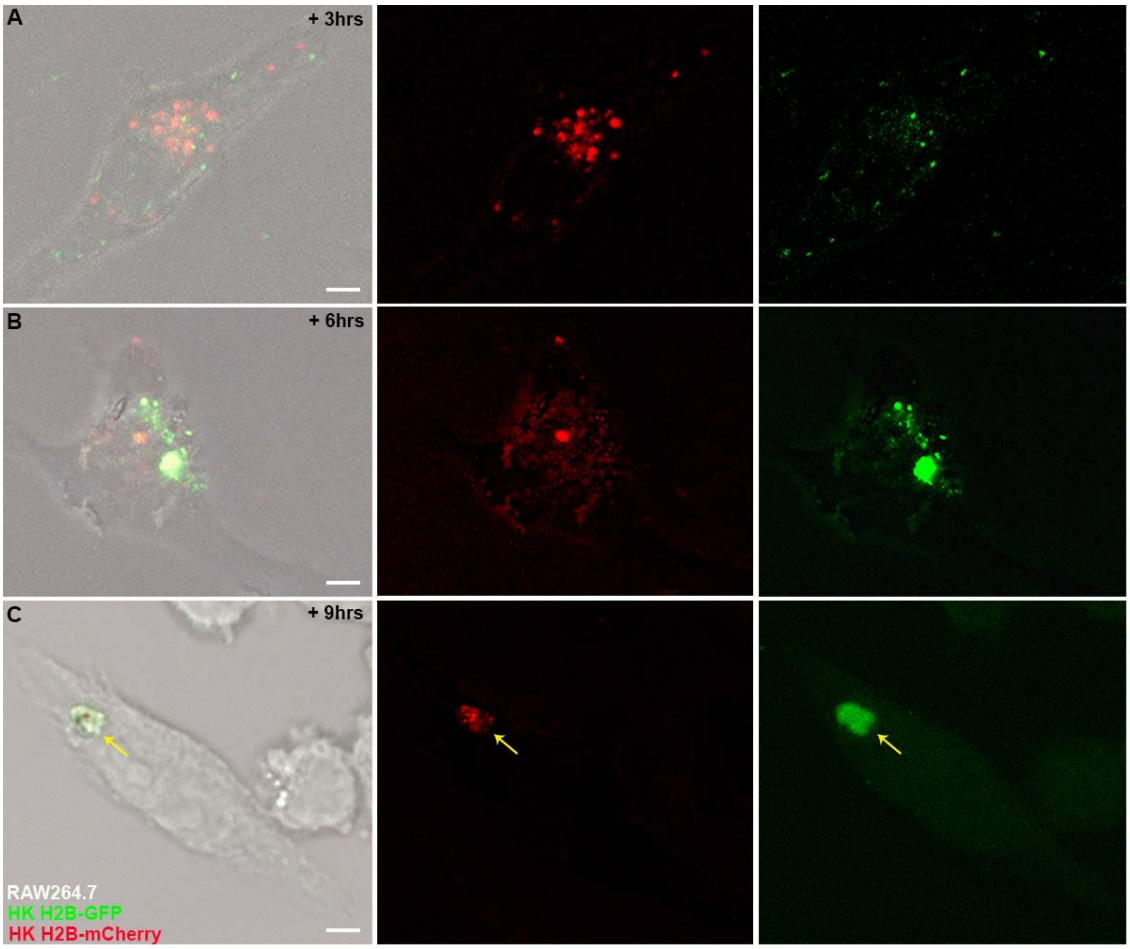

Figure 6: Homotypic fusion in RAW 264.7 macrophages

Confocal images of chemically fixed RAW 264.7 macrophages after engulfment of apoptotic HeLa Kyoto cells labeled with *Tg(H2B::GFP)* and *Tg(H2B::mCherry)*. (A) Cells fixed 3 hours after apoptosis induction. (B) Cells fixed 6 hour after apoptosis induction. (C) Cells fixed 9 hours after apoptosis induction. Arrow indicates compartment where both fluorophores co-localize. Scale bar 5 µm.

In both systems, zebrafish microglia and cultured macrophages, we see a convergence of phagosome through fusion events. The type of fission described for hypothesis 2 therefore remains an unlikely mechanism for size reduction. It should also be considered that a cell performing autophagy, or indeed phagocytosis as shown by Krajcovic et al., in order to survive starvation, is facing quite the opposite challenge from that of a professional phagocyte who is dealing with an abundance of metabolites. It is well documented that there is an extensive overlap between the phagocytic and autophagic pathways with regard to maturation and digestion (ref), where the objective of the pathway remains the same. There is however, no reason to assume they deal with the resulting metabolic end products in an identical manner. Our evidence instead supports the third hypothesis, that shrinkage is driven by transport of osmolytes from the phagosome lumen to the cytoplasm, passively forcing out water in the process.

In their thesis two former PhD students described a mutant for the solute carrier transport protein Slc37a2 (Henke 2011, Moritz 2014). This mutant called *Bubblebrain* (blb), initially *Blubberblaeschen*, was first discovered as part of a mutagenesis screen conducted at the Max Planck Institute (MPI) for Developmental Biology in Tübingen. The phenotype of this mutant is characterized by the appearance of a single big vacuole inside the microglia of the optic tectum. This vacuole was shown to form as a consequence of phagocytic activity. It was also found that increasing the osmolarity in the brain was sufficient to collapse the large vacuole. To investigate the role of Slc37a2 in phagocytosis, and potentially in phagosome shrinkage, I have studied the blb mutant in further detail in collaboration with Ambra Villani, a fellow PhD student.

3.3 Initial characterization of the *bubblebrain* mutant:

In the original screen F_2 embryos were selected for abnormal microglial morphology using neutral red staining (figure 7 B). The blb mutant displayed very unusual bubble-like microglia in the optic tectum of larvae 4 days post fertilization (figure 7 A). Transgenic reporter lines specifically labeling microglia *Tg(ApoE::LynGFP)* (Henke 2011) or macrophages *Tg(pU1::Gal4-UAS::GFP/RFP)* (Moritz 2014) confirm that the phenotype was indeed specific to microglia (figure 7 C). It was determined by Katrin Henke, through genetic mapping, that the mutation underlying the phenotype was localized to chromosome 5, and within a region encoding for the gene *Slc37a2* (figure 7 E). Sequencing of the affected locus revealed two non-complementing alleles with mutations resulting in premature stop codons. We verified this by generating a knock out for *Slc37a2* using the CRISPR-Cas9 system resulting in F_1 embryos that were a phenocopy of blb mutants (figure 7 D).

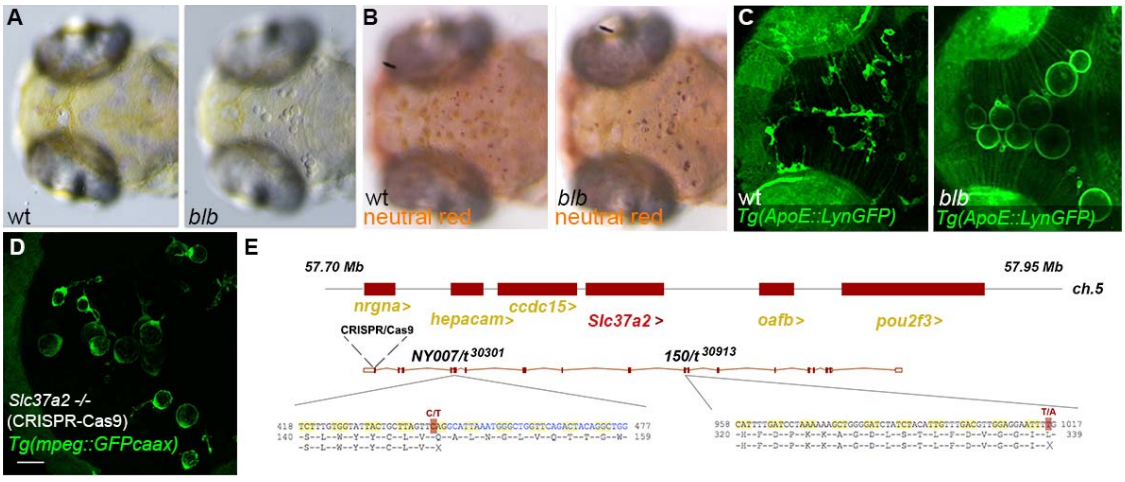

Figure 7: Characterization of the *blb* mutant I

(A) Images of wild type (left) and blb mutant (right) embryos at 4 dpf. (B) Neutral red staining of wild type (left) and *blb* mutant (right) embryos at 4 dpf. (C) Confocal image of wild type (left) and *blb* mutant (right) embryos at 4 dpf. Microglia labeled with *Tg(ApoE::LynGFP)*. (D) Confocal image of *Slc37a2* knock out generated using CRISPR-Cas9. Microglia labeled with *Tg(mpeg::GFPcaax).* Scale bar 30 µm. (E) Schematic of *slc37a2* locus. Sequences show the two mutated alleles. Target sequence for CRISPR-Cas9 indicated in exon 1.

The bubble-like morphology of the mutant microglia resulted from a single vacuole which received engulfed apoptotic neurons, demonstrated using a transgenic reporter line for neurons *Tg(nbt::LexPR-LexOP::RFP)* (Henke 2011), acridin orange staining of apoptotic cells (Moritz 2014) and a transgenic reporter for apoptotic neurons (figure 8 A). They also found that fluorescently labeled *Escherichia. coli.*, when injected into the brain of mutant larvae, were ingested by the microglia and ended up in the vacuoles (Moritz 2014). The phenotype could also be experimentally provoked in macrophages by inducing apoptosis in the trunk of mutant larvae (figure 8 B) and rescued in the opotic tectum by blocking apoptosis using the caspase inhibitor Z-VAD-fmk (figure 8 C). In his thesis Christian Moritz establishes that, in the absence of microglia, the number of apoptotic cells available to be phagocytized was the same in wild type and mutant larvae.

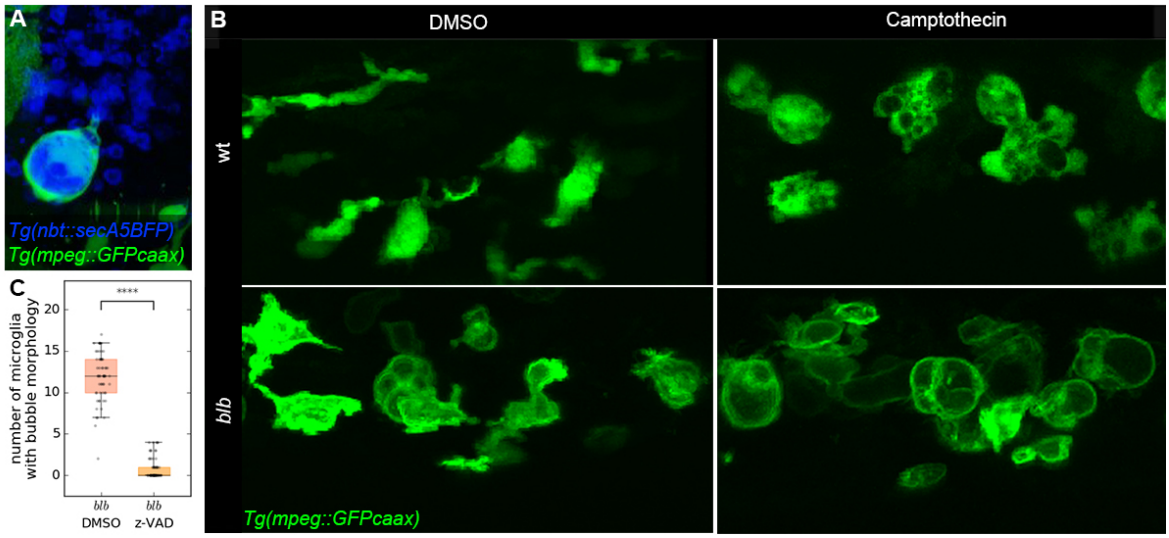

Figure 8: Characterization of the *blb* mutant II

(A) *blb* microglia labelled with *Tg(mpeg::GFPcaax)* coloured in green. Vacuole filled with material from apoptotic neurons labelled with *Tg(nbt::lexPR-lexOP::secA5BFP)* coloured in blue. (B) Trunk macrophages from wild type (top) and *blb* (bottom) embryos under control conditions (left) and with induced apoptosis (right). (C) Plot showing quantification of *blb* microglia with bubble morphology under control conditions (left) and with caspase inhibition (right). n=61, p-value <0.0001.

A morpholino against pU1 was used to deplete larvae of microglia and acridin orange staining was used to identify apoptotic cells for quantification (figure 9). This excluded the possibility that mutant cells acquire their phenotype by engulfing more apoptotic neurons than their wild type counterparts. He also showed that upon laser ablation of the microglia in mutant larvae the optic tectum was repopulated by normal looking macrophages that went on to develop the same bubble-like phenotype as the cells that had been ablated.

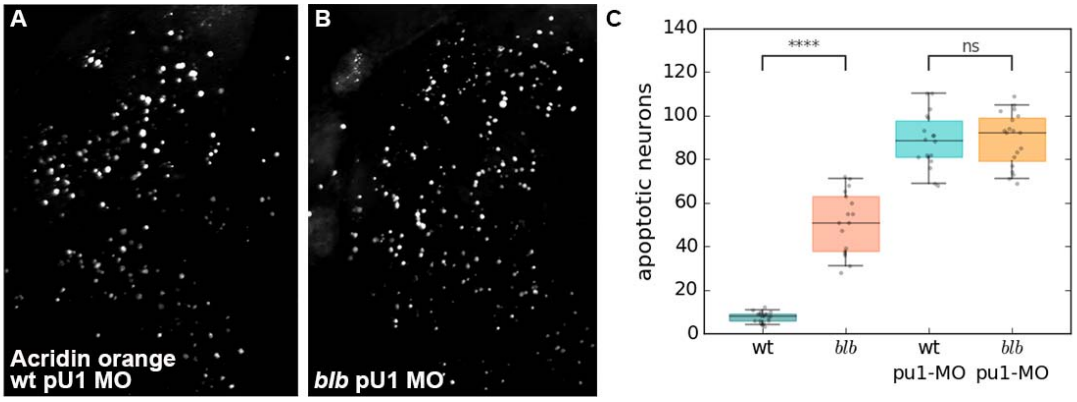

Figure 9: Characterization of the *blb* mutant III

(A-B) Acridin orange staining used for quantification of apoptotic cell. (A) Wild type embryo without microglia. (B) *blb* embryo without microglia. (C) Plot comparing number of apoptotic cells under control conditions (left) and without microglia (right) in wild type and blb embryos. For control condition wild type (n=20), blb (n=17) and without microglia wild type (n=18) and *blb* (n=19). P-value <0.0001.

Initial electron microscopy characterization of mutant microglia was carried out by Katrin Henke in collaboration with Dr. Heinz Schwarz of the electron microscopy unit at the MPI in Tubingen. In her thesis she describes that mutant microglia were easily identified by electron microscopy due to their large electron lucent vacuole, while wild type microglia were indistinguishable from surrounding tissues. Based on the above observations it was hypothesized that G6P, the predicted substrate of Slc37a2, from engulfed neurons would accumulate in the vacuole would lead to osmotic pressure forcing water into the vacuole. Finally, it was concluded that the aberrant morphology of mutant microglia constrain their movement and as a result they were less efficient in responding to injury (Moritz 2014).

Despite their thorough work describing the mutant line and the behavioral differences of the microglia, where exactly Slc37a2 acts and the identity of the vacuole was not uncovered. Beyond placing the defect somewhere in the phagocytic pathway, and the vacuole giving the appearance of being mainly filled with an aqueous solution, we did not know the nature or origin of the affected compartment.

3.4 The transporter Slc37a2 localizes directly on phagosomes:

To assess the role of Slc37a2 in phagosome shrinkage I made the same comparison of phagosome diameter in mutant microglia as I had previously done for wild type cells. Phagosomes had a comparable size upon formation in mutant and wild type larvae. However, in later phagosomes the size distribution differed significantly with larger phagosomes in the mutant, indicating they were deficient in reducing phagosome size (figure 10 A).

3.4.1 SPIM imaging of the blb mutant:

Mutant larvae were also imaged by SPIM (figure 10 D), analyzed and quantified in the same way as previously described for the wild type. By tracking individual phagosomes and measuring their diameters I did not detect any reduction in their size (figure 10 B). The small fluctuations that can be observed in figure 10 B are due to inaccuracies in the measurements caused by the phagosome not being spherical, but rather temporarily taking on a more oval shape as various forces in its environment acts on it. In these cases, the diameter was measured diagonally which gives a close approximation, but not a precise measurement of size. Phagosomes in mutant microglia also underwent homotypic fusion as seen in wild type, but more commonly they were seen to undergo fusion directly with the large vacuole that characterizes these cells. Absence of size reduction was further confirmed by plotting phagosome diameters from only the first and last time point of the tracks which shows that there is no actual change in mutant phagosome size over time (figure 10 E). For this plot the first time point was defined as the time point (t -1) in which the microglia completely surrounded the apoptotic cell and the last time point as the time point before any fusion event (t 0) (i.e. with another phagosome or the vacuole in case of the mutant). The larger shift in diameter (> 1 μm) that were found in wild type phagosomes was not observed in mutant ones.

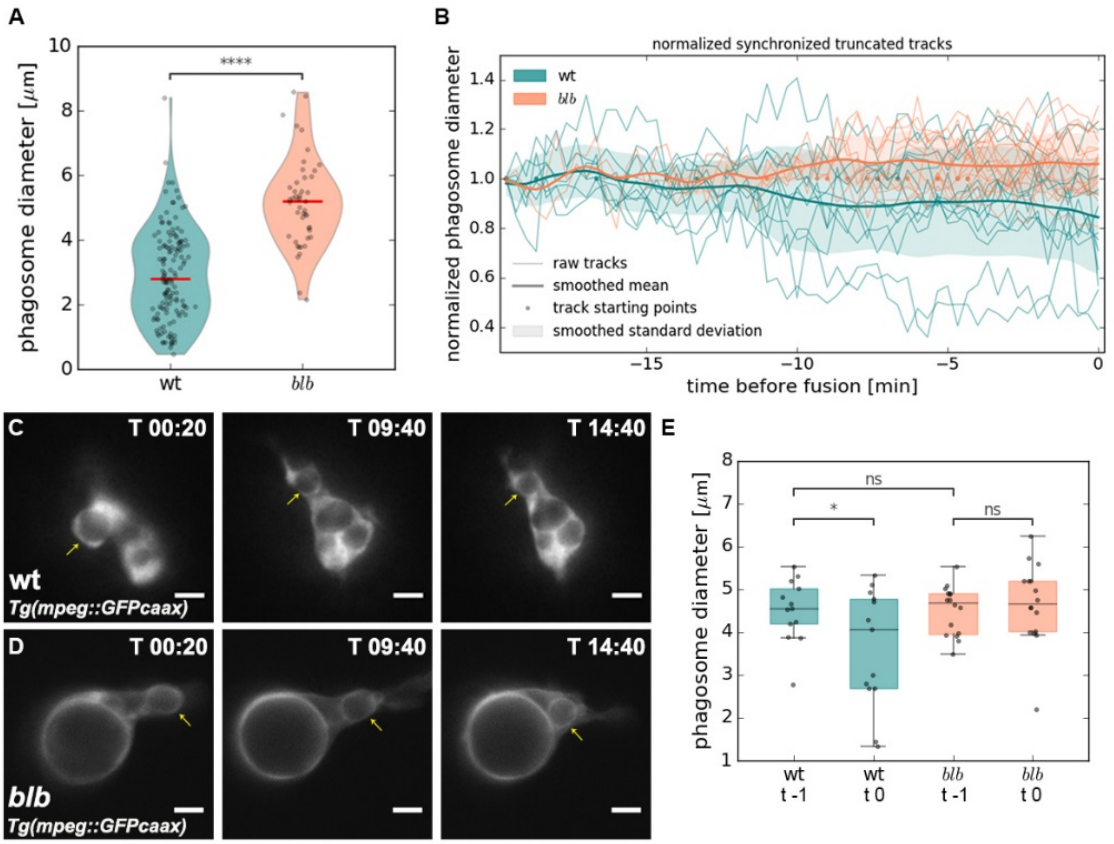

Figure 10: SPIM imaging in wild type and *blb* mutants

(A) Plot showing diameter of phagosomes (µm) from wild type (left) (N=27; n=141) and *blb* (right) (N= 27; n=47) embryos. P-value < 0.0001. (B) Quantification of phagosome diameter over time (min) in wild type (n=13) and *blb* (n=16). Data normalized against initial phagosome size. t 0 corresponds to first fusion even. (C-D) Time series of phagosome from wild type (C) and *blb* (D) microglia labeled with *Tg(mpeg::GFPcaax)* . Arrows indicate phagosome. Time in mm:ss. Scale bar 5 µm. (E) Quantification of phagosome diameter (µm) at formation (t -1) and before first fusion event (t 0). P-value <0.05.

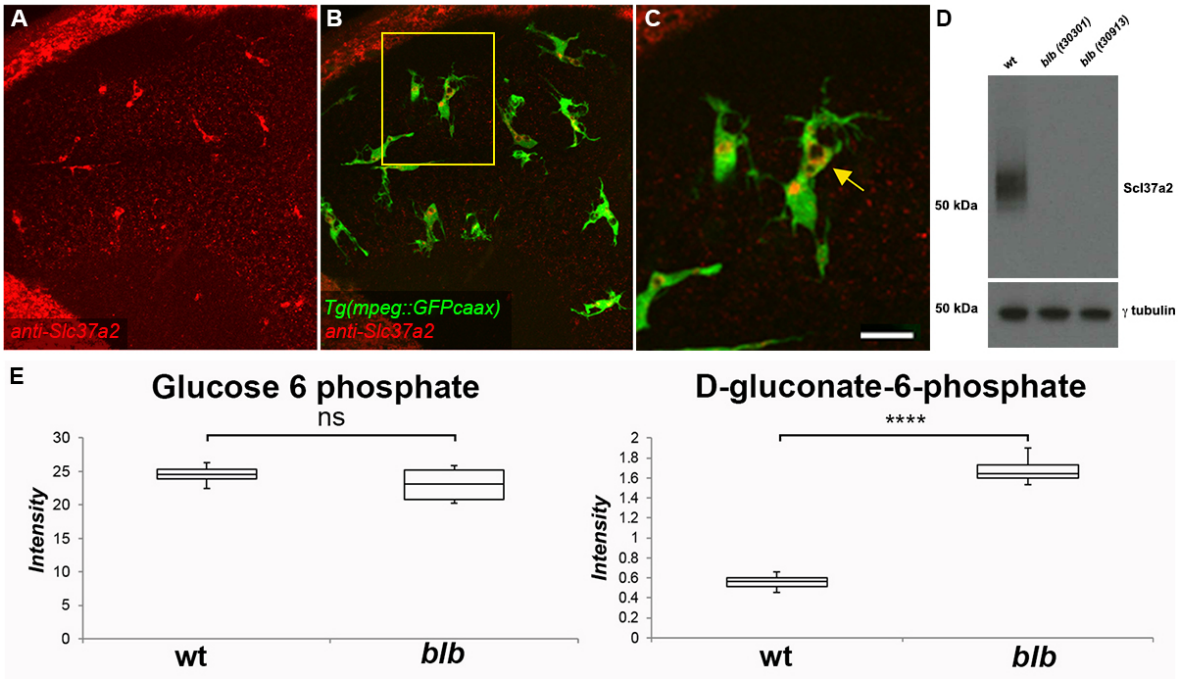

Figure 11: Slc37a2 localizes directly on phagosomes

(A-C) Confocal image of wild type embryo labelled with anti-Slc37a2 coloured in red and microglia labelled with *Tg(mpeg::GFPcaax)* coloured in green. (C) Arrow indicates phagosome positive for Slc37a2 Scale bar 15 µm. (D) Western blot analysis of Slc37a2 (55kDa) and Tubulin (48kDa) in wild type (left) and the two *blb* alleles (middle and right). (E) Mass-spectrometry data showing normalized intensities from wild type and *blb* embryos; of glucose 6-phosphate (left) and D-gluconate-6-phosphate (right), p Value < 0.0001.

3.4.2 Antibody staining against Slc37a2 shows localization to phagosomes:

The above result suggested that Slc37a2 act on phagosomes directly. To investigate protein localization, we performed antibody staining on wild type larvae using a mouse monoclonal antibody produced by the Monoclonal Antibodies Core Facility at EMBL Monterotondo (figure 11 A-C). Specificity of the antibody was confirmed by western blot. Extract from wild type zebrafish gave the expected 50 – 70 kD band whereas extract from *blb* mutants gave no band at all (figure 11 D). Antibody staining of larvae showed localization to several vesicles of various size. Some of the labeled structures were clearly phagosomes, about 5 µm in diameter, and easy to recognize based on my observations from tracking phagosomes. Other smaller vesicles could either be phagosomes that had already reduced in size or transport vesicles *en route* to phagosomes. Not all phagosomes were positive for Slc37a2 however,

indicating that it is only temporarily localized to and act on the phagosomes. This is also consistent with shrinkage seen in the data from tracking individual phagosomes.

3.4.3 Mass spectroscopy reveal high levels of d-gluconate-6-phosphate in blb mutants:

Given the absence of shrinkage in mutant phagosomes and the great number of phagosomes converging to the vacuole it seemed plausible that substantial amounts of Slc37a2's substrate would accumulate there. To investigate this further I worked with the Metabolomics Core Facility at EMBL Heidelberg to performed mass spectroscopy (MS) on extract from wild type and mutant larvae. Samples were obtained by decapitating larvae at 4 dpf, the time point reported for maximal vacuole size (Henke 2011, Moritz 2014), and lysing 50 pooled heads in 0.5 ml of methanol. Heads were homogenized by sonication and centrifuged to remove particulate matter before loading into the instrument.

Analysis of the MS results was carried out in collaboration with Dr. Andrew Palmer. This revealed a 3-fold increase in levels of D-gluconate-6-phosphate (figure 11 E). The predicted substrate of Slc37a2, G6P, was detected as well, but found to be at similar levels in wild type and mutants. Ours is the first evidence indicating that d-gluconate-6-phosphate might be a substrate for Slc37a2. The basis for previous predictions that it is a G6P transporter comes from similarities to the better characterized Slc37a4 and Slc37a2 has been shown to be capable of G6P transport over synthetic membranes, however, ours is the first in-vivo analysis conducted on the protein. It is of course possible that this one transporter has more than one substrate. These two sugar-phosphates are structurally similar and metabolically connected. Slc37a2 might be a transporter for d-gluconate-6-phosphate, either in addition to or instead of G6P. Alternatively, d-gluconate6-phosphate might be subject to further metabolic processing and the product of this process might be the actual substrate of Slc37a2. Further

biochemical studies will certainly be necessary to determine this fully, but the elevated levels of d-gluconate-6-phosphate that we detect fits well with our hypothesis and is an interesting candidate for further work.

3.5 Investigating the identity of the vacuole characteristic of the blb mutant:

In wild type microglia we had not been able to properly pinpoint the compartment acting as a point of convergence for phagosomes. Only when we tracked individual phagosomes over an extended period of time did we realize this occurred at all. In the *blb* mutant however, the vacuole appears as an obvious convergence point. To investigate if the large vacuole did constitute the same compartment we started by tracking phagosomes in mutant microglia shortly after their arrival in the optic tectum (2.5 dpf), before they acquire their characteristic phenotype. We found that the large vacuole indeed forms in a very similar fashion to the point of convergence in wild type cell. Several phagosomes, that fuse, but fail to shrink, eventually gives rise to a compartment that becomes recognizable as the mutant vacuole (figure 12 A). To further test this hypothesis we injected *blb* embryos with a morpholino against atp6v0a1, the a1 subunit of the proton pump vATPase which has been shown to block vesicular fusion (Peri and Nusslein-Volhard 2008). This resulted in microglia with many individual phagosomes, but no vacuole (figure 12 B-D).

SPIM imaging in combination with lysotracker staining revealed another peculiar property of the mutant vacuole. The vacuoles themselves were not always lysotracker positive, despite receiving material from already acidified phagosomes. Furthermore, when vacuoles that were lysotracker positive had less intensity than the phagolysosomes with which they fused. Upon fusion between a lysotracker positive phagosome and a negative vacuole material from the phagosome could be seen to enter the vacuole and retain a particulate shape for some time

during which it remained labeled with lysotracker (Figure 12 E). Neither of these observations fit the classical description of a lysosome which is the conventional end point of the phagocytic/endocytic pathway.

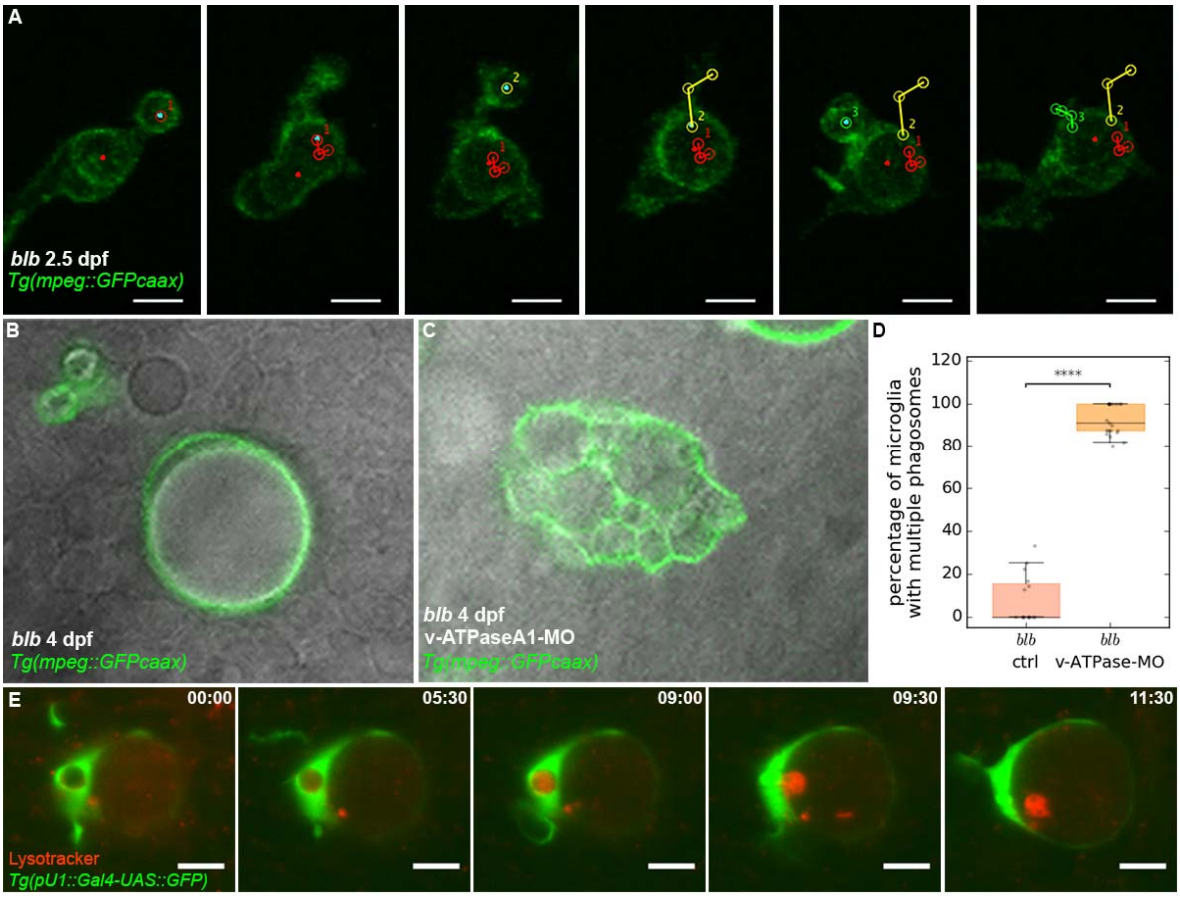

Figure 12: Description of the *blb* mutant vacuole

(A) Time series of microglia labeled with *Tg(mpeg::GFPcaax)* from a *blb* embryo 2.5 dpf. Red, yellow and green tracks indicate phagosomes fusing with a preexisting compartment (red dot). Scale bar 10 µm. (B-C) Microglia from 4 dpf *blb* embryos under control conditions (B) and with blocked vesicular fusion (C). Microglia labeled with *Tg(mpeg::GFPcaax)*. (D) Quantification of B and C. Percentage of microglia with more than 1 vesicle per cell, in control (n=15) and embryos injected with a morpholino against the a1-vATPase (n=21), p Value < 0.0001. (E) Time series of phagosome in *blb* microglia labeled with *Tg(pU1::Gal4-UAS::GFP)* coloured in green and lysotracker staining coloured in red. Time given in mm:ss. Scale bar 10 µm.

3.5.1 Development of a correlative light and electron microscopy approach, and ultrastructure analysis:

As concluded in the initial ultrastructural analysis of the blb mutant wild type microglia can be difficult to distinguish from surrounding tissue in vivo. While there are features of microglia that can be used as hallmarks, like a multi-lobed nucleus and dense cytoplasm compared to neurons, these are not necessarily reliable features that will be clear to interpret in any given cross-section of the sample and will ultimately depend on specific sample preparation protocols and subjective interpretation. For the purpose of obtaining in vivo ultrastructural data of the phagocytic process I therefore developed a workflow combining x-ray micro tomography (µCT) and correlative light and electron microscopy (CLEM), in collaboration with Dr. Matthia Karreman.

In short, CLEM is the combined use of any two or more imaging techniques in order to superimpose, or infer, information from one imaging modality to another. The term encompasses a large number of different strategies that is always adapted to the specific sample, whether it is a 2D or 3D correlation and what information is to be correlated. For this specific application we wanted to utilize the transgenic reporter lines already available to us to identify microglia by confocal microscopy, and correlate the information about their position inside the sample in order to target our acquisition by electron microscopy. The main challenge in this regard was shrinkage of the tissues due to the sample preparation necessary for electron microscopy. This shrinkage is not uniform within the sample meaning a simple scaling correction does not suffice to compensate for it. Our approach therefore relied on the use of fiducial markers detectable with both light microscopy and µCT in order to register one dataset to the other. These fiducial markers were created using near infrared branding (NIRB) in embryos that had been chemically fixed 3-4 dpf. Typically 12 to 16 brand marks were

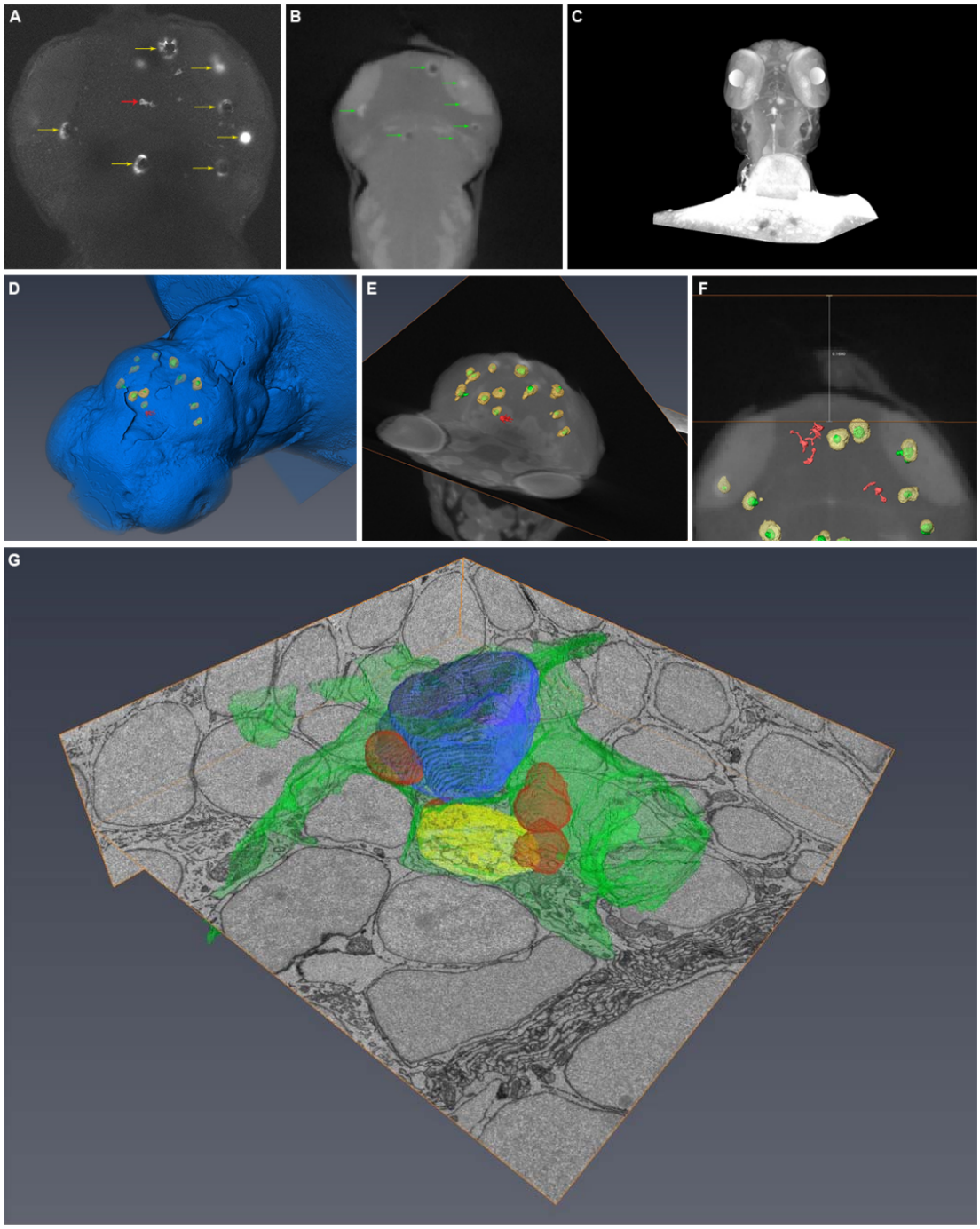

Figure 13: Correlative light and electron microscopy in zebrafish embryos

(A) Selected z-plane from 2-photon stack of chemically fixed zebrafish embryo. Yellow arrows indicate NIRB marks. Red arrow indicates microglia. (B) Corresponding z-plane from µCT data. Green arrows indicate same NIRB marks as in A. (C) Volume rendering based on µCT data. (D) Segmentation based on both imaging modalities. Sample outline in blue and NIRB marks in green based on µCT data. NIRB marks in yellow and microglia in red based on 2-photon data. (E) Same as D, with µCT data and without segmentation of the sample. (F) Top view of E, with measurement for targeted ultramicrotomy. (G) Segmentation and SBFSEM volume data of microglia. Microglia in green, nucleus in blue, phagosomes/phagolysosomes in red and compartment with lucent lumen in yellow.

created per sample, distributed randomly throughout the x, y and z dimensions with care taken that the final pattern would have a chirality. Samples were then imaged by confocal or 2-photon microscopy (figure 13 A). After sample preparation for electron microscopy blocks were trimmed with an ultramicrotome and x-ray tomograms were acquired (figure 13 B-C). Two 3D models were created based on segmentations of the different datasets. From light microscopy data both microglia and fiducial markers were segmented. From μCT data the fiducial markers and the surface of the resin block were segmented (figure 13 D-F). By transforming the confocal data to have the best possible overlap of segmented fiducial markers with the μCT segmentation I could predict the position of microglia within the block and distances to the block face could be measured (figure 13 F). The resulting 3D model was used to guide further trimming of the sample with an ultramicrotome. Samples were either serial sectioned and imaged by transmission electron microscopy (TEM) or imaged in a serial block face scanning electron microscope (SBFSEM) (figure 13 G).

In both mutant and wild type microglia I observed “fresh” phagosomes containing apoptotic cells with partially intact nucleus and mitochondria (figure 14 C). In wild type microglia I also found numerous compartments with a completely electron opaque lumen, of various different sizes and of an irregular spheroid shape (figure 14 D-E). These were mostly found in the perinuclear space and had little to no internal structure. Compartments of this characteristic were completely absent from mutant microglia where instead I found compartments with a more lucent lumen, however, much more packed with membranous debris, and smaller in size, than the large vacuole (figure 14 F). Based on the observation that wild type phagosomes undergo shrinkage, whereas mutant phagosomes do not, I propose that these opaque structures in wild type cells represent phagosomes containing material from apoptotic cells that has been extremely compacted and that these are the equivalent

structures that in the mutant appear more lucent and where membranous debris is clearly visible.

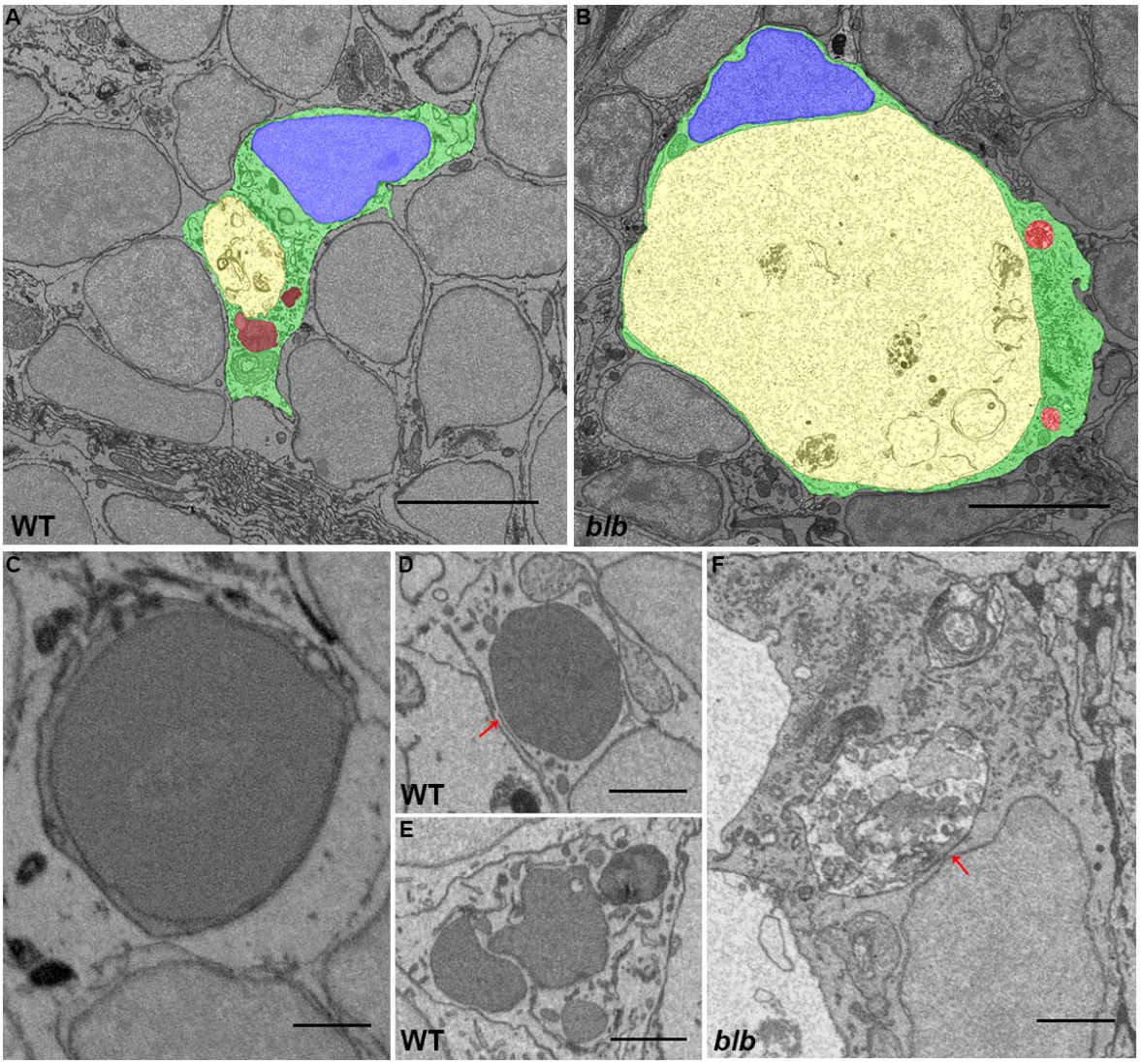

Figure 14: Ultrastructural comparison of wild type and *blb* microglia I

(A-B) Segmentation and data from a single SBFSEM z-plane of microglia. Microglia in green, nucleus in blue, phagosomes/phagolysosomes in red and compartment with lucent lumen/vacuole in yellow. (A) Wild type embryo. (B) *blb* embryo. Scale bar 5 µm. (C) Example of freshly formed phagosome with intact nucleus from a wild type microglia. Scale bar 1 µm. (D) Arrow indicates electron opaque compartment found in wild type microglia. Scale bar 1 µm. (E) Cluster of three electron opaque compartments from wild type microglia. Scale bar 1 µm. (F) Arrow indicates electron lucent compartment with membranous debris found in *blb* microglia. Another similar compartment is visible in the upper right corner, but sliced more obliquely. The vacuole is partly visible on the left. Scale bar 1 µm.

In some wild type microglia I was also able to identify a compartment with the same ultrastructural characteristic as that observed for the vacuole in blb mutants (figure 15). Although much smaller in size (~5 µm) and less spherical in shape than the mutant vacuole, it had an electron lucent lumen containing debris of lipid bilayers confined within a limiting membrane consisting of a single bilayer. They had a perinuclear localization and were regularly found directly adjacent to the opaque compartments (figure 15 A-B).

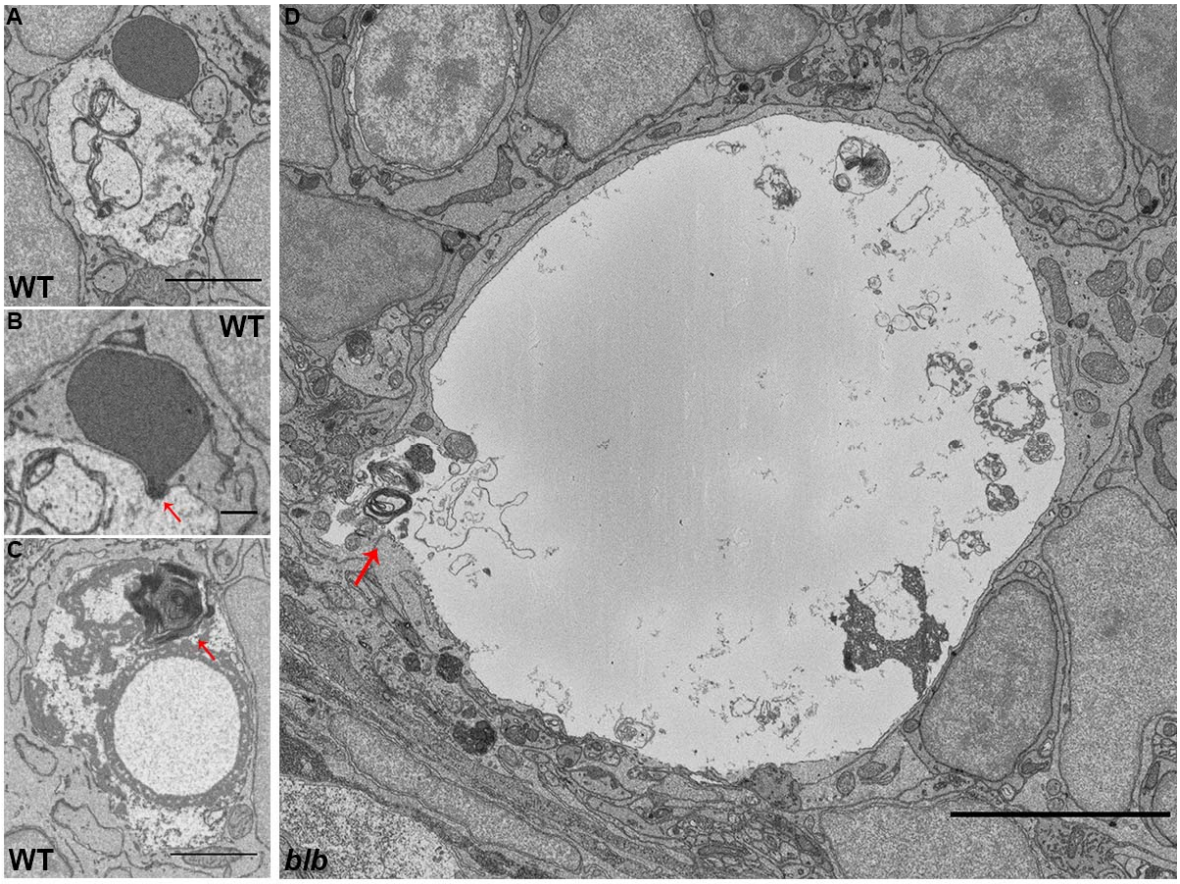

Figure 15: Ultrastructural comparison of wild type and *blb* microglia II

(A) Example of electron lucent compartment found in wild type microglia directly adjacent to an opaque compartment. Scale bar 2 µm. (B) Different z-plane of the same two compartments from A. Arrow indicates possible site of fusion. Scale bar 0.5 µm. (C) Another example of electron lucent compartment found in wild type microglia. Arrow indicates material from possibly recent fusion event. . Scale bar 2 µm. (D) Vacuole from *blb* microglia. Arrow indicates possible fusion event. Scale bar 5 µm.

3.5.2 Cell culture CLEM and antibody staining:

A simpler 2D CLEM approach was used to obtain ultrastructural data from the cultured macrophages. Cells were cultured in glass bottom dishes with a coordinate grid etched into it and the phagocytosis assay was conducted as described before. 9 hours after HeLa cells were turned apoptotic the co-culture was chemically fixed and the dishes inspected by confocal microscopy (figure 16 A). Images were acquired of cells where red and green fluorophores were found to localize to the same compartment and care was taken that the coordinate from the grid was visible in the image. Sample processing for EM was then carried out in the culture dish and after the resin was polymerized the block containing the sample was removed from the culture dish retaining a negative imprint of the coordinate grid. The grid was then used for targeted ultramicrotomy. Serial sections of the cell of interest was collected and inspected by TEM.

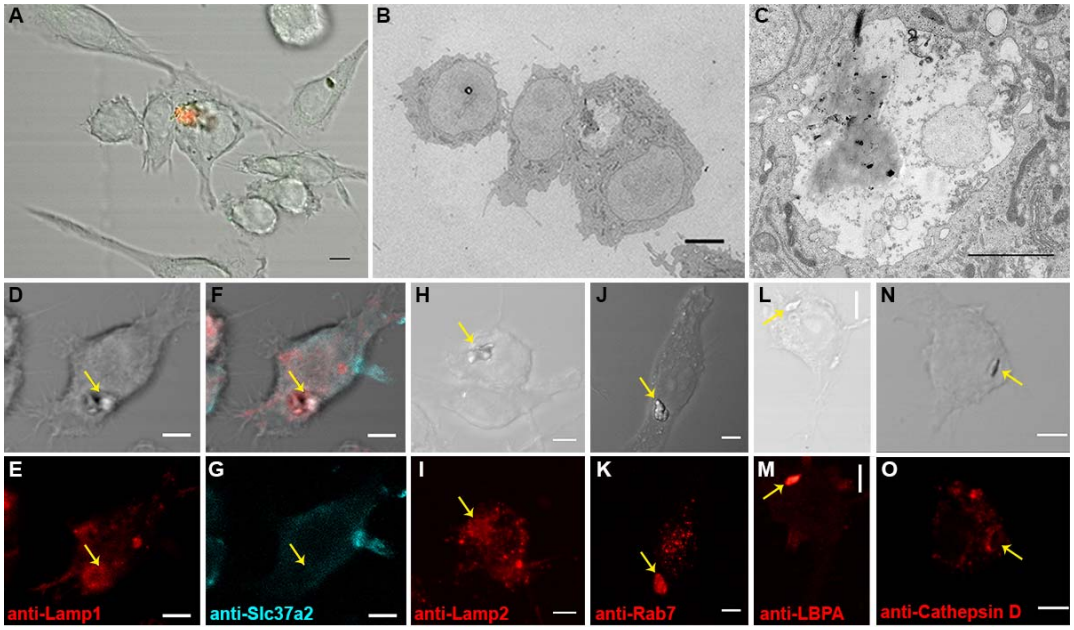

Figure 16: Ultrastructural and immunohistochemical analysis in RAW 264.7 macrophages

(A) Confocal images overlayed with bright field image of chemically fixed RAW 264.7 macrophage containing compartment of interest. Scale bar 5 µm. (B) TEM image of ultrathin section through the same cell as A. Scale bar 5 µm. (C) Higher magnification image of the same ultrathin section as in B. Scale bar 2 µm. (D-O) Antibody staining on chemically fixed RAW 264.7 macrophages. Arrows indicate compartment of interest. Scale bar 5 µm.

Also in the cultured cells I found the compartment in which the two flourophores co-localized to have ultrastructural characteristics similar to that of the mutant vacuole. It consisted of a single lipid bilayer with an electron lucent lumen and content consisting of membranous debris, intraluminal vesicles, and what appears to be an aggregate of lipids akin to lipofucin (figure 16 B-C).

To investigate the molecular identity of this compartment we conducted antibody staining against several known markers of the endocytic system. Antibody staining was carried out on cells co-cultured on cover slips, chemically fixed 9 hours after apoptosis induction and observed by confocal microscopy. LAMP1 and 2 Rab7 and LBPA were all found to localize to the compartment. Cathepsin D was not found to localize to the structure at all, and Slc37a2 was rarely found to localize to it (figure 16 D-O). Additionally we applied the lipid dyes Nile blue, BODIPY and Nile red to both RAW macrophages and blb mutants. All dyes label the compartment in RAW macrophages, as well as giving a more dispersed labeling of the vacuole in blb mutants consistent with the interpretation of the EM data that it is mostly water filled (figure 17).

This identifies the compartment as a hybrid between late endosome and lysosome (LAMP's and Rab7). The lack of Cathepsin D together with the presence of LBPA suggests a role in lipid metabolism rather than proteolysis, which is consistent with the content of the compartment observed by electron microscopy. The absence of Slc37a2 from the majority of compartments suggests the protein is actively removed after its substrate has been transported out of the phagosomal lumen.

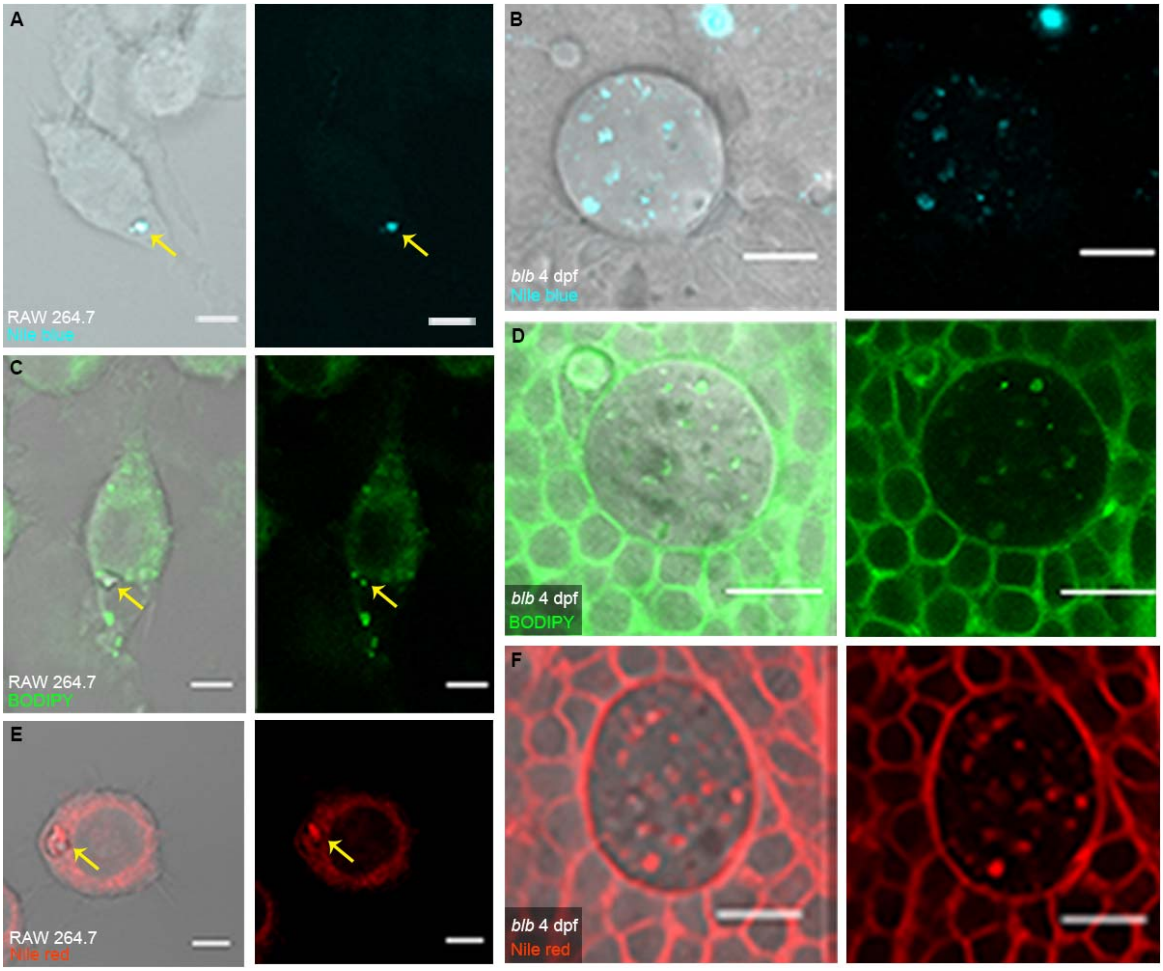

Figure 17: Lipid staining in RAW 264.7 macrophages and *blb* mutants

(A, C and E) RAW264.7 macrophages chemically fixed 9 hours after apoptosis induction in unlabeled HK cells. Stained with Nile blue (A), BODIPY (C) and Nile red (E). Arrows indicate compartment of interest. Scale bar 5 µm. (B, D and F) 4pf *blb* microglia stained with Nile blue (B), BODIPY (D) and Nile red (F). Scale bar 10 µm.

4 Discussion:

4.1 One transporter and one big bubble:

Antibody staining and quantification of phagosome size show that the protein Slc37a2 localizes to, and acts on, phagosomes. This is not necessarily in contrast to the initial finding that it localizes to the endoplasmic reticulum (ER) (Pan et al. 2011), but it is deserving of some closer examination. Pan et.al. reported co-localization, by antibody staining, of calreticulin with all four Slc37's as observed by fluorescence microscopy. The proteins were, however, overexpressed SLC's with a flag tag and antibody staining was carried out against the flag tag. There is a possibility that this artificial expression resulted in a miss localization of the protein. Furthermore, the experiment was carried out in Chinese hamster ovary cells which are not phagocytically active. As expression of Slc37a2 has been shown to be upregulated in response to phagocytosis (ref), the fact that there were no phagosomes around for the protein to localize to might also have resulted in miss localization. Additionally, interactions between the ER and phagosomes have been report (Gagnon et al. 2002), and although considered controversial by some (Touret, Paroutis, and Grinstein 2005) it is a possibility that the protein is preloaded on the ER and localizes to phagosomes on demand.

It is nonetheless striking that a mutation in a gene coding for a single transporter protein can inhibit a phagosomes ability to shrink its size so extensively. The cargo of these phagosomes, the apoptotic cell, is known to be made up of a huge variety of different substrates, yet we do not observe any size reduction from the presumed transport of these substrates out of phagosomes either.

One possible explanation for this is that the size reduction we observe is mainly due to the movement of water out of the phagosome. Water makes up the majority of the volume of all

cells and moves freely across the phagosomal membrane through aquaporins to create an equilibrium in the osmotic pressure on both sides of the membrane. As osmotic pressure depends on the molar concentration of solutes, as opposed to their total mass, catabolic activity will in general increase the amount of water needed in the compartment as long as no substrate is removed. Even if all the solutes that can be transported by other proteins were removed, if some catabolic process produces substrates uniquely transported out of phagosomes by Slc37a2 the amount of water required inside the phagosome might still be as high, or exceed, that of the same phagosome before any catabolic activity took place.

With this in mind it becomes of particular interest that the metabolite we did find a significant increase of in the *blb* mutant, D-gluconate-6-phosphate, belongs to the pentose phosphate pathway. Apoptotic cells contain large amounts of DNA and RNA which is known to be degraded into individual nucleotides and nucleosides. Hematopoietic cells do not express the enzymes necessary to produce nucleosides for themselves and it has therefore been hypothesized that, for these key metabolites, they rely entirely on external sources, including from phagocytized cells (Levin, Grinstein, and Canton 2016). It appears unlikely, however, that they would require several cells worth in the short period of time it takes microglia to clear the optic tectum of neurons. One interesting possibility then is that a portion of the nucleosides are further catalyzed producing sugar-phosphates and that these are what accumulate in mutant vacuoles.

4.2 On the identity of the vacuole:

To determine the identity of subcellular compartments we rely primarily on two criteria. Molecular markers that localizes specifically to the compartment of interest and the ultrastructural, morphological features of the compartments such as the number of lipid

bilayers that make up its limiting membrane and internal structures such as the cristae of mitochondria.

Many organelles can be easily identified by their ultrastructural morphology alone unless it is severely perturbed. The nucleus, mitochondria, Golgi apparatus and ER are good examples of these. Among the endocytic organelles however, things are considerably more complicated due to the natural flux state of the system. Whereas mitochondria can undergo both fission and homotypic fusion, this does not fundamentally alter their morphology or biochemical signature. Both the Golgi and the ER have various vesicles bud off from it, and fuse with it, but these are small in size relative to the organelles themselves and they retain their characteristic feature. It is therefore still identifiable as the same organelle afterwards.

The continuous flux of material through some compartments constitutes a conceptual problem that had experts in a deadlock for decades (Griffiths 1996). Two different hypothesis were competing to explain the nature of this transport between different organelles. The first, referred to as vesicular transport, or the Palade paradigm, held that the membranous compartments are fundamentally unchangeable. It defines a process whereby a part of the membrane of one preexisting compartment forms a vesicle which is targeted to, and fuses with, a second preexisting compartment (Palade 1975, Palade 1983).

For example, a new vesicle buds off from the preexisting plasma membrane, carrying with it engulfed material from an apoptotic cell. The vesicle would then proceed to fuse with an already preexisting early endosome. The early endosome would then go on to bud off a vesicle containing the engulfed material and this vesicle would fuse with an already preexisting late endosome and so forth. In this interpretation of events the early and late

endosomes would constitute unique organelles whereas the vesicles trafficking material between them were not.

The second hypothesis, referred to simply as maturation (Murphy 1991), held that after fission from the original membrane the composition of the limiting membrane gradually changes with new proteins being acquired onto the compartment from the cytoplasm. There is therefore no clear cut point at which this compartment seizes to belong to the early endosome organelles and starts belonging to the late endosome organelles.

Today the term maturation is unanimously used to describe the endocytic/phagocytic process. However, it is acknowledged that endosomes and phagosomes undergo a series of fusion events with late endosomes and lysosomes and that these fusion events constitutes part of the maturation process (Levin, Grinstein, and Canton 2016). While this hybrid hypothesis fits the data better than either of the two previously proposed models it makes it does not enable us to define lysosomes and endosomes as different organelles by the same criteria with which we define them as different from the Golgi or ER. These compartments all have different sets of markers and functions associated with them, but morphologically they are all, spherical or tubular, single lipid bilayer, structures (ref). Sometimes their luminal content can help distinguish them, ILV's are a clear hallmark of MVB's, but not all late endosomes will have visible ILV's. A very electron dense lumen is often considered to be suggestive of lysosomes, but not exclusively enough to constitute proof and not all structures with biomarkers for lysosomes have this feature (Huotari and Helenius 2011). Furthermore, the content of a digestive compartment will depend heavily on what is being digested making comparisons difficult. Similarly, the extensive literature on biomarkers associated with the endocytic system sometimes struggle to make a clear cut distinctions regarding the identity

of compartments as a certain degree of overlap in biomarkers is known to occur (Vieira, Botelho, and Grinstein 2002, Lu and Zhou 2012).

The identity of the mutant vacuole can then only be described as a hybrid between a late endosome and a lysosome. In order to distinguish it from “pure” endosomes and lysosomes we named this compartment the gastrosome. Based on the presence of various membranous debris together with the lipid LBPA, as well as the absence of a key proteolytic enzyme, Cathepsin D, we conclude that it is most likely involved in lipid metabolism and it could be a key actor in the, as of yet, elusive mechanism behind phagosome resolution. Although Slc37a2 was found to act mostly on phagosomes upstream of the gastrosome it also appears to play a role in the resolution process as evident by the arrest of this process in mutant cells. Furthermore the extent of homotypic fusion of phagosomes that I here describe as giving rise to the formation of the gastrosome might also play an important role.

4.3 The problem of resolution:

To explore these ideas further I will here attempt to resolve a phagosome. It appears obvious that the structure we refer to as the phagosome must at one point cease to exist, otherwise cells would accumulate unresolved compartments. The premise then appears to be to explain how a compartment can mature into non-existence.

If one considers a single phagosome, it starts out with a limiting membrane more or less just sufficient to contain its own volume. It must therefore reduce its volume before it will be able reduce its surface area. As demonstrated by us here, as well as by Freeman et.al. 2018 this reduction in volume can be facilitated by transport of soluble content across the phagosomal membrane. If the content of the phagosome is fully liquid this transport can start immediately after the relevant transporters can localize to the phagosomes limiting membrane, as was the

case with Freeman et.al. 2018. However, if the content of the phagosome is in a semisolid state, like that of an apoptotic cell, catalytic processes must proceed transport across the membrane. As osmolytes are extracted from the phagosome the hydrostatic pressure will also reduce as water is forced out. The resulting volume reduction allows the surface area, made up of the lipid bilayer, to reduce as well. While some of this membrane might be recycled through the budding off of recycling endosomes or lysosomes not all of it appears to be recyclable. Some of it is internalized into ILV's and destined for further digestion. The total reduction in surface area is therefore limited to the minimum area required to contain this new volume of internalized membrane and protein. The resulting compartment can now undergo a new cycle of catalysis, volume reduction and surface area reduction, but no number of iterations of this process can result in the compartment no longer existing.

Now consider a number of phagosomes, all maturing in parallel. If they continue their individual maturation the number of unresolved phagosomes will equal the number of phagosomes formed. On the other hand, if these phagosomes are allowed to fuse freely with each other the number of resulting compartments will approach one over time. In this scenario individual phagosomes essentially no longer need to resolve in order to effectively cease to exist. Instead such a hypothesis would predict the existence of at least one compartment that persists, but is not required to maintain any one specific identity as it transitions between catalysis, volume reduction and over time.

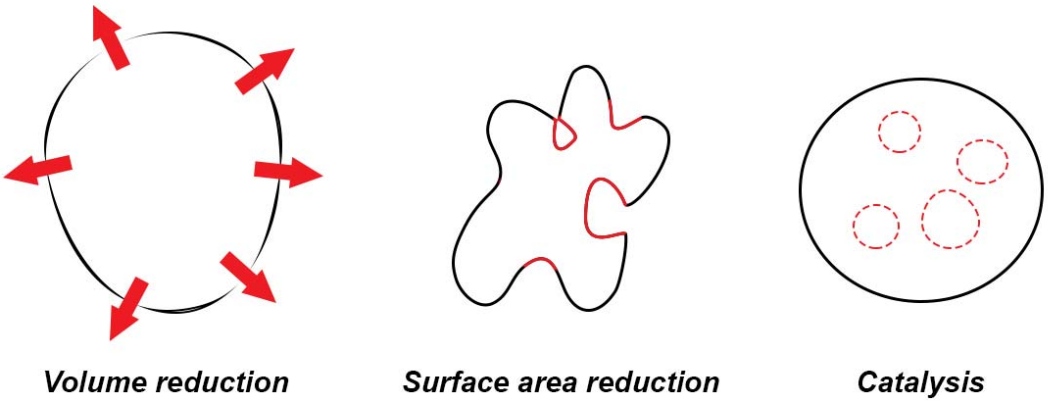

Figure 18: Sketches showing different states of a phagosome

5 Materials and Methods:

5.1 Zebrafish techniques:

5.1.1 Zebrafish husbandry:

Adult zebrafish were maintained and breeding for propagation of various lines was conducted according to "Zebrafish – A practical approach" (Nusslain-Volhard and Dahm, 2002). The aquarium systems used were from Aquaschwarz Aaquariumbaum (Göttingen, Germany) and Müller & Pfleger (Rockhausen, Germany). System water was maintained at 26.5 °C with a pH of 7 and conductivity of 200 – 350 µS. A 14/10 hour day/night cycle was maintained and animals were fed with a combination of artemia (*Artemia nauplii*) (Zeigler, USA) and dry flakes (Omega Sea Ltd, USA).

Mating of adult zebrafish was set up in the evening in 1 liter boxes with one male and one female. The boxes contained a metal lattice separating the animals from the bottom of the box. Eggs were collected the following morning by removing the adult animals and the lattice and pouring the water through a strainer.

Eggs were kept at 28.5 °C in E3 medium in a petri dish until bleached. To avoid contamination by pathogens/parasites eggs were bleached 10 - 28 hpf in 10-15% NaOCl. Two rounds of bleaching for 5 min was conducted with intermittent rinsing in water and eggs were transferred to a clean petri dish.

After bleaching embryos were kept in E3 medium containing 3mg/ml N-phenythiourea (PTU) to avoid pigmentation.

Before experiments were conducted embryos were dechorionated either manually using two sets of forceps or enzymatically using pronase.

Anesthetizing of zebrafish embryos was done using 40 µg/ml Tricaine (3-amino Benzoic acidethylseter) in E3 medium.

Medium	Composition	Concentration
E3 60x	NaCl	3 mM
	KCl	0.17 mM
	$CaCl_2 * 2H_2O$	0.33 mM
	$MgSO_4 * 6H_2O$	0.33 mM
PBS 1x pH 7.4	NaCl	137 mM
	KCl	2.7 mM
	$Na_2 * HPO_4$	10 mM
	KH_2PO_4	2 mM

Reagents	Stock solution	Supplier
Sodium hypochlorite (bleach)	10 – 15 % NaOCL	Sigma (425044)
Pronase	30 mg/ml	Roche (11459643001)
PTU	100x: 750 g in 250 ml PBS	Sigma (P7629)
Tricane	100x: 2 g in 489.5 ml H_2O pH adj. pH with Tris 1 M	Sigma (A5040)

5.1.2 Transgenic lines:

Zebrafish here referred to as wild type were either from the WIK, Golden, Tübingen or TLF lines.

The following transgenic reporter lines were used in experiments for this thesis:

a) *Tg(mpeg::GFPcaax)*: mpeg is a macrophage specific promoter used to drive the expression of the fluorophore GFP fused with the membrane anchor caax (Ellet 2011).
b) *Tg(nbt::lexPR-lexOP::secA5BFP)*: nbt is a neuron specific beta tubulin promoter used to drive a constitutively active expression of a Annexin5-BFP fusion protein. Annexin5 is excreted by the neurons and localize to apoptotic cells (Mazarati and Breus 2014).
c) *Tg(nbt::lexPR-lexOP::DsRed)*: nbt is a neuron specific beta tubulin promoter used to drive a constitutively active expression of the fluorophore DsRed. This line had been selected for mosaic expression of the transgene to label some, but not all neurons (Peri and Nusslein-Volhard 2008)..
d) *Tg(pU1::Gal4UAS::GFP)*: PU.1, also known as SPI 1, is a transcription factor involved in myeloid and lymphoid cell differentiation. In zebrafish expression is restricted to 12 to 30 hpf. Gal4UAS is therefore used to enhance and prolong expression of GFP. In brain tissue only microglia have any expression (Peri and Nusslein-Volhard 2008).
e) *Tg(pU1::Gal4UAS::tagRFP)*: same as d) with a different fluorophore (Sieger 2012).
f) *Tg(apoE::lyn-eGFP)*: In zebrafish apolipoproteinE is uniquely expressed in microglia in the time period 3 to 6 dpf. In this line the apoE promotor is used to drive expression of eGFP fused with the membrane anchor lyn (Peri and Nusslein Volhard 2008).

5.1.3 Mounting zebrafish embryos for confocal microscopy:

Embryos were anesthetized with tricane and mounted in MatTek glassbottom dishes (MatTek Corporation, P35G-1.5-10-C) using 1.3% (w/v) low melting point agarose (Peqlab 352010) for support. After the agarose had solidified the dish was filled up with E3 containing PTU and tricane.

5.1.4 Microinjections of glucose in zebrafish embryos:

Embryos were mounted similarly to that for confocal microscopy, but using 1.5% (w/v) low meting point agarose. Injections were performed directly into the brain of anesthetized zebrafish larvae using the injections setup build on the Andor Spinning Disk confocal microscope.

5.2 Cell culture:

5.2.1 RAW 264.7 macrophages:

Cells were bought from ATCC (TIB-71) and grown in Dulbecco's Modified Eagle's Medium with High Glucose and L-Glutamine from ATCC (30-2002) with 10% (v/v) Heat Inactivated Fetal Bovine Serum from Gibco (10500-064) added to it. Cells were incubated in a cell culture incubator at 37 °C and with 5% CO_2 atmosphere and handled in a sterile cell culture hood. Cells were grown for 2-3 day or until 70 - 80% confluence before splitting. For splitting, cells were rinsed with sterile filtered 1xPBS and trypsinized with 0.05% trypsin-EDTA from Gibco (25300-054) was used to detach them from the flask. After 10 - 15 min incubation 20 ml growth medium was added and the cells were transferred to a 50 ml Falcon tube. They were then centrifuged for 5 min at 1000 rpm, resuspended in 6 ml of growth medium and ceded in a fresh culture flask at the desired concentration.

5.2.2 HeLa Kyoto:

HeLa Koyoto *Tg(H2B:EGFP)* were gifted by Lars Velten and Lars Steinmetz, EMBL. HeLa Kyoto *Tg(H2B:mCerry)* were gifted from Mitocheck consortium, EMBL. Cells were grown in a DMEM-1g/L D-Glucose, Pyruvate from Gibco (11880-028) with 10% (v/v) Heat Inactivated Fetal Bovine Serum from Gibco (10500-064), 1% Penecilin/Streptomycin from Gibco (15140-122) and 1% GlutMAX-I 100x from Gibco (35050-061) added to it. Cells were incubated in a cell culture incubator at 37 °C and with 5% CO_2 atmosphere and handled in a sterile cell culture hood. Cells were grown for 2-3 day or until 70 - 80% confluence before splitting. For splitting, cells were rinsed with sterile filtered 1xPBS and trypsinized with 0.05% trypsin-EDTA from Gibco (25300-054) was used to detach them from the flask. After 2 - 5 min incubation 20 ml growth medium was added and the cells were transferred to a 50 ml Falcon tube. They were then centrifuged for 5 min at 500 rpm, resuspended in 6 ml of growth medium and ceded in a fresh culture flask at desired concentration

5.2.3 Phagocytosis assay:

RAW 264.7 macrophages and HeLa Kyoto cells were ceded in a 1:1 ratio and co-cultured until 30 - 50% confluent in RAW 264.7 growth medium. For experiments conducted for light microscopy inspection cells were ceded on cover slips (22 mm) placed in a 6-well cell culture plates (Sigma, SIAL0516-50EA). For experiments conducted for correlative light and electron microscopy cells were ceded on MatTek Glass bottom dishes with a Finders Grid (MatTek, P35G-1.5-14-CGRD) HeLa-specific apoptosis was induced by adding Recombinant Human TRAIL/TNFS10 from R&D Systems (375-TEC-010) to a final concentration of 80ng/ml to the growth medium. After 1 hour incubation the medium containing the drug was removed and replaced with fresh growth medium. Incubation continued for 3, 6 or 9 hours after the drug was initially added. Samples for light microscopy inspection were washed with sterile filtered

1x PBS and chemically fixed using 4% paraformaldehyde from Sigma (441244) in PBS. Samples for CLEM were chemically fixed by adding 2x fixative (4% PFA + 0.1% GA in 0.1M PHEM) to the growth medium in a 1:1 ratio with the growth medium. After 5 minutes on the bench this was replaced with 1x fixative.

5.3 Molecular biology techniques:

5.3.1 CRISPR/Cas9 genome editing:

CRISPR gene editing was performed entirely by my colleague Ambra Villani and here I will report the method she used.

5.3.1.1 Target design:

The CRISPR-Cas9 technology is based on a bacterial system of programmable DNA endonucleases. Using sgRNA that is complementary to a specific target sequence the Cas9 endonuclease is able to induce cleavage of double stranded DNA, 4 base pairs upstream of the PAM sequence (NGG). It then relies on the cells own repair mechanisms to join the break in the DNA strand. This can happen either through non-homologous end joining which is error-prone and therefore can reliably produce random mutations at the target site, or a template can be provided together with the Cas9 which allows for insertion of a specific sequence through homology direct repair. In our experiment we relied on the latter to insert a STOP-codon cassette, a 20 base pair sequence which will result in a stop codon regardless of the reading frame of the insertion, into the first exon of *Slc37a2*. sgRNA was designed using CHOPCHOP (http://chopchop.cbu.uib.no) based on a transcript ID from the ENSEMBL database (ENSDART00000038602.6). Only coding regions were considered as targets and the sgRNA was designed to be 20 nucleotides long + the full PAM sequence (NGG) at the 3'. The sgRNA target was selected based on its position 81 base pairs from ATG, its GC percentage between 60 - 70 % and the target score which takes into consideration self-complementary,

efficiency and absence of predicted off-targets. The cassette was ordered as an oligo purified by HPLC from Sigma. It was designed by flanking the STOP-codon cassette with 30 nucleotides specific to the target region on the gene.

5.3.1.2 sgRNA synthesis:

A DNA template was made for sgRNA synthesis using PCR and four primers. These primers were all ordered as oligos, purified by HPLC from Sigma. One primer, a 81 base pair oligo was used as a template. It contains the T7 promoter sequence followed by target sequence (in red) and a 40 nucleotide tail.

Primer name	**Length**	**Sequence (5'-3')**
Template	81 nt	GCGTAATACGACTCACTATAGTGATAGGCTTTCGAGAGAGAGTTTTAGAGCT AGAAATAGCAAGTTAAAATAAGGCTAGTC
66F	20 nt	GCGTAATACGACTCACTATA
66R	20 nt	GCACCGAGTCGGTGCGGATC
67R	81 nt	GATCCGCACCGACTCGGTGCCACTTTTTCAAGTTGATAACGGACTAGCCTTATTTT AACTTGCTATTTCTAGCTCTAAAAC

Successful amplification was verified by electrophoresis. 3 µl PCR product was run on a 1.5 % agarose gel in 1x TAE. Bands were visualized using SYBR safe and a DNA ladder was used to reference molecular weight. The PCR product was purified by column using the QIAauick PCR Purificatioin Kit according to the manufacturer's specification. Concentration was measured by Nanodrop (NanoDrop 8000 pectrophotometer, Thermo Fisher Scientific).

sgRNA was then synthesized *in-vitro* using the MEGAshortscript T7 kit in accordance with the manufacturer's specification. It was further purified by column using the miRNeasy kit from step 6 in the manufacturer's protocol onwards and sgRNA was eluted with 60 µl RNAse free water.

PCR mix:

Reagent	Volume in µl	Supplier
Buffer 10x	5	Genaxxon Bioscience (M3454)
X7 Pfu polymerase	0.5	Protein Expression and Purification Facility, EMBL, Heidelberg, Germany
10 mM dNTPs	1	Thermo Fisher Scientific (R0192)
100 µM template	0.4	Sigma
100 µM 67R	0.4	Sigma
100 µM 66F	2.5	Sigma
100 µM 66R	2.5	Sigma
H_2O	37.7	

PCR conditions:

Temperature	Time	Cycles
94 °C	3 min	1 x
94 °C	15 sec	40 x
50 °C	15 sec	
72 °C	15 sec	
72 °C	5 min	1 x
4 °C	Hold	1 x
Storage at 4 °C		

PCR was performed on an Eppendorf Mastercycler (Sigma).

Reagents used:

Reagent/material	Stock solution	Supplier
TAE	50x stock solution: 121g TRIZMA base + 50 ml EDTA 0.5M (pH 8.0) + 28.55 ml glacial acetic acid. Bring to 500 ml with Millipore H2O and autoclave before use.	EMBL laboratory kitchen
Agarose	-	Sigma (A9539)
SYBR Safe DNA gel stain	10000x	Thermo Fisher Scientific (S33102)
GeneRuler 100 bp DNA ladder	-	Thermo Fisher Scientific (SM0241)
6x DNA loading Dye	6x	Thermo Fisher Scientific (R0611)
QIAquick PCR Purification Kit	-	Qiagen (28104)
MEGAshortscript T7	-	Thermo Fisher Scientific (AM1354)
miRNeasy Mini Kit	-	Qiagen (217004)

5.3.2 Microinjections of zebrafish embryos:

Injection plates were prepared according to Nusslein-Volhard and Dahm 2002 using 2% (w/v) agarose in E3 medium containing methylene blue. A polyethylene mold was used to create groves to help position the eggs for injection. Microinjection needles were made from borosilicate capillaries (Harvard Apparatus No. 30-0035) pulled on a Stutter P9 Micropipette Puller (Stutter) using the following settings: heat 630, pull 80, velicity 75, time 90. Freshly collected eggs were placed on the injection plate and a Pneumatic PicoPump microinjector (WPI, SYS-PV820) was used for injections under a Zeiss STEMI 2000 stereo microscope.

5.3.2.1 Morpholino injections:

Morpholinos (Gene Tools, LLC. Oregan, USA) were diluted in dH_2O with 0.1M KCl and 0.2% Phenol red (Sigma) and injected into the yolk of embryos at the 1-cell stage.

Gene targeted	Sequence (5'-3')	Concentration	Reference
pU.1	GATATACTGATACTCCATTGGTGGT	0.5 mM	Rhodes et al., 2005
Caspase 3	TTGCGTCCACACAGTCTCCGTTCAT	0.1 mM	Yamashita, 2003
BAI-1	CTAGAACTCTAACACACTTACTCAT	1 mM	Mazaheri et al., 2014
TIM4	CATAGTTTATCAACACTTACCATCA	0.7 mM	Mazaheri et al., 2014
a1vATPase	CCTCGCTACGAAACAGCTCCCCCAT	0.4 mM	Peri and Nüsslein-Volhard, 2008

5.3.2.2 CRISPR-Cas9 injections:

Injection mixture was prepared according to the table below and incubated at 37 °C for 20 min to allow the Cas9 protein to refold before injection. Injections were then made into the cell of embryos at the single cell stage.

Reagent	Stock concentration	Final concentration	Volume
sgRNA	600 ng/µl	200 ng/µl	1.36 µl
Cassette	5.4 µM	1 µM	0.74 µl
KCl	1M	300 mM	0.9 µl
Cas9	4000 ng/µl	1000 ng/µl	1 µl

5.3.3 Protein extraction:

Protein was extracted from 50 pooled embryos 4 dpf in 0.2 ml lysis buffer (Fiorotto et al., 2016) with a protease inhibitor cocktail (Roche) added to it. A microfuge pestle was used to homogenize embryos and the lysate was incubated for 30 min at 4 °C under rotation before centrifugation for 30 min at 4 °C. The supernatant was transferred to a new tube and total protein extracted was measured by Coomassie Protein Assay Reagent (Thermo Fisher Scientific, 1856209). Using a spectrophotometer (Eppendorf BioPhotometer plus).

Lysis buffer:	Concentration	Supplier
Tris-HCl [1M, pH 7.5]	50 mM	EMBL laboratory kitchen
EDTA [10mM]	1 mM	EMBL laboratory kitchen
Octyl b-D-glucopyranoside	2 %	Sigma (O8001)
2-Mercaptoethanol	5 mM	Sigma (M6250)
NaCl [3M]	0.25 M	Merck (1.06404.1000)
Na_3VO_4	1 mM	Sigma (S6508)
NaF	20 mM	Sigma (201154)
Glycerol	5%	Merck (1.04093.1000)
Triton X-100	100 µL	Sigma (T9284)

5.3.4 SDS-PAGE:

Discontinuous gel electrophoresis under denaturing conditions was used for protein separation of zebrafish lysates. 800 µg of extracted protein was solubilized in 20 µl 1x Laemmli buffer with 10% 2-Mercaptoethanol and warmed for 10 min to 37°C. Protein was separated by electrophoresis in precast polyacrylamide gels for 90 min at 200V using MOPS or MES buffer for big or small proteins respectively.

Reagent	Supplier
Laemmli buffer 4x	Biorad (161-0747)
2-Mercaptoethanol	Sigma (M6250)
NuPAGE 4-12% Bis-Tris Protein Gels	Novex (NP0321BOX)
NuPAGE MOPS SDS Running Buffer (20x)	Novex (NP0001)
NuPAGE MES SDS Running Buffer (20x)	Novex (NP0002)

5.3.5 Immunoblotting:

To identify specific proteins recognized by antibodies immunoblotting was performed. Proteins separated by SDS-PAGE was transferred by electrophoresis onto nitrocellulose membrane. Transfer took place at room temperature for 1 hour at 170 mA. Membranes were

rinsed in TBS-T (0.1% Tween-20), before blocking with 5% fat-free milk powder in TBS-T for 1 hour at room temperature. The membrane was then incubated with the primary antibody, diluted in blocking buffer, overnight at 4°C with constant gentle agitation. Membranes were washed 3 x 10 min in TBS-T buffer before incubation with the secondary antibody diluted 1:2500 in blocking buffer for 1 hour at room temperature. Membranes were again washed 3 x 10 min in TBS-T buffer before HRP detection systems and autoradiography films according to the manufacturer's instructions.

Reagent/material	**Supplier**
Nitrocellulose membranes, 0.2 µm pore size	Novex (LC2000)
NuPAGE transfer buffer 20x	Novex (NP0006)
Tween-20	Sigma (P9416)
Immobilion Western	Millipore (WBKLS0500)
Super signal West Pico PLUS	Thermo Fisher Scientific (34579)
Amersham Hyperfilm MP	GE Healthcare (28906845)
Anti-zebrafish Slc37a2 (dilute 1:100)	EMBL Rome (MACF)
Anti-mouse g-Tubulin (dilute 1:2000)	Sigma (T6557)

5.3.6 Antibody staining on zebrafish larvae:

Zebrafish larvae of the *Tg(mpeg1:eGFP)* were chemically fixed with 4% PFA in PBS overnight at 4 °C. They were then permeabilized for 5x30 min in PBS + 0.8 % Triton (PBST) and rinsed in 10x blocking buffer before a 1 hour incubation in 10x blocking buffer at room temperature. Primary antibody was diluted according to the table below in 1x blocking buffer. Samples were incubated overnight with the primary antibody at 4 °C with gentle rocking. Samples were then rinsed extensively in PBST followed by rinsing with 10x blocking buffer and a 1 hour incubation with 10x blocking buffer. Secondary antibody was diluted 1:500 in 1x blocking buffer together with a GFP booster diluted 1:200. Samples were incubated with this cocktail overnight t 4 °C

with gentle rocking. Samples were then rinsed 3x30 min in PBST before they were mounted for confocal microscopy.

Reagent	Composition
Permeabilizing solution	Triton (Tx100) in PBS (800 µl in 100ml)
Blocking Solution 10x	10 % NGS in permeabilizing solution
Blocking solution 1x	1:10 dilution of blocking buffer solution 10x

5.3.7 Antibody staining on RAW 264.7 macrophages:

Cells were cultured and prepared on coverslips as described above before fixation with 4 % PFA in PBS overnight. After fixation coverslips were rinsed 3x5 min in PBS and permeabilized for 7 minutes in PBS + 0.2 % Triton (PBST). Blocking was then performed using 3 % BSA in PBST for 1 hour at room temperature with gentle rocking. Primary antibody was diluted according to the table below, in blocking buffer. Coverslips were incubated with the primary antibody solution overnight at 4 °C. They were then rinsed 3x5 min with PBS before incubation for 1 hour with the appropriate secondary antibody, diluted according to the table below, in blocking buffer. Afterwards they were rinsed in PBS and mounted using a Vectrashield kit with DAPI stain added to it in accordance with the manufacturer's instructions (Vector Laboratories, Inc., Burlingame, CA).

Reagent	Composition
Permabilizating solution	Triton (Tx100) in PBS (200 µl in 100ml)
Blocking Solution	3 % BSA in permeabilizing solution

Reagents/Material	Supplier
Triton X-100	Sigma (T9284)
Bovine Serum Albumine	Sigma (A2153)
Normal Goat Serum (NGS)	Merck (S26)

5.3.8 List of antibodies used:

Antibody	Species	Supplier	Dilution
Anti-zebrafish Slc37a2	Mouse, monoclonal	EMBL, Rome	1:20
Anti-mouse Slc37a2	Rabbit, polyclonal	Invitrogen (PA5-20916)	1:100
Anti-muse Rab7	Rabbit, monoclonal	Abcam (Ab137029)	1:100
Anti-mouse LBPA	Hamster, monoclonal	Millipore (MABT837)	1:100
Anti-mouse Lamp1	Rat, monoclonal	Abcam (Ab25245)	1:100
Anti-mouse Lamp2	Rat, monoclonal	Abcam (Ab25339)	1:100
Anti-rat Cathepsin D	Rabbit	Gift from Bernard Hoflack	1:100
Anti-Rabbit IgG Alexa 488	Goat	Abcam (ab150077)	1:500
Anti-Mouse IgG Alexa 488	Goat	Abcam (ab150113)	1:500
Anti-Rabbit IgG Alexa 594	Goat	Abcam (ab150080)	1:500
Anti-Rat IgG Alexa 594	Goat	Abcam (ab150160)	1:500

5.4 Light microscopy techniques:

5.4.1 Chemical treatment of zebrafish embryos:

5.4.1.1 Z-VAD-fmk treatment:

Z-VAD-fmk (Carbobenzoxy-valyl-alanyl-aspartyl-[O-methyl]-fluoromethylketone) (Bachem, 4027403) was used to reduce levels of apoptosis in zebrafish embryos. It was applied at a concentration of 300 µM in E3 medium with 1 % (v/v) DMSO added to it. Embryos were kept on this solution from 1 dpf until they were inspected by microscopy.

5.4.1.2 Camptothecin treatment:

Camptothecin (CPT) (Sigma, C9911) was used to induce apoptosis in embryos to higher levels than normal or in tissues where it is not naturally prevalent. It was applied at a concentration of 1 µM in E3 medium with 1 % (v/v) DMSO added to it. Embryos were incubated for in this solution for 8 hours before inspection by microscopy.

5.4.2 Laser induced injury:

Injuries with laser ablation was performed using a 532 nm ablation laser attached to a Olympus FV1200 confocal microscope or a 355 nm ablation laser attached to a Andora Spinning Disc confocal microscope. For the FV1200 tornado pattern was used and the laser intensity set to 45% in a region of 30x30 pixels. For the Andora Spinning Disc the frequency was set to 2500 Hz, and the laser intensity to 100 % and 1000 pulses/point.

5.4.3Stainings with chemical dyes:

5.4.3.1 Acridin orange:

To label apoptotic cells zebrafish embryos were incubated with 10 µg/ml acridin orange (Sigma, A6014) in E3/PTU for 1 hour and extensively rinsed before mounting for light microscopy.

5.4.3.2 Neutral red:

Neutral red staining was used to visualize microglia in zebrafish larvae. A 5 µg/ml neutral red (Sigma, N4638) solution in E3/PTU was used for staining for 2 hours at 28 °C. Before mounting for light microscopy samples were extensively rinsed with E3/PTU.

5.4.3.3 Lysotracker:

Embryos were stained in a solution made from 12 µl Lysotracker DND-99 (Thermo Fisher Scientific, L7528) added to 30 ml of E3/PTU and 1% (v/v) DMSO for 1 hour, in the dark, at 28 °C. Embryos were then rinsed trice in in E3/PTU medium before mounting for microscopy.

5.4.3.4 Staining for lipids:

Both zebrafish embryos and cultured cells were stained with several dyes specifically labeling lipids. Live zebrafish larvae were stained at 4 dpf for 30 min at 28 °C. They were then rinsed trice in in E3/PTU medium before mounting for microscopy. Cultured cells were stained after performing the phagocytosis assay on cells that had been chemically fixed 9 hours post

treatment. They were rinsed once with PBS before staining for 30 min at room temperature. After staining cells were again rinsed trice in PBS for 5 min and mounted for light microscopy using a Vectashield Kit (Vector Laboratories, Inc., Burlingame, CA).

Reagent	Stock	Concentration used	Supplier
BODIPY 493/503	1 mg/ml in DMSO	1µg/ml	Thermo Fisher (D3922)
Nile red	1 mg/ml in DMSO	5µg/ml	Thermo Fisher (N-1142)
Nile Blue Chloride	1 mg/ml in H2O	5-10µg/ml	Sigma (222550)

5.4.4 Confocal microscopy:

Zebrafish embryos were tricanated and mounted in glassbottom dishes using low melting point agarose as described above. Imaging was performed using either an Olympus FV1200, a Leica SP8 or an Andor Spinning disk with 40x/NA1.15 or 20x/NA0.7 objectives. The entire optic tectum was imaged with an average of 30-40 z-step of 1.5 µm. Laser intensity was usually set between 1-10 % depending on the fluorophore and adjusted to optimize signal to noise. All images and videos were analyzed in Fiji or Imaris.

5.4.5 Single plane illumination microscopy:

5.4.5.1 Mounting zebrafish embryos for single plane illumination imaging:

Embryos were anesthetized with tricane as described above. For imaging with the Leica SP8 (DLS) embryos were mounted in Mattek glass bottom dishes (MatTek Corporation, P35G-1.5-10-C) using 1.3% (w/v) low melting point agarose (Peqlab 352010). A big dome was made in the middle of the cover glass from the agarose and a single embryo was mounted at its apex. Two sides of the dome were then cut away using a scalpel leaving a slice < 1 mm thick to fit in between the mirrors of the microscope. For imaging with the Zeiss Lightsheet Z.1 and Luxendo MuVi SPIM embryos in melted agarose were pulled into a glass capillary in the agarose before it solidified. The glass capillary was then mounted in the microscope for

imaging and the now solidified agarose containing the embryo was pushed out with a piston so the embryo was clear of the glass during imaging.

5.4.5.2 Image acquisition:

SP8 DLS and Luxendo MuVi microscopes were fitted with a 25x detection objective and the Zeiss Lightsheet Z.1 with a 20x detection objective. Z-stacks were set up to contain as much of the optic tectum as possible with a temporal resolution of 20 seconds. 5 – 10 % laser power was used, adjusted for optimal signal to noise ratio and a 50 ms exposure time per plane. Imaging was set up with two channels, one for visualizing microglia specific fluorescent reporters and the other for apoptotic cells (also transgenic reporter) or lysotracker dye.

5.4.5.3 Data analysis:

For initial viewing as well as Tracking and cropping of individual microglia the Big Data Tool plug-in (https://github.com/tischi/fiji-plugin-bigDataTools) for Fiji was used. Crops from this process were then used to track individual phagosomes using the MTrackJ plug-in (https://imagescience.org/meijering/software/mtrackj) for Fiji. The center z-plane of each individual phagosome was carefully selected this way and their diameter was measured using the measuring tool in Fiji. Intensity values for the lysotracker staining was extracted based on these tracks (python script by Dr. Nils Norlin). For creating graphical representation combining these data a python script was written by Jonas Hartmann (https://github.com/WhoIsJack/TrackTree).

5.5 Mass spectroscopy:

5.5.1 Sample preparation:

Zebrafish embryos (4 dpf) were anaesthetized using tricane as described above. They were then decapitated using a scalpel and heads were collected in an eppendorf tube. 50 heads were pooled per tube and all residual medium was removed before adding 0.5 ml methanol. Samples were then stored at 4 °C until further processed.

Before loading onto the column they were homogenized by vortexing for 5 min vigorously followed by sonication in ice for 10 min. Extracts were centrifuged at 3,500 rpm for 10min at 4°C and the supernatant transferred to a 2ml eppendorf tube. All samples were centrifuge again at 14,000 rpm for 5 min to remove particulate matter.

5.5.2 Analytical method:

LC-MS/MS analysis was performed on a Vanquish UHPLC system coupled to a Q-Exactive plus HRMS (Thermo Scientific, MA, USA) in ESI negative mode. Separation of metabolites was performed using a Luna amino (150 X 2 mm; 3uM) at a flow rate of 0.3 ml/min and maintained at 35 °C. The mobile phase consisted of solvent A (7.5 mM Ammonium acetate with 0.05% NH4OH) and solvent B (acetonitrile). The UHPLC system was run in gradient mode as described in the table below.

Metabolites were detected with HRMS full scan at the mass resolving power R=70000 in mass range of 60-900 m/z. The data-dependent tandem (MS/MS) mass scans were obtained along with full scans using higher energy collisional dissociation (HCD) of normalized collision energies of 10, 20 and 30 units which were at the mass resolving power R=17500. The MS parameters in the Tune software (Thermo Scientific) were set as: spray voltage of 4 kV (for negative mode 3.5 kV), sheath gas 30 and auxiliary gas 5 units, S-Lens 65 eV, capillary temperature 320oC and vaporization temperature of auxiliary gas was 300 °C. Data was

acquired in full scan mode and data dependent tandem mass spectra (MS/MS) for all precursors corresponding to targeted metabolites.

Time (min)	% B
0	85
2	85
24	5
30	5
31	85
35	85

5.5.3 Quality control and analysis sequence:

Sequence of LC-MS analysis was randomized. A pooled quality control sample was prepared from mixing equal volume of each samples and processed in a similar manner. Blanks and quality controls were injected at the beginning of the analysis sequence to stabilize the LC-MS system. Between every 4 samples a quality control sample was injected to assess the stability of instrument and analytical method (%CV <20). Chromatograms were evaluated manually and stability of quality control samples checked before proceeding to data analysis.

5.5.4 Data analysis:

Data analysis was performed using Thermo software (Xcalibur Quan) including the generation of extracted ion chromatograms, peak integration and raw data visualization. The peak areas were exported to a spreadsheet for further data analysis, including concentration calculated, quality control evaluation and statistical analysis. All data was evaluated for consistency of peak integration and manual integration was performed whenever necessary. The Optimus pipeline (https://github.com/MolecularCartography/Optimus) was used for comparative analysis allowing for an m/z deviation of 3ppm. Features were retained if they were above the noise threshold of 100,00 and ms/ms spectra were acquired in at least one sample.

Median normalization was applied, absent features were zero filled and a two-tailed t-test was used to compare the mutant and wild type samples using Benferroni multiple correction testing. The identity of metabolite peaks in deprotonated from [M-H] were confirmed by matching its retention time and exact mass (+ 5 ppm) with respective authentic standards.

5.6 Correlative light and electron microscopy:

5.6.1 Zebrafish embryos:

5.6.1.1 Light microscopy:

Zebrafish embryos were anesthetizes with tricane and immersed in fixative (2.5% GA and 4% FA in 0.1M PHEM buffer). They were immediately decapitated with a scalpel and fixation and quenching (150 mM glycine in 100 mM PHEM) was carried out in a PELCO Biowave equipped with a ColdSpot (Ted Pella) as detailed below. I discovered that storing the samples overnight on 0.1M PHEM buffer at 4 °C increased the background autofluorescence just enough to be helpful for brand-marking, but not too much to interfere with detection of the microglia. Individual heads were then mounted in a MatTek glass bottom dish using 1.3 % (w/v) low melting point agarose for stabilizing the sample. After the agarose had solidified samples were covered in 0.1 M PHEM buffer to keep them hydrated during imagin. Imaging and near infrared branding was performed either on a FEI Corrsight prototype or 780 NLO two photon microscope (Zeiss). 12 – 16 brand marks were created with a diameter of 20 -30 µm in in a constellation in three different planes, with the middle plane approximately at the depth of the cell of interest, and with a non-symmetric distribution as to create a pattern with a chirality. A high resolution z-stack was acquired using a 40x water immersion objective positioned such that all the brand marks as well as the cell of interest was within the field of view. Individual samples were stored in 0.1M PHEM buffer at 4 °C for up to 2 days before further processing.

5.6.1.2 Sample preparation:

Sample preparation of zebrafish larvae for SBF-SEM was adapted to the Biowave from Hua et al 2015. This protocol consists of an initial post-fixation with 2% OsO_4 in cacodylate buffer followed by a separate treatment with 2.5% ferrocyanide in cacodylate buffer, a treatment with 6.67 mg/ml thiocarbohydrazide in water and a second post-fixation with 2% OsO_4 in water. Samples were then stained with 1% uranyl acetate in water followed by 4.4 mg/ml lead aspartate in water as no post section staining is possible with this form of microscopy. After staining samples were dehydrated in a graded series of ethanol (EtOh) (25%, 50%, 75%, 90%, 95% and 2x100%) and infiltration with DURCPOPAN resin mixture (Electron Microscopy Sciences #14020) was done in a graded series of resin diluted in 100% EtOH (30%, 50%, 70%, 90% and 100%) Excessive resin was drained off the sample by touching it against a filter paper and samples were mounted in insect needles for polymerized for 24 hours at 60 °C as described in (Schieber et al. 2017).

5.6.1.3 µCT scanning:

Samples were mounted on microtome stubs (Agar Scientific, G1092450) using an EPO-TEK adhesive (Electron Microscopy Sciences, #12670-EE), a conductive silver glue, at the base of the sample and polymerized for 48 h at 60 °C. Great care was taken to keep the sides of the sample free of the EPO-TEK adhesive. This was the same stub as the sample remained mounted on for SBF-SEM which was important for keeping the orientation of the sample. Before scanning the front of the sample was trimmed to a flat surface using an EM UC7 ultramicrotome (Leica) with a diamond trimming tool (Diatome).

µCT scan was performed on a Phoenix Nanotom m (GE Sensing & Inspection Technologies, Fairfield, CT) operating under xs control and Phoenix datos|x acquisition software (both GE Sensing & Inspection Technologies). X-ray tomograms were acquired with the x-ray source

running at 430 µA and 60 kV. Images were acquired with a voxel size of 0.7 µm, 1440 rotation steps, 1000 ms exposure time and 4 time averaging. Volume data was reconstructed using the Phoenix datos|x reconstruction software (GE Sensing & Inspection Technologies).

5.6.1.4 Amira modeling and ultramicrotomy:

Two 3D models were constructed using Amira (version 6.2.0) (FEI Company). One model was made from the light microscopy dataset and contained segmentations of the brand mark and the cell of interest. The other model was made from the µCT scan and contained segmentation of the sample surface and the brand marks. These two models were then overlaid to give the best possible fit for the constellation of brand marks from both models, allowing the light microscopy coordinates to be transformed but not the µCT data. The position of the cell of interest could then be measured relative to the trimmed front face of the block.

The sample was then be mounted in the microtome and trimmed down to the position of the cell. Typically it was necessary to remove 200 – 300 µm of material to reach the cell. Upon reaching within 20 – 30 µm of the target position semi thick sections were collected with an ultra 45° diamond knife (Diatome) and stained with toluidine blue solution. These sections were compared to the sample features in the x-ray scan. This was used to determine the accuracy of the approach and the trimming of the final µm of material was adjusted accordingly.

5.6.1.5 Serial Block Face Scanning Electron microscopy:

Once trimming was completed the sample was transferred to the electron microscope and left under vacuum overnight to be degassed. SBF-SEM was performed on a FEI Teneo VolumeScope (VS) with the VS plugin for Maps software (FEI Company). The microscope was

operated at 1.78 kV and 0.1 nA. The imaging parameters used were 2.5 nanometer pixel size, with a dwell time of 100 nanoseconds and 4 times line averaging.

For samples of the blb mutant no CLEM was required as vacuoles could be detected directly by µCT or at low magnification in the electron microscope.

5.6.1.6 Data processing:

The microtome was set to section 30 nanometer slices. Post-acquisition processing of images was performed using Fiji. A Gaussian blur, sigma 2.0 was applied for de-noising before scaling of the image in x and y by a factor of 0.5 and the grayscale was inverted. For creating segmentations, 3D models and animations from the EM data Amira (version 6.2.0) (FEI Company) was used.

5.6.2 Cell culture:

5.6.2.1 Light microscopy:

Before samples were imaged fixative was quenched with 150 mM glycine in 100 mM PHEM buffer in a PELCO Biowave equipped with a ColdSpot (Ted Pella) as detailed below. Light microscopy for CLEM on cultures cells was carried out either on an FV 1200 confocal microscope (Olympus) or Axio Observer.Z1 widefield microscope with a side mounted Axio MRm camera (Zeiss). Images were acquired with a 10x objective for low magnification overview images and a 40x objective for identifying a cell of interest. Laser power was set between 10 – 20 % to optimize signal to noise ratio. Care was taken that the coordinate grid was clearly visible in the bright field image.

5.6.2.2 Sample preparation:

All sample preparation was conducted in a PELCO Biowave equipped with a ColdSpot (Ted Pella) as detailed below with the exception of tannic acid treatment. All processing steps were carried out in the the MatTek petri dish and care was taken that the cells not detach from the

glass when solutions were exchanged. A second round of fixation was performed after light microscopy imaging using 2.5% GA and 4% FA in 0.1 M cacodylate buffer, followed by rinsing with 0.1 M cacodylate and post-fixation with 1% osmium tetroxide (OsO4) and 0.8% potassium ferrocyanide (K3Fe(CN)6) in water. Samples were again rinsed in 0.1 M cacodylate buffer before staining with 1% tannic acid for 20 min on ice. Tannic acid solution was removed and samples rinsed with water, before staining with 1% uranyl acetate (UA) (in water), and rinsed with water. Dehydration of samples was done in a graded series of ethanol (EtOh) (25%, 50%, 75%, 90%, 95% and 2x100%). Infiltration with very hard EPON resin mixture (Serva, 45359-1EA-F) was done in a graded series of resin diluted in 100% EtOH (30%, 50%, 70%, 90% and 100%) Samples were finally covered in in a thin layer of pure resin and a gelatin cylinder was placed on top of it and filled with resin in order to create a dummy block. Samples were incubated for 48 hours at 60 °C for the resin to polymerize.

5.6.2.3 Ultramicrotomy:

When samples were removed from the Matek dish the surface of the resin block retained a negative imprint of the finder grid. This was used to guide trimming of the sample, by razorblade for course trimming, and a diamond trimming tool (Diatome) for fine trimming. Ultramicrotomy was performed on a EM UC7 ultramicrotome (Leica) with an ultra 45° diamond knife (Diatome) Serial sections were cut with a 70 nm feed, collected on slot grids (Plano, G2500C) with a formvar film and inspected by transmission electron microscopy.

5.6.3 Transmission electron microscopy:

Post section staining was performed using a 2% solution of uranyl acetate in water for 5 min followed by Reynolds lead citrate for 30 seconds. After each staining grids were rinsed in 5 consecutive baths of water and air dried. A Biotwin CM120 electron microscope (FEI) was

used to inspect the grids and images were acquired with a bottom mounted 1K CCD Camera (Keen View, SIS)

5.6.4 Biovawe processing:

Processing step:	Wattage:	Duration:	Vacuum:	Cycling intervals:	Temperature:
GA/PFA fixation OsO_4 postfixation	100	16 min	Yes	2 min	20 °C
Thiocarbohydrazide	100	16 min	Yes	2 min	40 °C
Uranyl acetate Lead aspertate	100	16 min	Yes	2 min	50 °C
Resin infiltration	250	3 min	Yes	3 min	20 °C
Rinses, quenching and EtOH	250	40 sec	No	-	20 °C

5.6.5 Table of chemicals for electron microscopy:

Reagent	Stock solution	Source
Paraformaldehyde (PFA)	16 %	Electron Microscopy Sciences, 15710
Glutaraldehyde (GA)	25 %	Electron Microscopy Sciences, 16020
Osmium tetroxide	4%	Electron Microscopy Sciences, RT 19112
Sodium cacodylate	98 %	C4945-10G
Potassium ferrocyanide trihydrate	Pure crystals	Carlo Erba (Italy) 471484
Thiocarbohydrazide	Pure crystals	Science Services
Tannic acid	Pure crystals	Electron Microscopy Sciences, RT 21700
Uranyl acetate	Pure crystals	Serva, 77870.01
Lead acetate	Pure crystals	Polaron Equipment Ltd
Aspartic acid	Pure crystals	Sigma, A9256
Durcopan	Compound resin	Sigma, 44610-1EA
EPON	Compound resin	Serva, 21045

PHEM buffer:	
	60mM PIPES
	25mM HEPES
	10mM EGTA
	2mM Magnesium chloride: pH 6.9

5.7 Statistical analysis:

Statistical analysis was carried out using either scipy.stats library (version 0.19.0) for python 2.7.11 or Prism 7. All hypothesis were tested without parametric assumptions with a two-tailed Mann-Whitney U test (scipy.stat.mannwhitneyu) for all comparisons unless otherwise specified. Python scripts for analysis were written by Jonas Hartmann.

P value	**Wording**	**Summary**
< 0.0001	Extremely significant	****
0.0001 – 0.001	Extremely significant	***
0.001 – 0.01	Very significant	**
0.01 – 0.05	Significant	*
>= 0.05	Not significant	ns

6 References:

Abraham, R. T. 2015. "Cell biology. Making sense of amino acid sensing." *Science* 347 (6218):128-9. doi: 10.1126/science.aaa4570.

Adachi, H., and M. Tsujimoto. 2002. "FEEL-1, a novel scavenger receptor with in vitro bacteria-binding and angiogenesis-modulating activities." *J Biol Chem* 277 (37):34264-70. doi: 10.1074/jbc.M204277200.

Aguzzi, A., B. A. Barres, and M. L. Bennett. 2013. "Microglia: scapegoat, saboteur, or something else?" *Science* 339 (6116):156-61. doi: 10.1126/science.1227901.

Araki, N., T. Hatae, A. Furukawa, and J. A. Swanson. 2003. "Phosphoinositide-3-kinase-independent contractile activities associated with Fcgamma-receptor-mediated phagocytosis and macropinocytosis in macrophages." *J Cell Sci* 116 (Pt 2):247-57.

Arandjelovic, S., and K. S. Ravichandran. 2015. "Phagocytosis of apoptotic cells in homeostasis." *Nat Immunol* 16 (9):907-17. doi: 10.1038/ni.3253.

Bajno, L., X. R. Peng, A. D. Schreiber, H. P. Moore, W. S. Trimble, and S. Grinstein. 2000. "Focal exocytosis of VAMP3-containing vesicles at sites of phagosome formation." *J Cell Biol* 149 (3):697-706.

Balasubramanian, K., and A. J. Schroit. 2003. "Aminophospholipid asymmetry: A matter of life and death." *Annu Rev Physiol* 65:701-34. doi: 10.1146/annurev.physiol.65.092101.142459.

Barclay, A. N., and M. H. Brown. 2006. "The SIRP family of receptors and immune regulation." *Nat Rev Immunol* 6 (6):457-64. doi: 10.1038/nri1859.

Bedell, V. M., S. E. Westcot, and S. C. Ekker. 2011. "Lessons from morpholino-based screening in zebrafish." *Brief Funct Genomics* 10 (4):181-8. doi: 10.1093/bfgp/elr021.

Bilimoria, P. M., and B. Stevens. 2015. "Microglia function during brain development: New insights from animal models." *Brain Res* 1617:7-17. doi: 10.1016/j.brainres.2014.11.032.

Bohdanowicz, M., D. M. Balkin, P. De Camilli, and S. Grinstein. 2012. "Recruitment of OCRL and Inpp5B to phagosomes by Rab5 and APPL1 depletes phosphoinositides and attenuates Akt signaling." *Mol Biol Cell* 23 (1):176-87. doi: 10.1091/mbc.E11-06-0489.

Brandhorst, D., D. Zwilling, S. O. Rizzoli, U. Lippert, T. Lang, and R. Jahn. 2006. "Homotypic fusion of early endosomes: SNAREs do not determine fusion specificity." *Proc Natl Acad Sci U S A* 103 (8):2701-6. doi: 10.1073/pnas.0511138103.

Brown, S., I. Heinisch, E. Ross, K. Shaw, C. D. Buckley, and J. Savill. 2002. "Apoptosis disables CD31-mediated cell detachment from phagocytes promoting binding and engulfment." *Nature* 418 (6894):200-3. doi: 10.1038/nature00811.

Cappello, A. R., R. Curcio, R. Lappano, M. Maggiolini, and V. Dolce. 2018. "The Physiopathological Role of the Exchangers Belonging to the SLC37 Family." *Front Chem* 6:122. doi: 10.3389/fchem.2018.00122.

Casano, A. M., M. Albert, and F. Peri. 2016. "Developmental Apoptosis Mediates Entry and Positioning of Microglia in the Zebrafish Brain." *Cell Rep* 16 (4):897-906. doi: 10.1016/j.celrep.2016.06.033.

Chen, Y., and X. Zhao. 1998. "Shaping limbs by apoptosis." *J Exp Zool* 282 (6):691-702.

Chou, J. Y., H. S. Jun, and B. C. Mansfield. 2010a. "Glycogen storage disease type I and G6Pase-beta deficiency: etiology and therapy." *Nat Rev Endocrinol* 6 (12):676-88. doi: 10.1038/nrendo.2010.189.

Chou, J. Y., H. S. Jun, and B. C. Mansfield. 2010b. "Neutropenia in type Ib glycogen storage disease." *Curr Opin Hematol* 17 (1):36-42. doi: 10.1097/MOH.0b013e328331df85.

Chou, J. Y., and B. C. Mansfield. 2014. "The SLC37 family of sugar-phosphate/phosphate exchangers." *Curr Top Membr* 73:357-82. doi: 10.1016/B978-0-12-800223-0.00010-4.

Claus, V., A. Jahraus, T. Tjelle, T. Berg, H. Kirschke, H. Faulstich, and G. Griffiths. 1998. "Lysosomal enzyme trafficking between phagosomes, endosomes, and lysosomes in J774 macrophages. Enrichment of cathepsin H in early endosomes." *J Biol Chem* 273 (16):9842-51.

Connor, J., C. C. Pak, and A. J. Schroit. 1994. "Exposure of phosphatidylserine in the outer leaflet of human red blood cells. Relationship to cell density, cell age, and clearance by mononuclear cells." *J Biol Chem* 269 (4):2399-404.

Cox, D., J. S. Berg, M. Cammer, J. O. Chinegwundoh, B. M. Dale, R. E. Cheney, and S. Greenberg. 2002. "Myosin X is a downstream effector of PI(3)K during phagocytosis." *Nature Cell Biology* 4 (7):469-477. doi: 10.1038/ncb805.

Cox, D., D. J. Lee, B. M. Dale, J. Calafat, and S. Greenberg. 2000. "A Rab11-containing rapidly recycling compartment in macrophages that promotes phagocytosis." *Proc Natl Acad Sci U S A* 97 (2):680-5.

Damiani, M. T., M. Pavarotti, N. Leiva, A. J. Lindsay, M. W. McCaffrey, and M. I. Colombo. 2004. "Rab coupling protein associates with phagosomes and regulates recycling from the phagosomal compartment." *Traffic* 5 (10):785-97. doi: 10.1111/j.1600-0854.2004.00220.x.

Davalos, D., J. Grutzendler, G. Yang, J. V. Kim, Y. Zuo, S. Jung, D. R. Littman, M. L. Dustin, and W. B. Gan. 2005. "ATP mediates rapid microglial response to local brain injury in vivo." *Nat Neurosci* 8 (6):752-8. doi: 10.1038/nn1472.

Davidson, A. J., and L. I. Zon. 2004. "The 'definitive' (and 'primitive') guide to zebrafish hematopoiesis." *Oncogene* 23 (43):7233-46. doi: 10.1038/sj.onc.1207943.

Desjardins, M., L. A. Huber, R. G. Parton, and G. Griffiths. 1994. "Biogenesis of phagolysosomes proceeds through a sequential series of interactions with the endocytic apparatus." *J Cell Biol* 124 (5):677-88.

Di, A., B. Krupa, V. P. Bindokas, Y. Chen, M. E. Brown, H. C. Palfrey, A. P. Naren, K. L. Kirk, and D. J. Nelson. 2002. "Quantal release of free radicals during exocytosis of phagosomes." *Nat Cell Biol* 4 (4):279-85. doi: 10.1038/ncb771.

Driever, W., L. Solnica-Krezel, A. F. Schier, S. C. Neuhauss, J. Malicki, D. L. Stemple, D. Y. Stainier, F. Zwartkruis, S. Abdelilah, Z. Rangini, J. Belak, and C. Boggs. 1996. "A genetic screen for mutations affecting embryogenesis in zebrafish." *Development* 123:37-46.

Duclos, S., G. Clavarino, G. Rousserie, G. Goyette, J. Boulais, V. Camossetto, E. Gatti, S. LaBoissiere, P. Pierre, and M. Desjardins. 2011. "The endosomal proteome of macrophage and dendritic cells." *Proteomics* 11 (5):854-64. doi: 10.1002/pmic.201000577.

Ellett, F., L. Pase, J. W. Hayman, A. Andrianopoulos, and G. J. Lieschke. 2011. "mpeg1 promoter transgenes direct macrophage-lineage expression in zebrafish." *Blood* 117 (4):e49-56. doi: 10.1182/blood-2010-10-314120.

Elliott, M. R., F. B. Chekeni, P. C. Trampont, E. R. Lazarowski, A. Kadl, S. F. Walk, D. Park, R. I. Woodson, M. Ostankovich, P. Sharma, J. J. Lysiak, T. K. Harden, N. Leitinger, and K. S. Ravichandran. 2009. "Nucleotides released by apoptotic cells act as a find-me signal to promote phagocytic clearance." *Nature* 461 (7261):282-6. doi: 10.1038/nature08296.

Ellis, R. E., D. M. Jacobson, and H. R. Horvitz. 1991. "Genes required for the engulfment of cell corpses during programmed cell death in Caenorhabditis elegans." *Genetics* 129 (1):79-94.

Erwig, L. P., and P. M. Henson. 2008. "Clearance of apoptotic cells by phagocytes." *Cell Death Differ* 15 (2):243-50. doi: 10.1038/sj.cdd.4402184.

Erwig, L. P., K. A. McPhilips, M. W. Wynes, A. Ivetic, A. J. Ridley, and P. M. Henson. 2006. "Differential regulation of phagosome maturation in macrophages and dendritic cells mediated by Rho GTPases and ezrin-radixin-moesin (ERM) proteins." *Proc Natl Acad Sci U S A* 103 (34):12825-30. doi: 10.1073/pnas.0605331103.

Fischer, K., D. Chatterjee, J. Torrelles, P. J. Brennan, S. H. Kaufmann, and U. E. Schaible. 2001. "Mycobacterial lysocardiolipin is exported from phagosomes upon cleavage of cardiolipin by a macrophage-derived lysosomal phospholipase A2." *J Immunol* 167 (4):2187-92.

Flannagan, R. S., J. Canton, W. Furuya, M. Glogauer, and S. Grinstein. 2014. "The phosphatidylserine receptor TIM4 utilizes integrins as coreceptors to effect phagocytosis." *Mol Biol Cell* 25 (9):1511-22. doi: 10.1091/mbc.E13-04-0212.

Flannagan, R. S., V. Jaumouille, and S. Grinstein. 2012. "The cell biology of phagocytosis." *Annu Rev Pathol* 7:61-98. doi: 10.1146/annurev-pathol-011811-132445.

Freeman, S. A., and S. Grinstein. 2018. "Resolution of macropinosomes, phagosomes, and autolysosomes: osmotically-driven shrinkage enables tubulation and vesiculation." *Traffic*. doi: 10.1111/tra.12614.

Fritz, S., A. Capitan, A. Djari, S. C. Rodriguez, A. Barbat, A. Baur, C. Grohs, B. Weiss, M. Boussaha, D. Esquerre, C. Klopp, D. Rocha, and D. Boichard. 2013. "Detection of haplotypes associated with prenatal death in dairy cattle and identification of deleterious mutations in GART, SHBG and SLC37A2." *PLoS One* 8 (6):e65550. doi: 10.1371/journal.pone.0065550.

Gagnon, E., S. Duclos, C. Rondeau, E. Chevet, P. H. Cameron, O. Steele-Mortimer, J. Paiement, J. J. Bergeron, and M. Desjardins. 2002. "Endoplasmic reticulum-mediated phagocytosis is a mechanism of entry into macrophages." *Cell* 110 (1):119-31.

Gardai, S. J., K. A. McPhillips, S. C. Frasch, W. J. Janssen, A. Starefeldt, J. E. Murphy-Ullrich, D. L. Bratton, P. A. Oldenborg, M. Michalak, and P. M. Henson. 2005. "Cell-surface calreticulin initiates clearance of viable or apoptotic cells through trans-activation of LRP on the phagocyte." *Cell* 123 (2):321-34. doi: 10.1016/j.cell.2005.08.032.

Garin, J., R. Diez, S. Kieffer, J. F. Dermine, S. Duclos, E. Gagnon, R. Sadoul, C. Rondeau, and M. Desjardins. 2001. "The phagosome proteome: insight into phagosome functions." *J Cell Biol* 152 (1):165-80.

Ginhoux, F., M. Greter, M. Leboeuf, S. Nandi, P. See, S. Gokhan, M. F. Mehler, S. J. Conway, L. G. Ng, E. R. Stanley, I. M. Samokhvalov, and M. Merad. 2010. "Fate mapping analysis reveals that adult microglia derive from primitive macrophages." *Science* 330 (6005):841-5. doi: 10.1126/science.1194637.

Gotthardt, D., H. J. Warnatz, O. Henschel, F. Bruckert, M. Schleicher, and T. Soldati. 2002. "High-resolution dissection of phagosome maturation reveals distinct membrane trafficking phases." *Mol Biol Cell* 13 (10):3508-20. doi: 10.1091/mbc.e02-04-0206.

Graham, D. K., T. L. Dawson, D. L. Mullaney, H. R. Snodgrass, and H. S. Earp. 1994. "Cloning and mRNA expression analysis of a novel human protooncogene, c-mer." *Cell Growth Differ* 5 (6):647-57.

Griffin, F. M., Jr., C. Bianco, and S. C. Silverstein. 1975. "Characterization of the macrophage receptro for complement and demonstration of its functional independence from the receptor for the Fc portion of immunoglobulin G." *J Exp Med* 141 (6):1269-77.

Griffiths, G. 1996. "On vesicles and membrane compartments." *Protoplasma* 195 (1-4):37-58. doi: Doi 10.1007/Bf01279185.

Gude, D. R., S. E. Alvarez, S. W. Paugh, P. Mitra, J. Yu, R. Griffiths, S. E. Barbour, S. Milstien, and S. Spiegel. 2008. "Apoptosis induces expression of sphingosine kinase 1 to release sphingosine-1-phosphate as a "come-and-get-me" signal." *FASEB J* 22 (8):2629-38. doi: 10.1096/fj.08-107169.

Guerra, C. R., S. H. Seabra, W. de Souza, and S. Rozental. 2014. "Cryptococcus neoformans is internalized by receptor-mediated or 'triggered' phagocytosis, dependent on actin recruitment." *PLoS One* 9 (2):e89250. doi: 10.1371/journal.pone.0089250.

Haffter, P., and C. Nusslein-Volhard. 1996. "Large scale genetics in a small vertebrate, the zebrafish." *Int J Dev Biol* 40 (1):221-7.

Hanayama, R., M. Tanaka, K. Miwa, A. Shinohara, A. Iwamatsu, and S. Nagata. 2002. "Identification of a factor that links apoptotic cells to phagocytes." *Nature* 417 (6885):182-7. doi: 10.1038/417182a.

Hara, K., K. Yonezawa, Q. P. Weng, M. T. Kozlowski, C. Belham, and J. Avruch. 1998. "Amino acid sufficiency and mTOR regulate p70 S6 kinase and eIF-4E BP1 through a common effector mechanism." *J Biol Chem* 273 (23):14484-94.

Harris, E., and J. Cardelli. 2002. "RabD, a Dictyostelium Rab14-related GTPase, regulates phagocytosis and homotypic phagosome and lysosome fusion." *J Cell Sci* 115 (Pt 18):3703-13.

Henke, K. 2011. "Microglia in the zebrafish embryo: Isolation and characterization of molecules involved in their function and colonization of the brain.".

Herbomel, P., B. Thisse, and C. Thisse. 1999. "Ontogeny and behaviour of early macrophages in the zebrafish embryo." *Development* 126 (17):3735-45.

Herbomel, P., B. Thisse, and C. Thisse. 2001. "Zebrafish early macrophages colonize cephalic mesenchyme and developing brain, retina, and epidermis through a M-CSF receptor-dependent invasive process." *Dev Biol* 238 (2):274-88. doi: 10.1006/dbio.2001.0393.

Hirano, T., A. Saluja, P. Ramarao, M. M. Lerch, M. Saluja, and M. L. Steer. 1991. "Apical secretion of lysosomal enzymes in rabbit pancreas occurs via a secretagogue regulated pathway and is increased after pancreatic duct obstruction." *J Clin Invest* 87 (3):865-9. doi: 10.1172/JCI115091.

Hochreiter-Hufford, A. E., C. S. Lee, J. M. Kinchen, J. D. Sokolowski, S. Arandjelovic, J. A. Call, A. L. Klibanov, Z. Yan, J. W. Mandell, and K. S. Ravichandran. 2013. "Phosphatidylserine receptor BAI1 and apoptotic cells as new promoters of myoblast fusion." *Nature* 497 (7448):263-7. doi: 10.1038/nature12135.

Horvitz, H. R., H. M. Ellis, and P. W. Sternberg. 1982. "Programmed cell death in nematode development." *Neurosci. Comment.* (1):56-65.

Hsu, C. L., W. Lin, D. Seshasayee, Y. H. Chen, X. Ding, Z. Lin, E. Suto, Z. Huang, W. P. Lee, H. Park, M. Xu, M. Sun, L. Rangell, J. L. Lutman, S. Ulufatu, E. Stefanich, C. Chalouni, M. Sagolla, L. Diehl, P. Fielder, B. Dean, M. Balazs, and F. Martin. 2012. "Equilibrative nucleoside transporter 3 deficiency perturbs lysosome function and macrophage homeostasis." *Science* 335 (6064):89-92. doi: 10.1126/science.1213682.

Huotari, J., and A. Helenius. 2011. "Endosome maturation." *EMBO J* 30 (17):3481-500. doi: 10.1038/emboj.2011.286.

Hwang, W. Y., Y. Fu, D. Reyon, M. L. Maeder, P. Kaini, J. D. Sander, J. K. Joung, R. T. Peterson, and J. R. Yeh. 2013. "Heritable and precise zebrafish genome editing using a CRISPR-Cas system." *PLoS One* 8 (7):e68708. doi: 10.1371/journal.pone.0068708.

Hwang, W. Y., Y. Fu, D. Reyon, M. L. Maeder, S. Q. Tsai, J. D. Sander, R. T. Peterson, J. R. Yeh, and J. K. Joung. 2013. "Efficient genome editing in zebrafish using a CRISPR-Cas system." *Nat Biotechnol* 31 (3):227-9. doi: 10.1038/nbt.2501.

Iacopetta, D., R. Lappano, A. R. Cappello, M. Madeo, E. M. De Francesco, A. Santoro, R. Curcio, L. Capobianco, V. Pezzi, M. Maggiolini, and V. Dolce. 2010. "SLC37A1 gene expression is up-regulated by epidermal growth factor in breast cancer cells." *Breast Cancer Res Treat* 122 (3):755-64. doi: 10.1007/s10549-009-0620-x.

Idzko, M., D. Ferrari, and H. K. Eltzschig. 2014. "Nucleotide signalling during inflammation." *Nature* 509 (7500):310-7. doi: 10.1038/nature13085.

Jutras, I., M. Houde, N. Currier, J. Boulais, S. Duclos, S. LaBoissiere, E. Bonneil, P. Kearney, P. Thibault, E. Paramithiotis, P. Hugo, and M. Desjardins. 2008. "Modulation of the phagosome proteome by interferon-gamma." *Mol Cell Proteomics* 7 (4):697-715. doi: 10.1074/mcp.M700267-MCP200.

Kanchanawong, P., G. Shtengel, A. M. Pasapera, E. B. Ramko, M. W. Davidson, H. F. Hess, and C. M. Waterman. 2010. "Nanoscale architecture of integrin-based cell adhesions." *Nature* 468 (7323):580-4. doi: 10.1038/nature09621.

Kaplan, G. 1977. "Differences in the mode of phagocytosis with Fc and C3 receptors in macrophages." *Scand J Immunol* 6 (8):797-807.

Kaur, B., D. J. Brat, N. S. Devi, and E. G. Van Meir. 2005. "Vasculostatin, a proteolytic fragment of brain angiogenesis inhibitor 1, is an antiangiogenic and antitumorigenic factor." *Oncogene* 24 (22):3632-42. doi: 10.1038/sj.onc.1208317.

Kerr, J. F., B. Harmon, and J. Searle. 1974. "An electron-microscope study of cell deletion in the anuran tadpole tail during spontaneous metamorphosis with special reference to apoptosis of striated muscle fibers." *J Cell Sci* 14 (3):571-85.

Kerr, J. F., A. H. Wyllie, and A. R. Currie. 1972. "Apoptosis: a basic biological phenomenon with wide-ranging implications in tissue kinetics." *Br J Cancer* 26 (4):239-57.

Kikuchi, D., M. Saito, K. Saito, Y. Watanabe, Y. Matsumoto, Y. Kanke, H. Onozawa, S. Hayase, W. Sakamoto, T. Ishigame, T. Momma, S. Ohki, and S. Takenoshita. 2018. "Upregulated solute carrier family 37 member 1 in colorectal cancer is associated with poor patient outcome and metastasis." *Oncol Lett* 15 (2):2065-2072. doi: 10.3892/ol.2017.7559.

Kim, D. H., D. D. Sarbassov, S. M. Ali, J. E. King, R. R. Latek, H. Erdjument-Bromage, P. Tempst, and D. M. Sabatini. 2002. "mTOR interacts with raptor to form a nutrient-sensitive complex that signals to the cell growth machinery." *Cell* 110 (2):163-75.

Kim, J. Y., K. Tillison, S. Zhou, Y. Wu, and C. M. Smas. 2007. "The major facilitator superfamily member Slc37a2 is a novel macrophage- specific gene selectively expressed in obese white adipose tissue." *Am J Physiol Endocrinol Metab* 293 (1):E110-20. doi: 10.1152/ajpendo.00404.2006.

Kinchen, J. M., J. Cabello, D. Klingele, K. Wong, R. Feichtinger, H. Schnabel, R. Schnabel, and M. O. Hengartner. 2005. "Two pathways converge at CED-10 to mediate actin rearrangement and corpse removal in C. elegans." *Nature* 434 (7029):93-9. doi: 10.1038/nature03263.

Krajcovic, M., S. Krishna, L. Akkari, J. A. Joyce, and M. Overholtzer. 2013. "mTOR regulates phagosome and entotic vacuole fission." *Mol Biol Cell* 24 (23):3736-45. doi: 10.1091/mbc.E13-07-0408.

Krieser, R. J., K. S. MacLea, D. S. Longnecker, J. L. Fields, S. Fiering, and A. Eastman. 2002. "Deoxyribonuclease IIalpha is required during the phagocytic phase of apoptosis and its loss causes perinatal lethality." *Cell Death Differ* 9 (9):956-62. doi: 10.1038/sj.cdd.4401056.

Krysko, D. V., G. Brouckaert, M. Kalai, P. Vandenabeele, and K. D'Herde. 2003. "Mechanisms of internalization of apoptotic and necrotic L929 cells by a macrophage cell line studied by electron microscopy." *J Morphol* 258 (3):336-45. doi: 10.1002/jmor.10161.

Krysko, D. V., G. Denecker, N. Festjens, S. Gabriels, E. Parthoens, K. D'Herde, and P. Vandenabeele. 2006. "Macrophages use different internalization mechanisms to clear apoptotic and necrotic cells." *Cell Death Differ* 13 (12):2011-22. doi: 10.1038/sj.cdd.4401900.

Lai, C., and G. Lemke. 1991. "An extended family of protein-tyrosine kinase genes differentially expressed in the vertebrate nervous system." *Neuron* 6 (5):691-704.

Lauber, K., E. Bohn, S. M. Krober, Y. J. Xiao, S. G. Blumenthal, R. K. Lindemann, P. Marini, C. Wiedig, A. Zobywalski, S. Baksh, Y. Xu, I. B. Autenrieth, K. Schulze-Osthoff, C. Belka, G. Stuhler, and S. Wesselborg. 2003. "Apoptotic cells induce migration of phagocytes via caspase-3-mediated release of a lipid attraction signal." *Cell* 113 (6):717-30.

Lee, W. L., M. K. Kim, A. D. Schreiber, and S. Grinstein. 2005. "Role of ubiquitin and proteasomes in phagosome maturation." *Mol Biol Cell* 16 (4):2077-90. doi: 10.1091/mbc.e04-06-0464.

Lee, W. L., D. Mason, A. D. Schreiber, and S. Grinstein. 2007. "Quantitative analysis of membrane remodeling at the phagocytic cup." *Mol Biol Cell* 18 (8):2883-92. doi: 10.1091/mbc.E06-05-0450.

Leonardi-Essmann, F., M. Emig, Y. Kitamura, R. Spanagel, and P. J. Gebicke-Haerter. 2005. "Fractalkine-upregulated milk-fat globule EGF factor-8 protein in cultured rat microglia." *J Neuroimmunol* 160 (1-2):92-101. doi: 10.1016/j.jneuroim.2004.11.012.

Levin, R., S. Grinstein, and J. Canton. 2016. "The life cycle of phagosomes: formation, maturation, and resolution." *Immunol Rev* 273 (1):156-79. doi: 10.1111/imr.12439.

Lu, N., and Z. Zhou. 2012. "Membrane trafficking and phagosome maturation during the clearance of apoptotic cells." *Int Rev Cell Mol Biol* 293:269-309. doi: 10.1016/B978-0-12-394304-0.00013-0.

Matsuo, H., J. Chevallier, N. Mayran, I. Le Blanc, C. Ferguson, J. Faure, N. S. Blanc, S. Matile, J. Dubochet, R. Sadoul, R. G. Parton, F. Vilbois, and J. Gruenberg. 2004. "Role of LBPA and Alix in multivesicular liposome formation and endosome organization." *Science* 303 (5657):531-4. doi: 10.1126/science.1092425.

Maxfield, F. R., and D. J. Yamashiro. 1987. "Endosome acidification and the pathways of receptor-mediated endocytosis." *Adv Exp Med Biol* 225:189-98.

Mazaheri, F., O. Breus, S. Durdu, P. Haas, J. Wittbrodt, D. Gilmour, and F. Peri. 2014. "Distinct roles for BAI1 and TIM-4 in the engulfment of dying neurons by microglia." *Nat Commun* 5:4046. doi: 10.1038/ncomms5046.

McCourt, P. A., B. H. Smedsrod, J. Melkko, and S. Johansson. 1999. "Characterization of a hyaluronan receptor on rat sinusoidal liver endothelial cells and its functional relationship to scavenger receptors." *Hepatology* 30 (5):1276-86. doi: 10.1002/hep.510300521.

Medina, C. B., and K. S. Ravichandran. 2016. "Do not let death do us part: 'find-me' signals in communication between dying cells and the phagocytes." *Cell Death Differ* 23 (6):979-89. doi: 10.1038/cdd.2016.13.

Meier, P., A. Finch, and G. Evan. 2000. "Apoptosis in development." *Nature* 407 (6805):796-801. doi: 10.1038/35037734.

Mercanti, V., S. J. Charette, N. Bennett, J. J. Ryckewaert, F. Letourneur, and P. Cosson. 2006. "Selective membrane exclusion in phagocytic and macropinocytic cups." *J Cell Sci* 119 (Pt 19):4079-87. doi: 10.1242/jcs.03190.

Miksa, M., D. Amin, R. Wu, T. S. Ravikumar, and P. Wang. 2007. "Fractalkine-induced MFG-E8 leads to enhanced apoptotic cell clearance by macrophages." *Mol Med* 13 (11-12):553-60. doi: 10.2119/2007-00019.Miksa.

Moritz, C. 2014. "Studying microglial responses to neuronal cell death in the living zebrafish brain.".

Moritz, C., F. Berardi, C. Abate, and F. Peri. 2015. "Live imaging reveals a new role for the sigma-1 (sigma1) receptor in allowing microglia to leave brain injuries." *Neurosci Lett* 591:13-8. doi: 10.1016/j.neulet.2015.02.004.

Mullins, M. C., M. Hammerschmidt, P. Haffter, and C. Nusslein-Volhard. 1994. "Large-scale mutagenesis in the zebrafish: in search of genes controlling development in a vertebrate." *Curr Biol* 4 (3):189-202.

Murphy, R. F. 1991. "Maturation models for endosome and lysosome biogenesis." *Trends Cell Biol* 1 (4):77-82.

Nagata, K., K. Ohashi, T. Nakano, H. Arita, C. Zong, H. Hanafusa, and K. Mizuno. 1996. "Identification of the product of growth arrest-specific gene 6 as a common ligand for Axl, Sky, and Mer receptor tyrosine kinases." *J Biol Chem* 271 (47):30022-7.

Nagata, S. 2007. "Autoimmune diseases caused by defects in clearing dead cells and nuclei expelled from erythroid precursors." *Immunol Rev* 220:237-50. doi: 10.1111/j.1600-065X.2007.00571.x.

Nagata, S. 2018. "Apoptosis and Clearance of Apoptotic Cells." *Annu Rev Immunol* 36:489-517. doi: 10.1146/annurev-immunol-042617-053010.

Nagata, S., R. Hanayama, and K. Kawane. 2010. "Autoimmunity and the clearance of dead cells." *Cell* 140 (5):619-30. doi: 10.1016/j.cell.2010.02.014.

Nimmerjahn, A., F. Kirchhoff, and F. Helmchen. 2005. "Resting microglial cells are highly dynamic surveillants of brain parenchyma in vivo." *Science* 308 (5726):1314-8. doi: 10.1126/science.1110647.

Nishimori, H., T. Shiratsuchi, T. Urano, Y. Kimura, K. Kiyono, K. Tatsumi, S. Yoshida, M. Ono, M. Kuwano, Y. Nakamura, and T. Tokino. 1997. "A novel brain-specific p53-target gene, BAI1, containing thrombospondin type 1 repeats inhibits experimental angiogenesis." *Oncogene* 15 (18):2145-50.

O'Bryan, J. P., R. A. Frye, P. C. Cogswell, A. Neubauer, B. Kitch, C. Prokop, R. Espinosa, 3rd, M. M. Le Beau, H. S. Earp, and E. T. Liu. 1991. "axl, a transforming gene isolated from primary human myeloid leukemia cells, encodes a novel receptor tyrosine kinase." *Mol Cell Biol* 11 (10):5016-31.

Ohashi, K., K. Nagata, J. Toshima, T. Nakano, H. Arita, H. Tsuda, K. Suzuki, and K. Mizuno. 1995. "Stimulation of sky receptor tyrosine kinase by the product of growth arrest-specific gene 6." *J Biol Chem* 270 (39):22681-4.

Palade, G. 1975. "Intracellular aspects of the process of protein synthesis." *Science* 189 (4206):867. doi: 10.1126/science.189.4206.867-b.

Palade, G. E. 1983. "Membrane biogenesis: an overview." *Methods Enzymol* 96:xxix-lv.

Pan, C. J., S. Y. Chen, H. S. Jun, S. R. Lin, B. C. Mansfield, and J. Y. Chou. 2011. "SLC37A1 and SLC37A2 are phosphate-linked, glucose-6-phosphate antiporters." *PLoS One* 6 (9):e23157. doi: 10.1371/journal.pone.0023157.

Pan, C. J., S. Y. Chen, S. Lee, and J. Y. Chou. 2009. "Structure-function study of the glucose-6-phosphate transporter, an eukaryotic antiporter deficient in glycogen storage disease type Ib." *Mol Genet Metab* 96 (1):32-7. doi: 10.1016/j.ymgme.2008.10.005.

Park, B., J. Lee, H. Moon, G. Lee, D. H. Lee, J. H. Cho, and D. Park. 2015. "Co-receptors are dispensable for tethering receptor-mediated phagocytosis of apoptotic cells." *Cell Death Dis* 6:e1772. doi: 10.1038/cddis.2015.140.

Park, D., C. Z. Han, M. R. Elliott, J. M. Kinchen, P. C. Trampont, S. Das, S. Collins, J. J. Lysiak, K. L. Hoehn, and K. S. Ravichandran. 2011. "Continued clearance of apoptotic cells critically depends on the phagocyte Ucp2 protein." *Nature* 477 (7363):220-4. doi: 10.1038/nature10340.

Park, D., A. Hochreiter-Hufford, and K. S. Ravichandran. 2009. "The phosphatidylserine receptor TIM-4 does not mediate direct signaling." *Curr Biol* 19 (4):346-51. doi: 10.1016/j.cub.2009.01.042.

Park, D., A. C. Tosello-Trampont, M. R. Elliott, M. Lu, L. B. Haney, Z. Ma, A. L. Klibanov, J. W. Mandell, and K. S. Ravichandran. 2007. "BAI1 is an engulfment receptor for apoptotic cells upstream of the ELMO/Dock180/Rac module." *Nature* 450 (7168):430-4. doi: 10.1038/nature06329.

Park, S. Y., M. Y. Jung, H. J. Kim, S. J. Lee, S. Y. Kim, B. H. Lee, T. H. Kwon, R. W. Park, and I. S. Kim. 2008. "Rapid cell corpse clearance by stabilin-2, a membrane phosphatidylserine receptor." *Cell Death Differ* 15 (1):192-201. doi: 10.1038/sj.cdd.4402242.

Park, S. Y., K. B. Kang, N. Thapa, S. Y. Kim, S. J. Lee, and I. S. Kim. 2008. "Requirement of adaptor protein GULP during stabilin-2-mediated cell corpse engulfment." *J Biol Chem* 283 (16):10593-600. doi: 10.1074/jbc.M709105200.

Parkhurst, C. N., G. Yang, I. Ninan, J. N. Savas, J. R. Yates, 3rd, J. J. Lafaille, B. L. Hempstead, D. R. Littman, and W. B. Gan. 2013. "Microglia promote learning-dependent synapse formation through brain-derived neurotrophic factor." *Cell* 155 (7):1596-609. doi: 10.1016/j.cell.2013.11.030.

Peltier, J., A. Hartlova, and M. Trost. 2017. "Assessing the Phagosome Proteome by Quantitative Mass Spectrometry." *Methods Mol Biol* 1519:249-263. doi: 10.1007/978-1-4939-6581-6_17.

Penberthy, K. K., J. J. Lysiak, and K. S. Ravichandran. 2018. "Rethinking Phagocytes: Clues from the Retina and Testes." *Trends Cell Biol* 28 (4):317-327. doi: 10.1016/j.tcb.2018.01.004.

Penberthy, K. K., and K. S. Ravichandran. 2016. "Apoptotic cell recognition receptors and scavenger receptors." *Immunol Rev* 269 (1):44-59. doi: 10.1111/imr.12376.

Peri, F., and C. Nusslein-Volhard. 2008. "Live imaging of neuronal degradation by microglia reveals a role for v0-ATPase a1 in phagosomal fusion in vivo." *Cell* 133 (5):916-27. doi: 10.1016/j.cell.2008.04.037.

Peter, C., M. Waibel, C. G. Radu, L. V. Yang, O. N. Witte, K. Schulze-Osthoff, S. Wesselborg, and K. Lauber. 2008. "Migration to apoptotic "find-me" signals is mediated via the phagocyte receptor G2A." *J Biol Chem* 283 (9):5296-305. doi: 10.1074/jbc.M706586200.

Politz, O., A. Gratchev, P. A. McCourt, K. Schledzewski, P. Guillot, S. Johansson, G. Svineng, P. Franke, C. Kannicht, J. Kzhyshkowska, P. Longati, F. W. Velten, S. Johansson, and S. Goerdt. 2002. "Stabilin-1 and -2 constitute a novel family of fasciclin-like hyaluronan receptor homologues." *Biochem J* 362 (Pt 1):155-64.

Proverbio, M. C., E. Mangano, A. Gessi, R. Bordoni, R. Spinelli, R. Asselta, P. S. Valin, S. Di Candia, I. Zamproni, C. Diceglie, S. Mora, M. Caruso-Nicoletti, A. Salvatoni, G. De Bellis, and C. Battaglia. 2013. "Whole genome SNP genotyping and exome sequencing reveal novel genetic variants and putative causative genes in congenital hyperinsulinism." *PLoS One* 8 (7):e68740. doi: 10.1371/journal.pone.0068740.

Reddy, A., E. V. Caler, and N. W. Andrews. 2001. "Plasma membrane repair is mediated by Ca(2+)-regulated exocytosis of lysosomes." *Cell* 106 (2):157-69.

Reinartz, S., and O. Distl. 2016. "Validation of Deleterious Mutations in Vorderwald Cattle." *PLoS One* 11 (7):e0160013. doi: 10.1371/journal.pone.0160013.

Renehan, A. G., C. Booth, and C. S. Potten. 2001. "What is apoptosis, and why is it important?" *BMJ* 322 (7301):1536-8.

Renshaw, S. A., and N. S. Trede. 2012. "A model 450 million years in the making: zebrafish and vertebrate immunity." *Dis Model Mech* 5 (1):38-47. doi: 10.1242/dmm.007138.

Ritchie, K., R. Iino, T. Fujiwara, K. Murase, and A. Kusumi. 2003. "The fence and picket structure of the plasma membrane of live cells as revealed by single molecule techniques (Review)." *Mol Membr Biol* 20 (1):13-8.

Roberts, R. L., M. A. Barbieri, J. Ullrich, and P. D. Stahl. 2000. "Dynamics of rab5 activation in endocytosis and phagocytosis." *J Leukoc Biol* 68 (5):627-32.

Rossi, F., A. M. Casano, K. Henke, K. Richter, and F. Peri. 2015. "The SLC7A7 Transporter Identifies Microglial Precursors prior to Entry into the Brain." *Cell Rep* 11 (7):1008-17. doi: 10.1016/j.celrep.2015.04.028.

Rothhammer, V., and F. J. Quintana. 2015. "Role of astrocytes and microglia in central nervous system inflammation." *Semin Immunopathol*. doi: 10.1007/s00281-015-0521-5.

Samejima, K., and W. C. Earnshaw. 2005. "Trashing the genome: the role of nucleases during apoptosis." *Nat Rev Mol Cell Biol* 6 (9):677-88. doi: 10.1038/nrm1715.

Sander, J. D., and J. K. Joung. 2014. "CRISPR-Cas systems for editing, regulating and targeting genomes." *Nat Biotechnol* 32 (4):347-55. doi: 10.1038/nbt.2842.

Schieber, N. L., P. Machado, S. M. Markert, C. Stigloher, Y. Schwab, and A. M. Steyer. 2017. "Minimal resin embedding of multicellular specimens for targeted FIB-SEM imaging." *Methods Cell Biol* 140:69-83. doi: 10.1016/bs.mcb.2017.03.005.

Seigneuret, M., and P. F. Devaux. 1984. "ATP-dependent asymmetric distribution of spin-labeled phospholipids in the erythrocyte membrane: relation to shape changes." *Proc Natl Acad Sci U S A* 81 (12):3751-5.

Sieger, D., C. Moritz, T. Ziegenhals, S. Prykhozhij, and F. Peri. 2012. "Long-range Ca2+ waves transmit brain-damage signals to microglia." *Dev Cell* 22 (6):1138-48. doi: 10.1016/j.devcel.2012.04.012.

Sierra, A., F. de Castro, J. Del Rio-Hortega, J. Rafael Iglesias-Rozas, M. Garrosa, and H. Kettenmann. 2016. "The "Big-Bang" for modern glial biology: Translation and comments on Pio del Rio-Hortega 1919 series of papers on microglia." *Glia* 64 (11):1801-40. doi: 10.1002/glia.23046.

Silva, M. T. 2010. "Secondary necrosis: the natural outcome of the complete apoptotic program." *FEBS Lett* 584 (22):4491-9. doi: 10.1016/j.febslet.2010.10.046.

Silverstein, R. L., and M. Febbraio. 1992. "Identification of lysosome-associated membrane protein-2 as an activation-dependent platelet surface glycoprotein." *Blood* 80 (6):1470-5.

Simhadri, V. R., J. F. Andersen, E. Calvo, S. C. Choi, J. E. Coligan, and F. Borrego. 2012. "Human CD300a binds to phosphatidylethanolamine and phosphatidylserine, and modulates the phagocytosis of dead cells." *Blood* 119 (12):2799-809. doi: 10.1182/blood-2011-08-372425.

Sisirak, V., B. Sally, V. D'Agati, W. Martinez-Ortiz, Z. B. Ozcakar, J. David, A. Rashidfarrokhi, A. Yeste, C. Panea, A. S. Chida, M. Bogunovic, Ivanov, II, F. J. Quintana, I. Sanz, K. B. Elkon, M. Tekin, F. Yalcinkaya, T. J. Cardozo, R. M. Clancy, J. P. Buyon, and B. Reizis. 2016. "Digestion of Chromatin in Apoptotic Cell Microparticles Prevents Autoimmunity." *Cell* 166 (1):88-101. doi: 10.1016/j.cell.2016.05.034.

Stitt, T. N., G. Conn, M. Gore, C. Lai, J. Bruno, C. Radziejewski, K. Mattsson, J. Fisher, D. R. Gies, P. F. Jones, and et al. 1995. "The anticoagulation factor protein S and its relative, Gas6, are ligands for the Tyro 3/Axl family of receptor tyrosine kinases." *Cell* 80 (4):661-70.

Streisinger, G., C. Walker, N. Dower, D. Knauber, and F. Singer. 1981. "Production of clones of homozygous diploid zebra fish (Brachydanio rerio)." *Nature* 291 (5813):293-6.

Suzuki, J., D. P. Denning, E. Imanishi, H. R. Horvitz, and S. Nagata. 2013. "Xk-related protein 8 and CED-8 promote phosphatidylserine exposure in apoptotic cells." *Science* 341 (6144):403-6. doi: 10.1126/science.1236758.

Suzuki, J., M. Umeda, P. J. Sims, and S. Nagata. 2010. "Calcium-dependent phospholipid scrambling by TMEM16F." *Nature* 468 (7325):834-8. doi: 10.1038/nature09583.

Swanson, J. A. 2008. "Shaping cups into phagosomes and macropinosomes." *Nat Rev Mol Cell Biol* 9 (8):639-49. doi: 10.1038/nrm2447.

Swanson, J. A., and S. C. Baer. 1995. "Phagocytosis by zippers and triggers." *Trends Cell Biol* 5 (3):89-93.

Swanson, J. A., M. T. Johnson, K. Beningo, P. Post, M. Mooseker, and N. Araki. 1999. "A contractile activity that closes phagosomes in macrophages." *J Cell Sci* 112 (Pt 3):307-16.

Tait, S. W., G. Ichim, and D. R. Green. 2014. "Die another way--non-apoptotic mechanisms of cell death." *J Cell Sci* 127 (Pt 10):2135-44. doi: 10.1242/jcs.093575.

Takahashi, Y., M. Miyata, P. Zheng, T. Imazato, A. Horwitz, and J. D. Smith. 2000. "Identification of cAMP analogue inducible genes in RAW264 macrophages." *Biochim Biophys Acta* 1492 (2-3):385-94.

Tamura, Y., H. Adachi, J. Osuga, K. Ohashi, N. Yahagi, M. Sekiya, H. Okazaki, S. Tomita, Y. Iizuka, H. Shimano, R. Nagai, S. Kimura, M. Tsujimoto, and S. Ishibashi. 2003. "FEEL-1 and FEEL-2 are endocytic receptors for advanced glycation end products." *J Biol Chem* 278 (15):12613-7. doi: 10.1074/jbc.M210211200.

Touret, N., P. Paroutis, and S. Grinstein. 2005. "The nature of the phagosomal membrane: endoplasmic reticulum versus plasmalemma." *J Leukoc Biol* 77 (6):878-85. doi: 10.1189/jlb.1104630.

Trost, M., L. English, S. Lemieux, M. Courcelles, M. Desjardins, and P. Thibault. 2009. "The phagosomal proteome in interferon-gamma-activated macrophages." *Immunity* 30 (1):143-54. doi: 10.1016/j.immuni.2008.11.006.

Truman, L. A., C. A. Ford, M. Pasikowska, J. D. Pound, S. J. Wilkinson, I. E. Dumitriu, L. Melville, L. A. Melrose, C. A. Ogden, R. Nibbs, G. Graham, C. Combadiere, and C. D. Gregory. 2008. "CX3CL1/fractalkine is released from apoptotic lymphocytes to stimulate macrophage chemotaxis." *Blood* 112 (13):5026-36. doi: 10.1182/blood-2008-06-162404.

Tsuboi, S., H. Takada, T. Hara, N. Mochizuki, T. Funyu, H. Saitoh, Y. Terayama, K. Yamaya, C. Ohyama, S. Nonoyama, and H. D. Ochs. 2009. "FBP17 Mediates a Common Molecular Step in the Formation of Podosomes and Phagocytic Cups in Macrophages." *J Biol Chem* 284 (13):8548-56. doi: 10.1074/jbc.M805638200.

van Ham, T. J., J. Mapes, D. Kokel, and R. T. Peterson. 2010. "Live imaging of apoptotic cells in zebrafish." *FASEB J* 24 (11):4336-42. doi: 10.1096/fj.10-161018.

Vieira, O. V., R. J. Botelho, and S. Grinstein. 2002. "Phagosome maturation: aging gracefully." *Biochem J* 366 (Pt 3):689-704. doi: 10.1042/BJ20020691.

Vieira, O. V., C. Bucci, R. E. Harrison, W. S. Trimble, L. Lanzetti, J. Gruenberg, A. D. Schreiber, P. D. Stahl, and S. Grinstein. 2003. "Modulation of Rab5 and Rab7 recruitment to phagosomes by phosphatidylinositol 3-kinase." *Mol Cell Biol* 23 (7):2501-14.

Wahe, A., B. Kasmapour, C. Schmaderer, D. Liebl, K. Sandhoff, A. Nykjaer, G. Griffiths, and M. G. Gutierrez. 2010. "Golgi-to-phagosome transport of acid sphingomyelinase and prosaposin is mediated by sortilin." *J Cell Sci* 123 (Pt 14):2502-11. doi: 10.1242/jcs.067686.

Weigert, A., N. Tzieply, A. von Knethen, A. M. Johann, H. Schmidt, G. Geisslinger, and B. Brune. 2007. "Tumor cell apoptosis polarizes macrophages role of sphingosine-1-phosphate." *Mol Biol Cell* 18 (10):3810-9. doi: 10.1091/mbc.e06-12-1096.

Weinhard, L., G. di Bartolomei, G. Bolasco, P. Machado, N. L. Schieber, U. Neniskyte, M. Exiga, A. Vadisiute, A. Raggioli, A. Schertel, Y. Schwab, and C. T. Gross. 2018. "Microglia remodel synapses by presynaptic trogocytosis and spine head filopodia induction." *Nat Commun* 9 (1):1228. doi: 10.1038/s41467-018-03566-5.

Wiley, S. R., K. Schooley, P. J. Smolak, W. S. Din, C. P. Huang, J. K. Nicholl, G. R. Sutherland, T. D. Smith, C. Rauch, C. A. Smith, and et al. 1995. "Identification and characterization of a new member of the TNF family that induces apoptosis." *Immunity* 3 (6):673-82.

Zhou, B., J. A. Weigel, L. Fauss, and P. H. Weigel. 2000. "Identification of the hyaluronan receptor for endocytosis (HARE)." *J Biol Chem* 275 (48):37733-41. doi: 10.1074/jbc.M003030200.

Acknowledgments:

Too many people have contributed to this calamitous conclusion for a complete and correct accounting. Nevertheless, the most notorious shall be named. First I must thank my supervisor, Francesca Peri, for giving me this opportunity, for challenging me in ways I did not know I needed challenging, and for her effort in making this experience rich and rewarding. I would also like to extend my gratitude to the members of my TAC committee for taking the time to guide me through the preposterous purgatory process of a PhD, in particular Yannick Schwab, for taking me in and giving me a second home at EMBL. Thank you for the great discussions, the encouragement, and for kicking my ass. I would also like to thank Gareth Griffiths, whose generosity and mentorship I am so extraordinarily lucky to be the beneficiary of. A very special thanks to Randi Olsen, for starting me off on this journey, and for introducing me to the wonderful world of electron microscopy. I will remain forever grateful. To Ambra Villani, I can sincerely say, thank you for everything. We have shared every high and every low and through all of them I was always glad to stand shoulder to shoulder with you. You have truly earned the respect of the otherwise disrespectful yours truly. A big thanks to all the current and former members of the Peri Group and the Schwab Team whose camaraderie and criticisms has been equally enjoyable over the past four years. Especially Matthia Karreman whose laughter haunts me still. Thank you to Kerstin Richter for all the help both in and outside of the lab. Without it I should not have survived German austerity. I tip my hat to Jonas Hartmann who possesses that most rare combination of virtues, a scholar and a gentleman, it has been a pleasure to make your acquaintances. If anyone remains that feel they should have been listed above, I assure you, you were not forgotten. I merely ran out of ink.